REF: SAF/O3M/IASB/VR/NO2/095
ISSUE: 4
DATE: 14.02.2011
PAGES: 74

O3M SAF VALIDATION REPORT

Validated data products:

Identifier	Name	Acronym
O3M-02	Near-Real-Time Total Nitrogen Dioxide	NTO/NO2
O3M-07	Offline Total Nitrogen Dioxide	OTO/NO2
O3M-36	Near-Real-Time Tropospheric Nitrogen Dioxide	NTO/NO2tropo
O3M-37	Offline Tropospheric Nitrogen Dioxide	OTO/NO2tropo

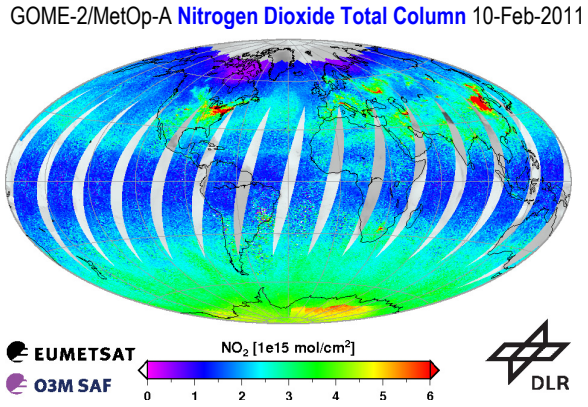

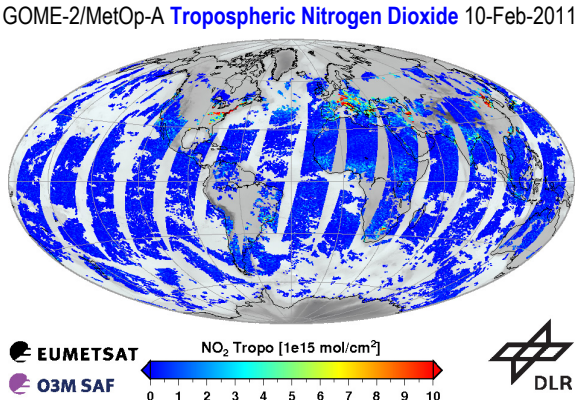

Authors:

Name	Institute	Email
Jean-Christopher Lambert	Belgian Institute for Space Aeronomy	at aeronomy.be
Gaia Pinardi	Belgian Institute for Space Aeronomy	at aeronomy.be
José Granville	Belgian Institute for Space Aeronomy	at aeronomy.be
Katrijn Clemer	Belgian Institute for Space Aeronomy	at aeronomy.be
Andy Delcloo	Royal Meteorological Institute of Belgium	at meteo.be
Pieter Valks	German Aerospace Centre	at dlr.de
Nan Hao	German Aerospace Centre	at dlr.de

Reporting period:

January 2007 – December 2010

Input data version:

GOME-2 L1b version 4.0, since 26 June 2008
GOME-2 L1b version 4.1, since 7 January 2009

Data processor version:

GDP version 4.3, since 26 May 2008
GDP version 4.4, since March 2010

authors / *auteurs*: G. Pinardi, J.-C. Lambert, J. Granville, K. Clemer, A. Delcloo, N. Hao, and P. Valks

contributeurs / *contributors*: V. Dorokhov, P. Eriksen, C. Fayt, M. Gil, F. Goutail, C. Hermans, G. Held, P. V. Johnston, K. Kreher, E. Kyrö, J. Leveau, D. Loyola, A. Pazmino, J.-P. Pommereau, O. Puentedura, A. Richter, H. K. Roscoe, V. Semenov, M. Van Roozendael, G. Vaughan, F. Wittrock, and M. Yela

edited by / *édité par*: G. Pinardi and J.-C. Lambert, BIRA-IASB, Brussels, Belgium

reference / *référence*: SAF/O3M/IASB/VR/NO2/095
TN-IASB-GOME2-O3MSAF-NO2-v4-2011

document type / *type de document*: O3M-SAF Validation Report
issue / *édition*: 4
revision / *révision*: 0
date of issue / *date d'édition*: 14 February 2011
products / *produits*: NTO/NO2, OTO/NO2, NTO/NO2tropo, OTO/NO2tropo
identifier / *identificateur*: O3M-02, O3M-07, O3M-36, O3M-37
product version / *version des données*: level-0-to-1 v4.0/4.1, level-1-to-2 GDP v4.3/4.4

distribution / *distribution*

Function	***Organisation***
O3M-SAF	EUMETSAT, BIRA-IASB, DLR, DMI, DWD, FMI, HNMS/AUTH, KNMI, LATMOS, MeteoFrance, RMI
GOME Team	DLR, ESA/ESRIN, BIRA-IASB, RTS, various
UPAS Team	DLR-IMF, DLR-DFD
NDACC UVVIS Working Group	BAS-NERC, BIRA-IASB, CAO, CNRS/IPSL/LATMOS, DMI, FMI-ARC, IFE/IUP, INTA, IPMet/UNESP, KSNU, NIWA, U. Manchester, U. Réunion/LACy, U. Wales

external contributors / *contributions externes au SAF*

NDACC teams contributing ground-based correlative measurements

Acronym	***Organisation***	***Country***
BAS-NERC	British Antarctic Survey – National Environment Research Council	United Kingdom
BIRA-IASB	Belgian Institute for Space Aeronomy	Belgium
CAO	Central Aerological Observatory	Russia
CNRS/LATMOS	CNRS / Laboratoire Atmosphère, Milieux, Observations Spatiales	France
DMI	Danish Meteorological Institute	Denmark
FMI-ARC	Finnish Meteorological Institute – Arctic Research Centre	Finland
IFE/IUP	Institut für Umweltphysik/Fernerkundung, University of Bremen	Germany
INTA	Instituto Nacional de Técnica Aeroespacial	Spain
IPMet/UNESP	Instituto de Pesquisas Meteorológicas, Universidade Estadual Paulista	Brazil
KSNU	Geophysical Laboratory, Kyrgyz State National University	Kyrgyzstan
NIWA	National Institute of Water and Atmospheric Research	New Zealand
U. Manchester	University of Manchester and University of Wales	United Kingdom
U. Réunion/LACY	Université de la Réunion	France

document change record / *historique du document*

Issue	***Rev.***	***Date***	***Section***	***Description of Change***
0		20.03.2008	all	Creation of this document
1		11.04.2008	all	Provisional validation report for ORR-A3
1	ORR-A3	29.04.2008	B	Implementation of ORR-A3 RIDs
2	0	17.09.2008	all	Update to 1.5 year of GOME-2 data + level-1B 3.9 to 4.0 + T-correction
2	ORR-B	24.11.2008	A, B, C	New Data Disclaimer; implementation of ORR-B RIDs; Section B.4 updated
3	0	10.05.2010	all	Validation update 2007-2009; full RTM MAX-DOAS; large swath issues; CHIMERE
4	0	14.02.2011	all	Validation update 2007-2010; GDP 4.3/4.4; MAX-DOAS; CHIMERE

MetOp-A GOME-2 GDP 4.3 / 4.4 total and tropospheric NO_2 validation: 2007 - 2010

CONTENTS

ACRONYMS AND ABBREVIATIONS

AMF	Air Mass Factor, or optical enhancement factor
BAS-NERC	British Antarctic Survey – National Environment Research Council
BIRA	Belgisch Instituut voor Ruimte-Aëronomie
CAO	Central Aerological Observatory
CNRS/LATMOS	Laboratoire Atmosphère, Milieux, Observations Spatiales du CNRS
DLR	German Aerospace Centre
DMI	Danish Meteorological Institute
DOAS	Differential Optical Absorption Spectroscopy
D-PAF	German Processing and Archiving Facility
Envisat	Environmental Satellite
ERS-2	European Remote Sensing Satellite -2
ESA	European Space Agency
EUMETSAT	European Organisation for the Exploitation of Meteorological Satellites
FMI-ARC	Finnish Meteorological Institute – Arctic Research Centre
GAW	WMO's Global Atmospheric Watch programme
GDOAS/SDOAS	GOME/SCIAMACHY WinDOAS prototype processor
GDP	GOME Data Processor
GOME	Global Ozone Monitoring Experiment
GVC	Ghost Vertical Column
H_2O	water vapour
IASB	Institut d'Aéronomie Spatiale de Belgique
IFE/IUP	Institut für Fernerkundung/Institut für Umweltphysik
IMF	Remote Sensing Technology Institute
INTA	Instituto Nacional de Técnica Aeroespacial
KSNU	Kyrgyzstan State National University
LOS	Line Of Sight
MIPAS	Michelson Interferometer for Passive Atmospheric Sounding
NDACC	Network for the Detection of Atmospheric Composition Change
NDSC	Network for the Detection of Stratospheric Change
NIWA	National Institute for Water and Atmospheric research
NO_2	nitrogen dioxide
O_3	ozone
O3M-SAF	Ozone and Atmospheric Chemistry Monitoring Satellite Application Facility
OCRA	Optical Cloud Recognition Algorithm
OMI	Ozone Monitoring Instrument
ROCINN	Retrieval of Cloud Information using Neural Networks
RRS	Rotational Raman Scattering
RTS	RT Solutions Inc.
SAOZ	Système d'Analyse par Observation Zénithale
SCD	Slant Column Density
SCIAMACHY	Scanning Imaging Absorption spectroMeter for Atmospheric CHartography
SNR	Signal to Noise Ratio
SZA	Solar Zenith Angle
TEMIS	Tropospheric Emission Monitoring Internet Service
UNESP	Universidade Estadual Paulista
UPAS	Universal Processor for UV/VIS Atmospheric Spectrometers
UVVIS	ground-based DOAS ultraviolet-visible spectrometer
VCD	Vertical Column Density
WMO	World Meteorological Organization

DATA DISCLAIMER FOR THE METOP-A GOME-2 TOTAL NO_2 (NTO/OTO) AND TROPOSPHERIC NO_2 (OTR) DATA PRODUCTS

In the framework of EUMETSAT's Satellite Application Facility on Ozone and Atmospheric Chemistry Monitoring (O3M-SAF), GOME-2 nitrogen dioxide (NO_2) total column and GOME-2 NO_2 tropospheric column data products, as well as associated cloud parameters, are delivered operationally in near-real-time (NTO, within 2:30 hours after sensing) and off-line (OTO). Those data products are generated at DLR from MetOp-A GOME-2 measurements using the UPAS environment version 1.2, the level-0-to-1 v4.0/4.1 processor and the level-1-to-2 GDP v4.3/4.4 DOAS retrieval processor (see TN-DLR-ATBD 2011 and TN-DLR-PUM 2010). BIRA-IASB, DLR and RMI ensure detailed quality assessment of algorithm upgrades and continuous monitoring of GOME-2 NO_2 data quality with a recurring geophysical validation using correlative measurements from the NDACC ground-based network and from other satellites, modelling support, and independent retrievals.

This report updates the validation of MetOp-A GOME-2 NO_2 column data (OTO/NTO) recorded over four years of operation, from January 2007 through December 2010. It also reports on the progress made with the set up of the validation process for GOME-2 NO_2 tropospheric column data (OTR), with validation results over the January 2007 – March 2010 time period. The stratospheric contribution to the NO_2 total column is validated against ground-based observations provided by the NDACC network of DOAS UV-Visible spectrometers. Those network measurements and independent GOME-2 retrievals are used to validate separately individual components of the tropospheric NO_2 retrieval chain, namely, the total slant column density and the stratospheric vertical columns density. Tropospheric NO_2 column data are compared to similar Envisat SCIAMACHY results, and to ground-based tropospheric columns retrieved from MAX-DOAS measurements at the pilot stations of OHP (Southern France) and Beijing (P.R. China).

The main results are summarized hereafter:

- The current quality of the MetOp-A GOME-2 radiance and irradiance spectra (level-1b data version 4.0/4.1) in the 425-445 nm spectral window enables stable DOAS retrievals. Resulting NO_2 slant columns and DOAS fit residuals are comparable to those obtained from ERS-2 GOME-1 spectra. GOME-2 GDP 4.3 and 4.4 NO_2 retrievals are consistent with independent retrievals to within 0.5 10^{14} molec.cm^{-2}, at nearly all latitudes.
- The previous and recent level-0-to-1B processor upgrades to version 4.0 and 4.1, respectively, impact hardly the quality of NO_2 column data retrieval. Monthly averages of the NO_2 column differences from one level-1 data version to another are smaller than 2.10^{13} molec.cm^{-2} at all latitudes.
- Qualitatively, all GOME-2 NO_2 column data products (total, stratospheric and tropospheric) are in good agreement with observations from the NDACC/UV-visible ground-based network, from ground-based MAX-DOAS instruments, and from the ERS-2 GOME and Envisat SCIAMACHY satellites. They all capture similarly global as well as finer structures of the NO_2 field, and its temporal variations at scales from days to months and years.
- Quantitatively, the estimated bias of GOME-2 NO_2 column products – estimated at first order as the absolute difference between GOME-2 and correlative vertical column data – depends on the latitude and on the presence of tropospheric NO_2. Expressed in percentage, the bias also varies – significantly – with the amplitude of the vertical column, which is a direct function of the season. After rejection of stations and/or episodes with high tropospheric NO_2, the quantitative agreement between GOME-2 and NDACC/UV-Visible network measurements in the Northern Hemisphere usually ranges from -0.6 to +0.6 10^{15} molec.cm^{-2}. The yearly mean/median agreement falls to a few 10^{14} molec.cm^{-2}. These results are close to the target bias requirements of 3-5 10^{14} molecule.cm^{-2} for unpolluted conditions, and well below the threshold bias requirement of 10 10^{14} molecule.cm^{-2}. Expressed as the

percentage relative difference, the agreement usually varies seasonally within the 8-20% range, depending on the value of the total column.

- In the Southern Hemisphere, again after rejection of episodes with high tropospheric NO_2, MetOp-A GOME-2 GDP 4.3/4.4 reports systematically smaller NO_2 column values than NDACC/UV-Visible network measurements, SCIAMACHY TEMIS and ERS-2 GOME GDP 4.1. This apparent negative offset is about $4\text{-}6 \cdot 10^{14}$ molec/cm^2 on an average or, expressed in percentage relative difference, of the order of 10-25%.
- Ground-based MAX-DOAS data retrieved at the OHP station have been used to test and set up a method for the end-to-end validation of GOME-2 NO_2 tropospheric column data. Pollution episodes are well reproduced by GOME-2. Quantitative comparisons with MAX-DOAS are encouraging, and conclude to a correlation coefficient of ~0.67 and a linear regression slope of ~0.8. Large scatter is observed in GOME-2 data in case of low tropospheric NO_2 conditions, but it is consistent with results reported in the literature, and a similar behaviour is also found when looking at other satellite data, such as the operational OMI NO_2 data produced by NASA/KNMI (AVDC, collection3).

A. INTRODUCTION

A.1. Scope of this document

The present document reports on the continuous validation of GOME-2/MetOp-A NO_2 column data acquired since the beginning of instrument operation in 2007. The data are produced operationally by the GOME Data Processor (GDP) operated at DLR in the framework of the EUMETSAT Satellite Application Facility on Ozone and Atmospheric Chemistry Monitoring (O3M-SAF). Based on an end-to-end validation approach, this report addresses the quality of individual components of the data processing, starting with DOAS fitting parameters. The report continues with comparisons of GOME-2 final data products with correlative observations from independent sources, namely, total (NTO/NO2, OTO/NO2) and tropospheric (NTO/NO2tropo, OTO/NO2tropo) column data produced with GDP versions 4.3 (operational since May 2008) and 4.4 (operational since March 2010). The NO_2 retrieval chain is identical in GDP 4.3 and 4.4, therefore the NO_2 data series produced by the two versions are analysed hereafter without distinction, unless stated explicitly.

A.2. Preliminary remarks

Validation techniques for NO_2 tropospheric column data derived from satellite measurements are in continuous development. Therefore this document details the progress of tropospheric NO_2 validation set-up.

Reported validations and supporting studies were carried out at the Belgian Institute for Space Aeronomy (IASB-BIRA, Brussels, Belgium), the DLR Remote Sensing Technology Institute (DLR-IMF, Oberpfaffenhofen, Germany), and the Royal Meteorological Institute of Belgium (RMI, Brussels, Belgium), in the framework of EUMETSAT Satellite Application Facility on Ozone and Atmospheric Chemistry Monitoring (O3M-SAF).

Ground-based validations rely on the early delivery of provisional data by NDACC/UVVIS network affiliates. This early delivery is the result of individual agreements arranged in the framework of the joint ESA/EUMETSAT RAO on the Calibration and Validation of EPS/MetOp data. Results relying on early-delivery data must always be considered as preliminary. Consolidated data from all ground-based stations and with official NDACC endorsement will be available via the NDACC Data Host Facility (see http://www.ndacc.org) within two years after acquisition, in accordance with NDACC Data Protocols.

A.3. Plan of this document

After presentation of the GOME-2 Data Disclaimer for NO_2 column products, this document is divided into the following sections:

A. This introduction

B. End-to-end validation: Results of the validation of individual components of the DOAS analysis – namely, slant column fit residuals, slant column densities, total (stratospheric) vertical column densities, and tropospheric vertical column densities. Ground-based validation of GOME-2 total NO_2. Ground-based validation and satellite-to-satellite comparisons of GOME-2 tropospheric NO_2. Studies using the CHIMERE model.

C. Conclusion of the present study

D. References

B. END-TO-END VALIDATION OF GOME-2 NO_2 COLUMN DATA

B.1. Rationale and method

Since the beginning of GOME-2 operation, several O3M-SAF NO_2 validation reports were issued on a regular basis. The present technical note updates these previous studies with the validation of GOME-2 NO_2 column data produced operationally by the GOME Data Processor versions 4.3 and 4.4. Despite their conclusive results, which endorse the operational production of NO_2 column data and their public release, accurate geophysical validation of NO_2 column observations from space remains a matter of scientific research and the object of field measurement intercomparison campaigns. Recurring issues are the multifaceted and variable behaviour of atmospheric NO_2, the particular way remote sensing samples and smoothes this variability vertically and horizontally, the poor availability of correlative (tropospheric column) measurements, the complexity of the data processing chain retrieving NO_2 column data from atmospheric spectra, and the lack of homogenisation of the validation methods being developed. For these reasons mainly the validation of satellite NO_2 column data in an operational environment remains also at the developmental stage. In addition of being an update, the work reported in the present technical note also constitutes a further step in the development of validation methods and facilities suitable to GOME-2 NO_2 column data.

Retrieval principles of GOME-2 NO_2 data are described in the Algorithm Theoretical Basis Document (ATBD, version January 2011) and the Product User Manual (PUM, version February 2010) available via the O3M-SAF web site (http://o3msaf.fmi.fi). The latest version 4.4 of the GOME Data Processor for NO_2 is also described in Valks et al. (2011). NO_2 column data are retrieved from the GOME-2 Earth radiance and solar irradiance spectra by several modules calculating intermediate parameters: the apparent slant column density along the optical path (SCD), the fractional cover (CF) and top pressure (CTP) of clouds interfering with the measurement scene, their optical thickness (COT) and albedo (CTA), the geometrical enhancement factor (AMF) needed to convert slant into vertical columns (VCD), and the NO_2 stratospheric reference needed to be subtracted from the total column to obtain the tropospheric column. In a latter stage those intermediate parameters are assembled to derive the final column data products: the total and the tropospheric column data. To ensure that the final product of such a complex production chain is validated meaningfully, validations cannot be limited to comparisons with correlative measurements of the total column data. An end-to-end validation of critical individual components of the level-1-to-2 retrieval chain can be necessary, e.g. to detect uncertainties affecting intermediate parameters but cancelling each other in the final data product.

The end-to-end validation approach adopted in this document consists in: (a) an assessment of the quality of GOME-2 DOAS analysis results, by means of confrontation of different GDP 4.3 retrievals performed on GOME-1 and GOME-2 spectra, and also performed with the NRT and off-line processing chains; (b) an assessment of the geophysical validity of total column measurements over areas free of tropospheric pollution, by comparison with stratospheric column measurements provided by zenith-sky DOAS UV-visible spectrometers affiliated with the Network for the Detection of Atmospheric Composition Change (NDACC); (c) an assessment of the validity of the stratospheric reference subtracted from the retrieved total column in order to obtain the tropospheric contribution, again with respect to NDACC zenith-sky DOAS measurements; and (d) an assessment of the validity of the GOME-2 tropospheric NO_2 column data, with respect to multiple-axis DOAS observations (MAX-DOAS). The validation of cloud data products falls beyond the scope of the present report.

B.2. Comparison of DOAS analysis results

B.2.1 Slant column density

To test the quality of the DOAS NO_2 slant column fit on two different sources of spectra, GDP 4.4 has been used to retrieve NO_2 slant column amounts from spectra recorded along a single orbit of GOME-2 (orbit #9524, August 20, 2008) and GOME-1 (orbit #17421, August 20, 1998). The GOME-2 orbit is based on level-1B version 4.0. The present subsection shows illustrative comparisons of the retrieved slant columns and of the associated DOAS fit residuals.

The two orbits are distant by ten years, but they cover more or less the same ground track over Eastern Asia. However, the pollution over China is much larger for the GOME-2 day in 2008 than for the GOME-1 day in 1998, which can be seen in the slant column picture. Differences in the cloud patterns are expected, however, cloud effects should not have a significant impact on the observed differences between the GOME-1 and GOME-2 DOAS residuals and SCDs, at least along an entire orbit.

Figure 2.1.1 shows the retrieved slant columns for GOME-2 and GOME-1 for the two individual orbits. If the GOME-2 swath is reduced to (approximately) the GOME-1 swath width (line-of-slight angle <30°), the scatter in the slant column is similar for the two instruments. It is timely to note that, because of the larger number of GOME-2 ground-pixels within the same swath-width (line-of-sight (LOS) < 30°) and the smaller pixel size of GOME-2, the scatter in the GOME-2 slant columns are slightly larger, as can be seen in the right part of the figure. The effect of the ground pixel size on the scatter in the NO_2 slant columns can be illustrated with a distribution plot, as shown in Figure 2.1.2. The distribution of the slant columns has been calculated for the equatorial Pacific for August 2008, using the original GOME-2 measurements (80x40 km^2, LOS < 30°), and GOME-2 measurements re-sampled to the spatial resolution of GOME-1 (320x40 km^2). As can be seen in Figure 2.1.2, the slant column distribution is narrower for the re-sampled GOME-2 measurements, illustrating the dependence of the scatter and S/N on the ground pixel size.

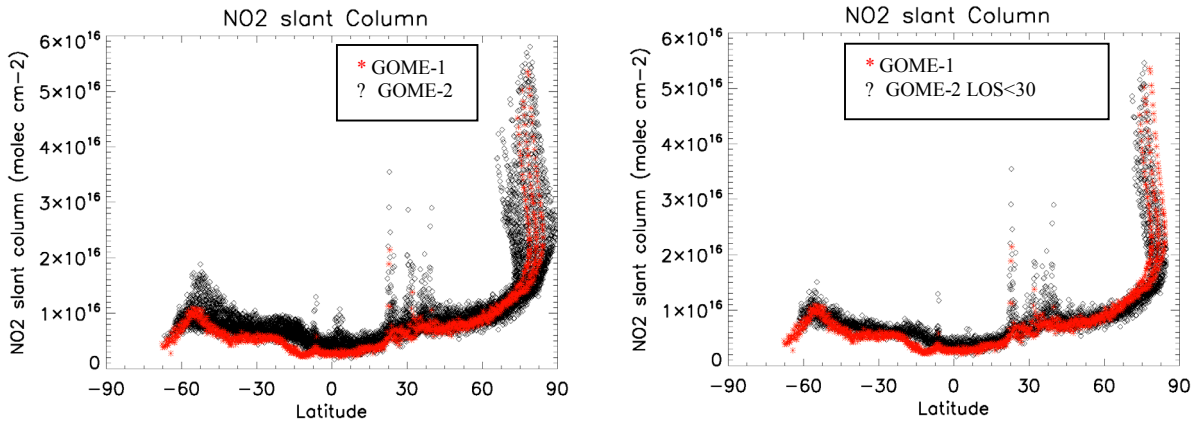

Figure 2.1.1 - NO_2 slant column along a single orbit of GOME-1 (August 20, 1998) and GOME-2 (August 20, 2008). For the picture on the right hand side, only GOME-2 data within a line-of-sight angle < 30° have been selected, in order to consider a swath width reduced to (approximately) the GOME-1 swath width.

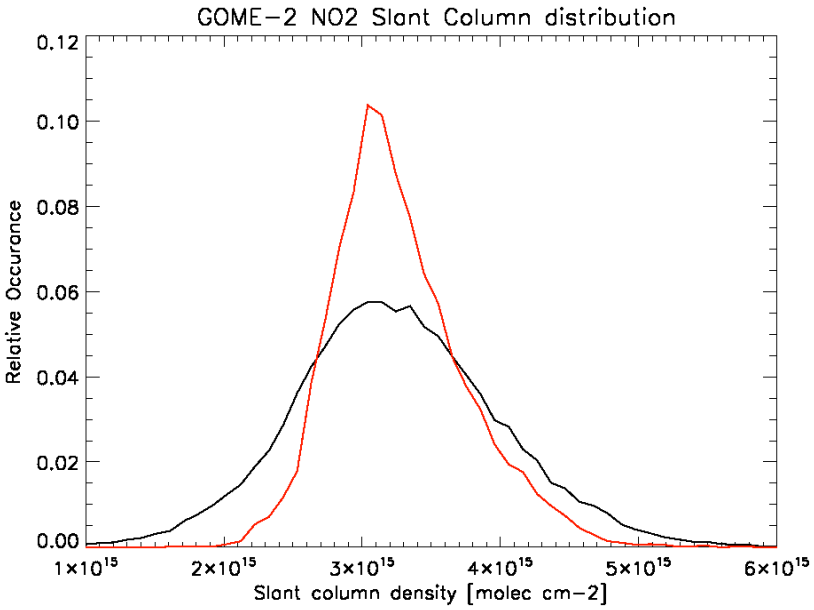

Figure 2.1.2 - Distribution of the GOME-2 NO_2 slant column densities for the equatorial Pacific region (10°S-10°N, 160-200°E). The black line shows the distribution of the original GOME-2 measurements (spatial resolution 80x40 km^2; line-of-sight angle < 30°). The red line shows the distribution of GOME-2 measurements resampled to the spatial resolution of GOME-1 (320x40 km^2; line-of-sight angle < 30°).

B.2.2 DOAS fit residuals

Figure 2.2.1 depicts the residual of the DOAS NO_2 slant column fit for the same two individual orbits, plotted as a function of the latitude and of the solar zenith angle. This figure illustrates the high quality of the DOAS fit in the NO_2 spectral fitting window (425-445 nm) selected for GOME-2: the fit residuals for GOME-2 are similar to those for GOME-1. However, the GOME-2 fitting residuals show larger along track variations than the GOME-1 fit residuals. This noisier behaviour can be attributed to the fact that GOME-2 measurements are limited by photon noise and not by undersampling effects. This means that GOME-2 NO_2 slant columns show reduced noise above bright scenes, such as produced by clouds.

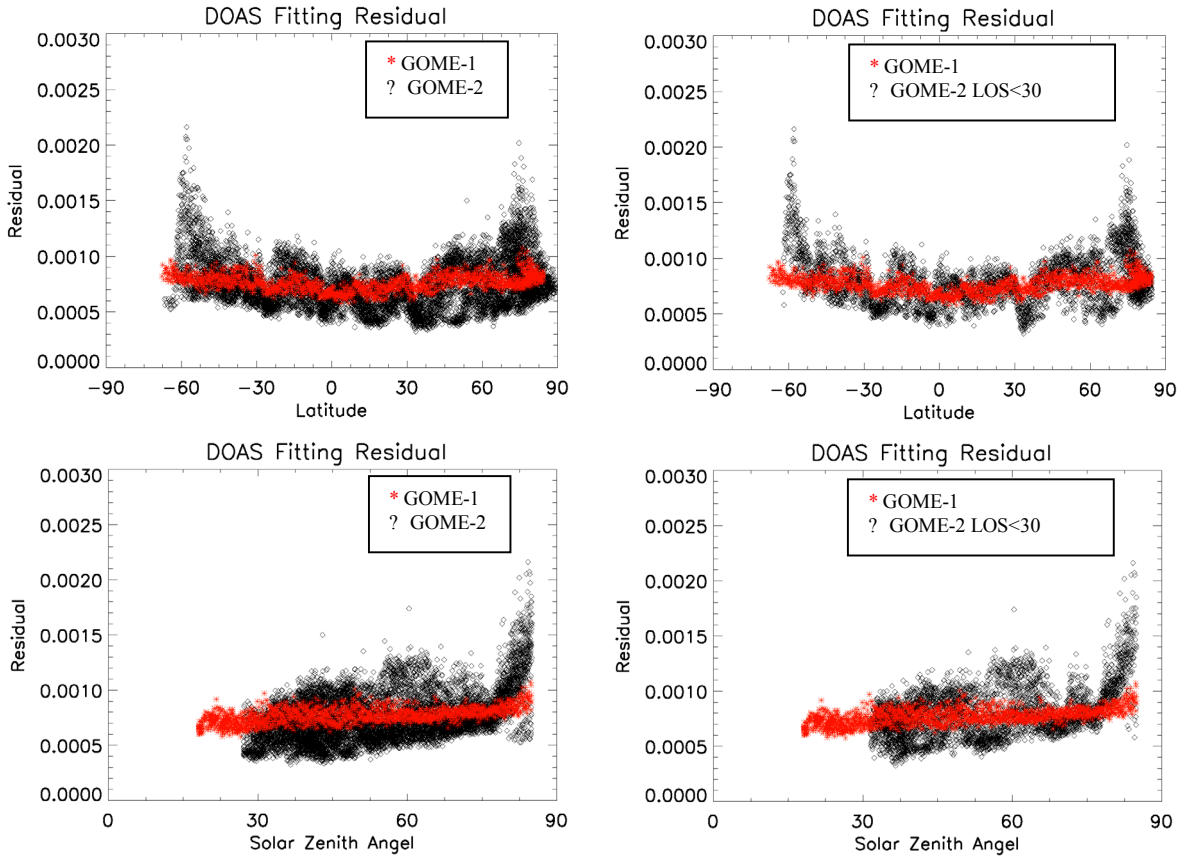

Figure 2.2.1 - DOAS fit residuals for the 425-445 nm NO_2 fitting window, as a function of the latitude (upper plots) and of the solar zenith angle (bottom plots). The residuals are shown for a single orbit of GOME-2 (August 20, 2008) and GOME-1 (August 20, 1998). For the pictures on the right hand side, only GOME-2 data within a line-of-sight angle < 30° have been selected, in order to consider a swath width reduced to (approximately) the GOME-1 swath width.

B.2.3 Time evolution of DOAS fit residuals and NO_2 slant column error

Figure 2.3.1 shows the evolution of the DOAS NO_2 slant column fit residual over the equatorial Pacific (10°S-10°N and 160-200°E), plotted as monthly averaged RMS values over the January 2007 – Dec 2010 time period. Changes in the average fit-residual over time are an indicator for possible degradation in the GOME-2 instrument (e.g. by contamination of the primary scan mirror or of the detectors). Changes in the level 0-to-1 processing could also have an impact on the fit residual – assuming the DOAS fit settings remain unchanged. As can be seen in Figure 2.3.1, the GOME-2 fit residual show a clear seasonal variation (especially in 2009 and 2010), and increases by about 10% per year. It is likely that the increase in the fit-residual is a result of the instrument degradation of the GOME-2 sensor in the visible wavelength range of Channel 3, as reported by Lang et al., 2009, and by Dikty et al., 2010.

The effect of the increase in the DOAS fit residual on the NO_2 slant column error has been determined with a statistical analysis of the GOME-2 measurements in the equatorial Pacific (20S-20N; 160-180E) (Valks et al., 2011). This region is divided into small boxes (2°×2°), and from the variation of the NO_2 columns within each box, an estimate of the slant column precision can be made. The analysis is based on the assumption that the variation in the total NO_2 columns in each box is a result of errors in the slant column only, originating from (random) instrument measurement noise. The deviation of each GOME-2 measurement from the corresponding box mean value is calculated on a daily basis. The slant column error is then derived

from the Gaussian-shaped distribution of the slant column deviations. Fig. 2.3.2 shows the estimated NO_2 slant column error for the GOME-2 instrument for the period January 2007 - December 2010. In the four years from the start of the operational GOME-2 measurements, the GOME-2 slant column error for NO_2 has increase from ~5.0×10^{14} molec/cm^2 in 2007 to ~6.5×10^{14} molec/cm^2 in 2010 (an increase of ~35%).

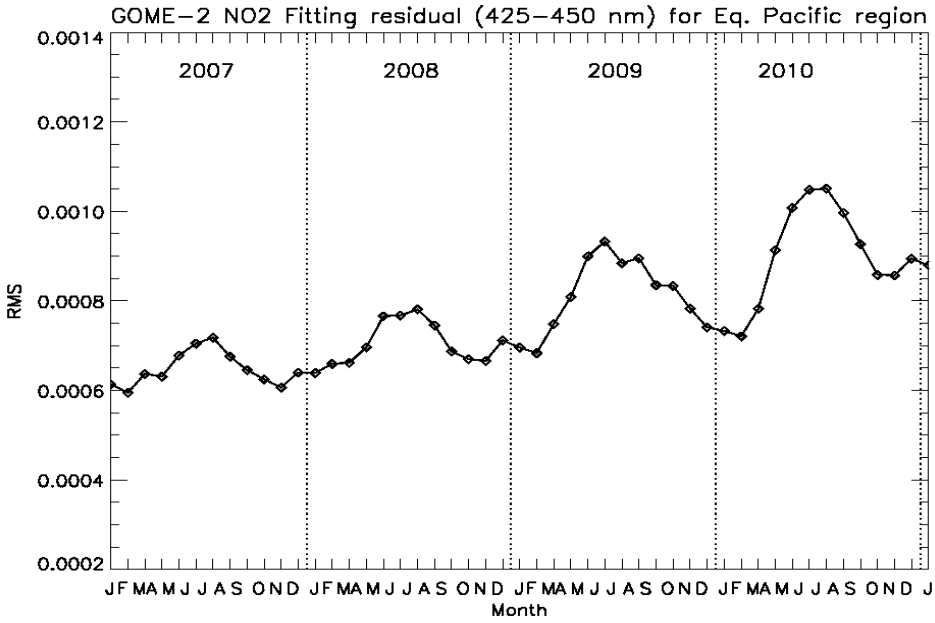

Figure 2.3.1 - Monthly averaged residual (RMS) of GOME-2 NO_2 slant column fits over the equatorial Pacific region from January 2007 to Dec 2010. Analyses are based on GOME-2 level1B-v4 (ir)radiance data.

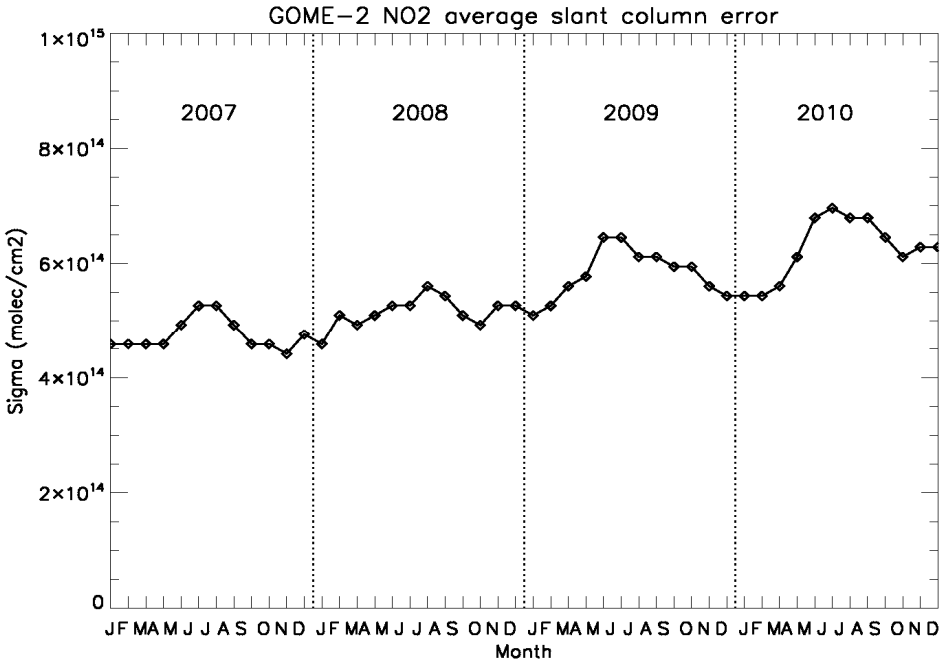

Figure 2.3.2 - Estimated NO_2 slant column error for GOME-2 instrument from January 2007 to December 2010.

B.2.4 Effect of NRT and off-line algorithm differences on tropospheric NO_2

The NRT and off-line tropospheric NO_2 retrievals differ slightly in the way the stratospheric NO_2 component is determined. As described in [TN-DLR-ATBD], this component is estimated using a spatial filtering which is applied on a global map of initial total NO_2 column data. The latter is constructed by binning 24 hours of GOME-2 data on a high resolution spatial grid. The NRT algorithm bins the GOME-2 data of the 24 hours before the actual measurement time, while the off-line algorithm bins the GOME-2 data of 12 hours before and after the actual measurement time (i.e. the off-line algorithm uses GOME-2 data of the "future").

As a consequence of these algorithm differences, the NRT and off-line tropospheric NO_2 column products are not identical. However, the day-to-day variability in the stratospheric NO_2 distribution is relatively small, and therefore the differences between the NRT and off-line tropospheric NO_2 column products also remain relatively small. This is illustrated in Figures 2.4.1 and 2.4.2 showing the GOME-2 tropospheric NO_2 distribution for August 2008 retrieved with the NRT and off-line algorithms, and the difference between the two. As can be seen from these figures, the monthly averaged difference between the NRT and off-line tropospheric NO_2 columns is mostly smaller than 1.10^{14} molec/cm^2. Such small differences can hardly be detected by means of comparisons with correlative measurements, since within the error bars of the latter.

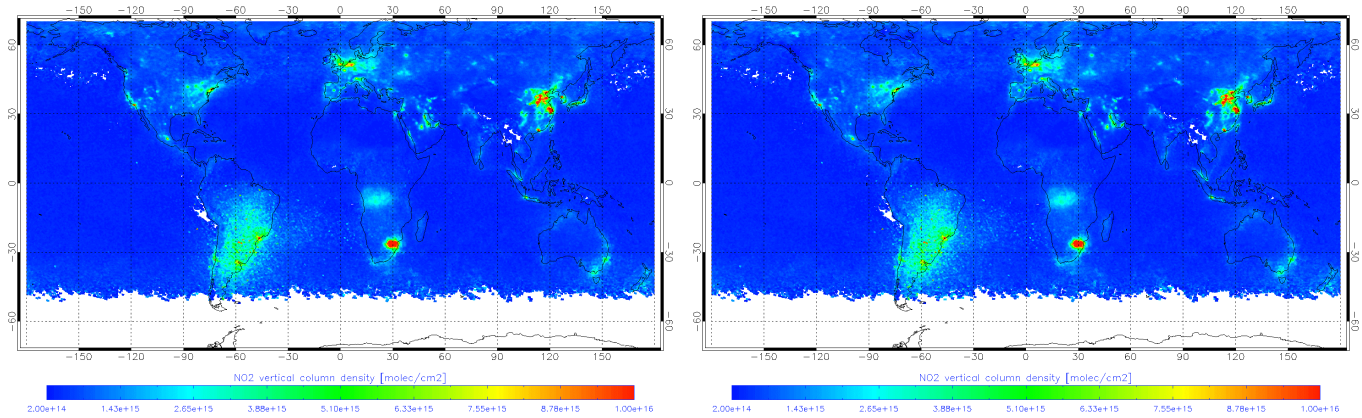

Figure 2.5.1 - GOME-2 tropospheric NO_2 distribution for August 2008 retrieved with the near-real time algorithm (left) and the off-line algorithm (right).

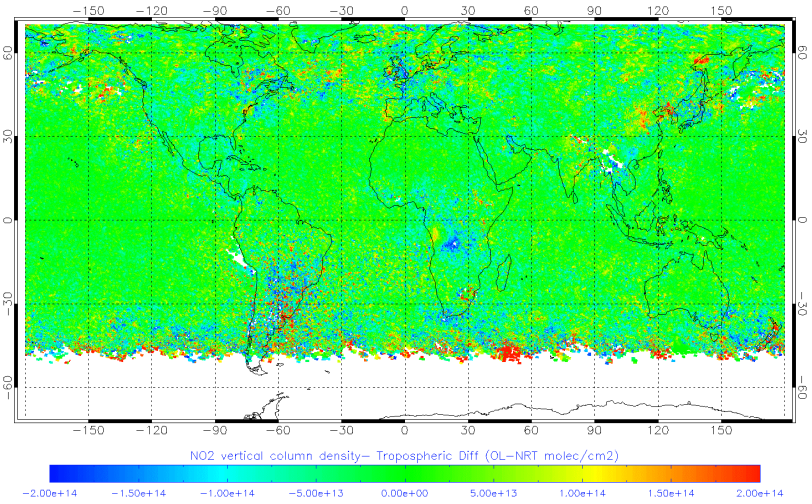

Figure 2.4.2 - Monthly averaged difference between the GOME-2 tropospheric NO_2 distributions of August 2008 retrieved with the near-real time and the off-line algorithms.

The differences between the NRT and off-line tropospheric columns for single GOME-2 measurements have been analysed for several polluted mid-latitude locations (note that the variability in the stratospheric NO_2 distribution usually is largest at middle and high latitudes). Figure 2.4.3 shows the correlation between the NRT and off-line tropospheric columns for Harestua, Bremen, OHP, Beijing and Lauder. As can been seen from this figure, the differences between the NRT and off-line tropospheric columns at these locations are generally smaller than 5.10^{14} molec/cm^2. Is should be noted that these differences are (much) smaller than the estimated total uncertainty in the GOME-2 tropospheric NO_2 column (see Table 3 in [TN-DLR-ATBD]).

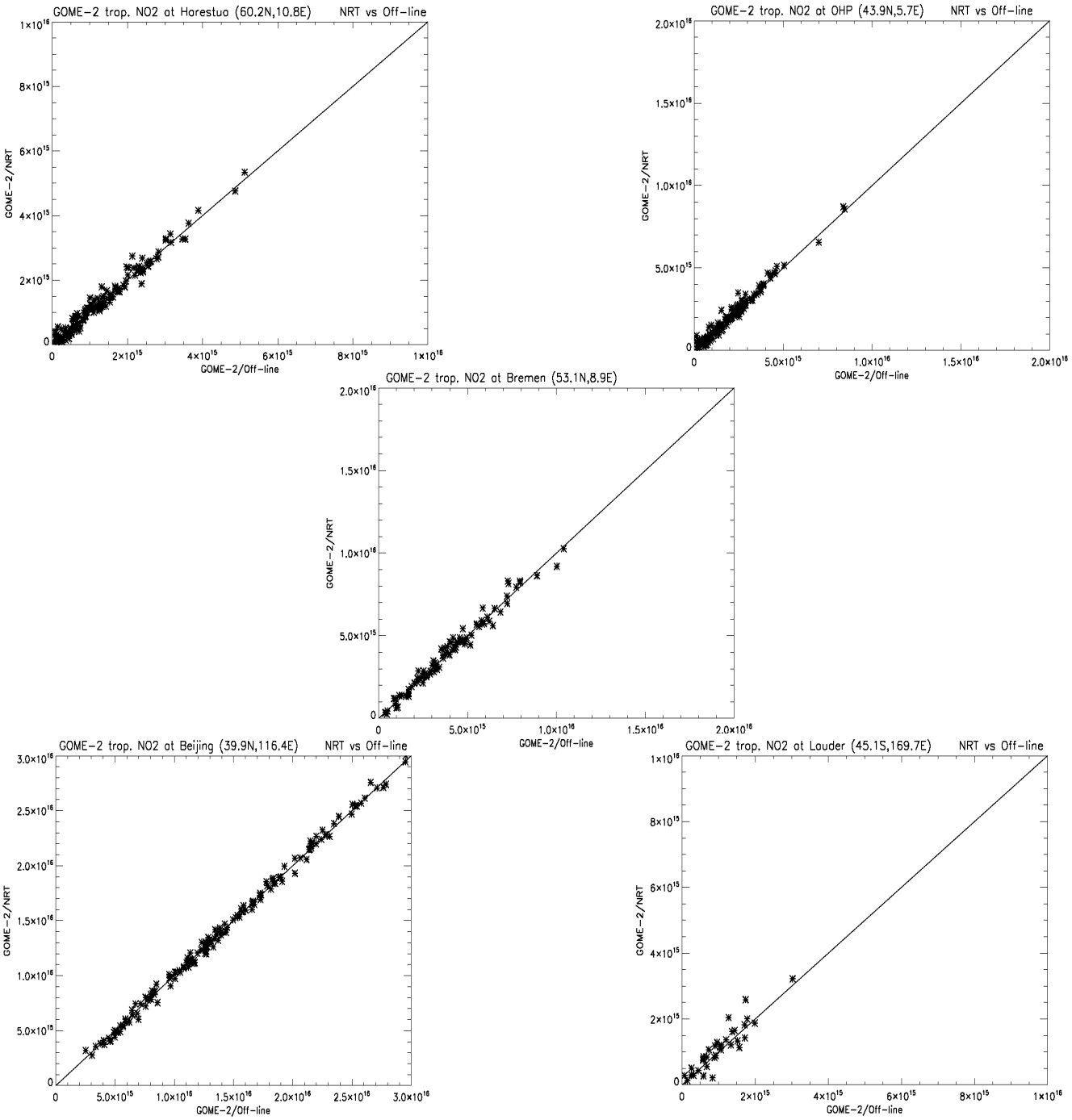

Figure 2.4.3 - Correlation between NRT and off-line NO_2 tropospheric columns from GOME-2 over May-June 2009, at five middle latitude sites experiencing pollution. Based on GOME-2 level-1B-v4 (ir)radiance data.

B.3 Validation of stratospheric vertical column density

Pole-to-pole validations of GDP 4.2 stratospheric/total columns had been conducted using stratospheric column measurements obtained by the NDACC UV-Vis network, and reported in VAL_ORR-A3_2008 and VAL_ORR-B_2008. The validation of GDP 4.2 NO_2 total column data had been performed as a check of the NO_2 total column in non-polluted regions, thus, where only stratospheric NO_2 contributes to the total column. Validations of GOME-1 (long-term, over a decade) and GOME-2 (March to June 2007) stratospheric NO_2 data had also been compared in VAL_INITIAL_2007, highlighting the importance of using a physically based method for the selection of overpass pixels (described in Lambert, 2005, and Balis *et al.*, 2007). The latter consists in estimating the optical path along which sunlight absorption by NO_2 occurs both for the UVVIS ground-based instruments and for the satellite, and comparing only data with a substantial overlap of the associated optical paths (also called "optical matching selection method").

Validations of GDP 4.2 data in VAL_ORR-A3_2008 and VAL_ORR-B_2008 had been presented according to observational conditions:

- Southern middle latitude stations, combining negligible tropospheric pollution, easy-to-handle diurnal cycle of stratospheric NO_2 (sunrise values relatively close to mid-morning values acquired by GOME-1), and sufficient SNR.
- Polar day, exhibiting a particular diurnal cycle sampled several times a day by GOME-1.
- Polar wintertime, with low NO_2 columns and SNR, and large relative variability at the vortex edge.
- Clean Northern middle latitude sites surrounded by large polluted areas.
- Equatorial stations, with low NO_2 columns observed under small SZA, which result in poor SNR, especially in the central Pacific Ocean.
- Tropical sites in the vicinity and far away from the South Atlantic Anomaly (SAA).

Comparison of GOME-2 and NDACC NO_2 columns in those conditions had been summarized as follows:

1. Over the period considered (2007-2008), correlative studies conclude to an excellent qualitative agreement of GOME-2, NDACC/UVVIS, GOME-1 and SCIAMACHY observations of the NO_2 field and of its temporal variations at scales from days to months.
2. GOME-2 GDP 4.2 reports systematically smaller NO_2 vertical column values than SCIAMACHY and than NDACC/UVVIS spectrometers in the Southern hemisphere. GOME-1 being in excellent agreement with NDACC/UVVIS observations, by transitivity, GOME-2 GDP 4.2 also reports systematically smaller values than GOME-1. The underestimation of these other global NO_2 data records is of the order of 4-6 10^{14} molec.cm^{-2}.
3. At a few stations, ground-based comparisons indicated possible time-dependent degradation of the agreement. Comparisons over one year show rather an annual cycle associated with the summertime activation of polar day photochemistry.

In this section we update validation studies of MetOp-A GOME-2 NO_2 data to versions 4.3/4.4 of GDP, and to cover four complete years, from January 2007 to December 2010. For an end-to-end component validation of the tropospheric NO_2 retrieval process, validation of stratospheric columns even over usually polluted stations is necessary. In those cases, direct comparisons of GOME-2 and NDACC NO_2 total column data are hampered by their difference in sensitivity to tropospheric NO_2 (the nadir-viewing geometry of GOME-2 is much more sensitive to tropospheric NO_2 than the zenith-sky viewing geometry of NDACC/UVVIS spectrometers), which content can vary significantly at scales of a few ten kilometres and a few hours. Hereafter a simple method enabling stratospheric validation at polluted stations is proposed. Other validation methods and principles remain the same as those described in previous validation reports.

B.3.1 Summary table of stratospheric validations over NDACC sites

The geographical distribution of NDACC/UVVIS stations which have contributed twilight measurements of the NO_2 total column, is displayed in Figure 3.1.1. Table 3.1 lists the contributing instruments and presents a summary of the comparison results. Results are discussed in the following subsections.

Table 3.1 – Statistical summary of absolute differences in NO_2 total column data between GOME-2 GDP 4.3/4.4 and contributing NDACC/UVVIS stations: range of monthly median difference, global median difference, and standard deviation (all in 10^{14} molecule/cm^2)

Station	Location	Institute	Latitude	Longitude	Range of monthly mean difference	Global mean difference	Global standard deviation
Ny-Ålesund	Spitsbergen	IUP/U.Bremen	78.91° N	11.93° E	-5 / +5	-1	4
Thule	Greenland	DMI	76.51° N	68.76° W	+1 / +6	+4	3
Scoresbysund	Greenland	CNRS/DMI	70.48° N	21.97° W	+4 / +5	-2	3
Kiruna	Sweden	NIWA	67.84° N	21.06° E	-5 / +4	0	3
Sodankylä	Finland	CNRS/FMI	67.37° N	26.67° E	-5 / +3	-3	4
Zhigansk	Eastern Siberia	CNRS/CAO	66.72° N	123.40° E	-3 / +1	-1	2
Harestua	Norway	BIRA-IASB	60.22° N	10.75° E	-3 / +9	+2	6
Bremen	Germany	IUP/UBremen	53.11° N	8.86° E	-7 / +9	+3	8
Jungfraujoch	Switzerland	BIRA-IASB	46.55° N	7.98° E	+3 / +10	+5	5
Moshiri	Japan	STEL/U.Tokyo	44.40° N	142.30° E	-3 / +3	-2	4
OHP	France	CNRS/LATMOS	43.94° N	5.71° E	-6 / +1	-3	5
Issyk-Kul	Kyrgyzstan	KSNU	42.63° N	76.98° E	-8 / +2	-1	5
Izaña	Tenerife	INTA	28.29°N	16.49° W	-7 / 0	-3	4
Mauna Loa	Hawaii	NIWA	19.54° N	155.58° W	-10 / -3	-7	3
Mérida	Venezuela	IUP/U.Bremen	8.60° N	71.14° W	-3 / +3	-1	3
Saint Denis	Reunion Isl.	CNRS/U.Reunion	21.07° S	55.48° E	-7 / 0	-3	3
Bauru	Brazil	CNRS/UNESP	22.35° S	49.03° W	-1 / +3	-5	9
Lauder	New Zealand	NIWA	45.03° N	169.68° E	-14 / -3	-7	4
Kerguelen	Indian Ocean	CNRS	49.36° S	70.26° E	-10 / -5	-7	3
Macquarie	Australia	NIWA	54.50° S	158.96° E	-19 / -5	-10	5
Marambio	Antarctica	INTA	64.23° S	56.72° W	-6 / +3	-3	5
Dumont d'Urville	Antarctica	CNRS	66.67° S	140.00° E	-5 / +2	-3	3
Rothera	Antarctica	BAS-NERC	67.57° S	68.13° W	-6 / -1	-4	3
Arrival Heights	Antarctica	NIWA	77.82° S	166.66° E	-5 / +2	-2	2
Belgrano	Antarctica	INTA	77.87° S	34.63° W	-6 / 0	-4	3

Note: at polar stations, data have not been considered where it is obvious that residual diurnal cycle effects degrade the accuracy of the validation method.

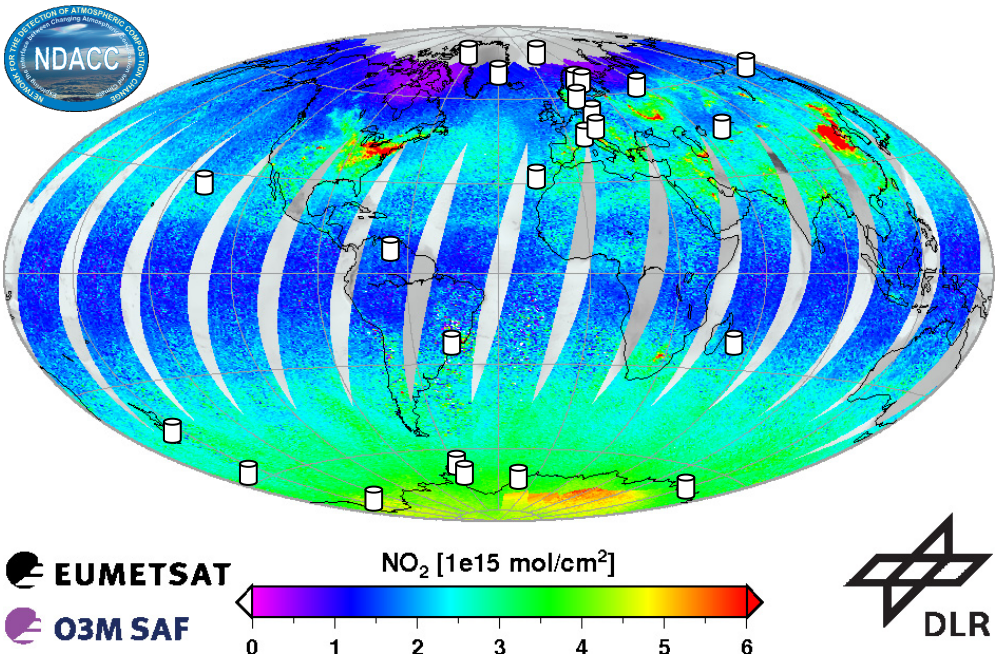

Figure 3.1.1. Geographical distribution of NDACC UVVIS spectrometers measuring the NO_2 total column at twilight, and used in this GOME-2 validation study. Stations are displayed on top of the global NO_2 field measured by GOME-2 on February 10, 2011.

B.3.2 Validation of stratospheric NO_2 column over unpolluted areas

At most **Southern Hemisphere middle latitude stations**, the NO_2 total column is predominantly in the stratosphere. As a result, GOME-2 vertical weighting functions resemble those of the zenith-sky UVVIS observations, enabling direct comparisons between GOME-2 and UVVIS data from the perspective of information content. The diurnal cycle of stratospheric NO_2 at those latitudes is well understood. Modelling studies carried out at IASB-BIRA in collaboration with U. Leeds (Lambert *et al.*, 2002, 2003) indicate that values measured at sunrise, that is, by UVVIS instruments, might be reasonably close – within a few 10^{14} molecule.cm^{-2} – to values measured in the mid-morning by GOME-2. GOME-2 data have been selected spatially using the optical matching method demonstrated for GOME-1 in VAL_INITIAL_2007.

Figure 3.1.2. shows that, at the NDACC station of Kerguelen in the Indian Ocean, GOME-2 GDP 4.3/4.4 and the SAOZ UVVIS instrument capture similarly NO_2 column variations at scales from seasons to days. The good qualitative agreement is particularly remarkable during high variability events like in October 2009.

Quantitatively, GOME-2 GDP 4.3/4.4 underestimates UVVIS values by a systematic negative offset of -0.6 to -0.9 10^{15} molec.cm^{-2}. This negative offset is relatively stable with time, except in November and December 2010 when it seems to increase by a few 10^{14} molec.cm^{-2} with respect to the 2007-2010 mean offset. It is necessary to continue the monitoring of GOME-2 data to check whether this apparent degradation will progress, remain stable, or disappear. Comparisons with the NIWA UVVIS system at the NDACC station of Lauder in New Zealand (45°S), depicted in Figure 3.1.3., also conclude to a systematic offset. But there is an annual cycle superimpose on the permanent offset, which might be related to a difference in the cross-sections used in the DOAS retrieval. As expected, the transition from GDP 4.3 to GDP 4.4 in March 2010 does not introduce any additional offset, any increase of noise or any other feature in the time series.

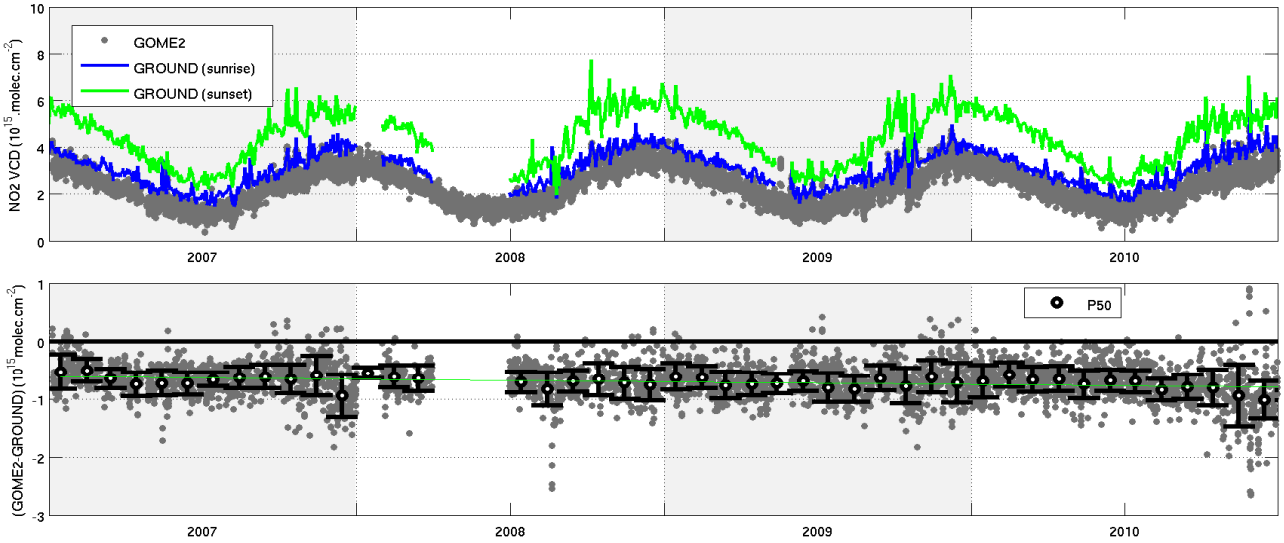

GOME2 OFL $GDP_{43a}nd_{44}$
Source: GOME2 OFL $GDP_{43a}nd_{44}$ NO2 VCD
9879 pixels in 1426 days (05/01/2007 - 12/02/2011)

UVVIS (Source: calval)
Source: calval
2893 values in 1460 days (19/07/2006 - 31/12/2010)

Method: zovp pixels vs. Twilights
Global agreement: -0.7 ± 0.3 (10^{15}mol.cm^{-2})
Linear drift: -0.05*t - 0.59 (10^{15}mol.cm^{-2}/year) , ψ = 0.244

	JAN	FEB	MAR	APR	MAY	JUN	JUL	AUG	SEP	OCT	NOV	DEC
2007	-0.5 ± 0.3	-0.5 ± 0.2	-0.6 ± 0.2	-0.7 ± 0.2	-0.7 ± 0.2	-0.7 ± 0.2	-0.7 ± 0.1	-0.6 ± 0.2	-0.6 ± 0.2	-0.7 ± 0.3	-0.6 ± 0.3	-0.9 ± 0.4
2008	-0.6 ± 0.1	-0.6 ± 0.2	-0.6 ± 0.2	-	-	-	-0.7 ± 0.2	-0.8 ± 0.3	-0.7 ± 0.2	-0.7 ± 0.3	-0.7 ± 0.3	-0.8 ± 0.3
2009	-0.6 ± 0.2	-0.6 ± 0.2	-0.8 ± 0.2	-0.7 ± 0.2	-0.7 ± 0.2	-0.7 ± 0.2	-0.8 ± 0.2	-0.8 ± 0.2	-0.6 ± 0.2	-0.8 ± 0.3	-0.6 ± 0.3	-0.7 ± 0.3
2010	-0.7 ± 0.3	-0.6 ± 0.2	-0.7 ± 0.2	-0.7 ± 0.2	-0.7 ± 0.2	-0.7 ± 0.2	-0.7 ± 0.2	-0.8 ± 0.2	-0.8 ± 0.2	-0.8 ± 0.3	-0.9 ± 0.5	-1.0 ± 0.3

Figure 3.1.2. Top: Total NO_2 VCD at the NDACC station of the Kerguelen Archipelago (Indian Ocean, 49°S), as measured by GOME-2 (GDP 4.3/4.4) and by the SAOZ UVVIS spectrometer operated by CNRS/LATMOS in 2007-2010. Bottom plot + table: absolute difference between GOME-2 and SAOZ UVVIS. Monthly medians (P50) and corresponding 68% interpercentile (error bars) are based on cloudy GOME-2 data and sunrise SAOZ data only.

To better understand the origin of the permanent offset between GOME-2 and ground-based data at Southern middle latitude stations, the same ground-based comparisons have been carried out with ERS-2 GOME NO_2 column data, processed operationally with the offline processor GDP 4.1. Such a comparison is illustrated in Figure 3.1.4., covering the GOME mission from 1995 till June 2003, when the failure of the onboard tape recorder started limiting the transmission of GOME data to those acquired in the vicinity of ground antennas. Figure 3.1.4. shows that no offset exists between ERS-2 GOME GDP 4.1 and NDACC/UVVIS data at Kerguelen. Moreover, the agreement remains stable within a few 10^{14} molec.cm^{-2} over the entire 1995-2003 period.

The offset between GOME-2 and the NDACC UVVIS spectrometer at Kerguelen does not seem to depend neither on the solar zenith angle, nor on the season, nor on the sub pixel index, as shown in Figure 3.1.5. The year-round stability with solar local time is an indicator that, at least at this station, the comparison method deals appropriately with diurnal cycle effects, and that the latter are probably not the cause of the permanent negative offset at this station. The independence on the sub pixel index, that is, on the off-nadir scan angle, is another element that vindicates the correctness of the diurnal cycle treatment: while there is a photochemical difference between pixels distant by 1920 km in longitude (the GOME-2 swath width), validation results for the two extreme positions (the most Eastern and Western pixels, respectively) do not differ statistically by more than 10^{14} molec.cm^{-2}.

In Figure 3.1.6. the negative offset at Kerguelen is shown to increase smoothly with the fractional cloud cover (CF), but not with the cloud top pressure (nor on the cloud top height, not shown here). Figure 3.1.7. indicates that the offset might vary also with the cloud top albedo (CTA) and the cloud optical thickness (COT), but it is hard to determine from this figure what the driving parameter is: CF, CTA or COT.

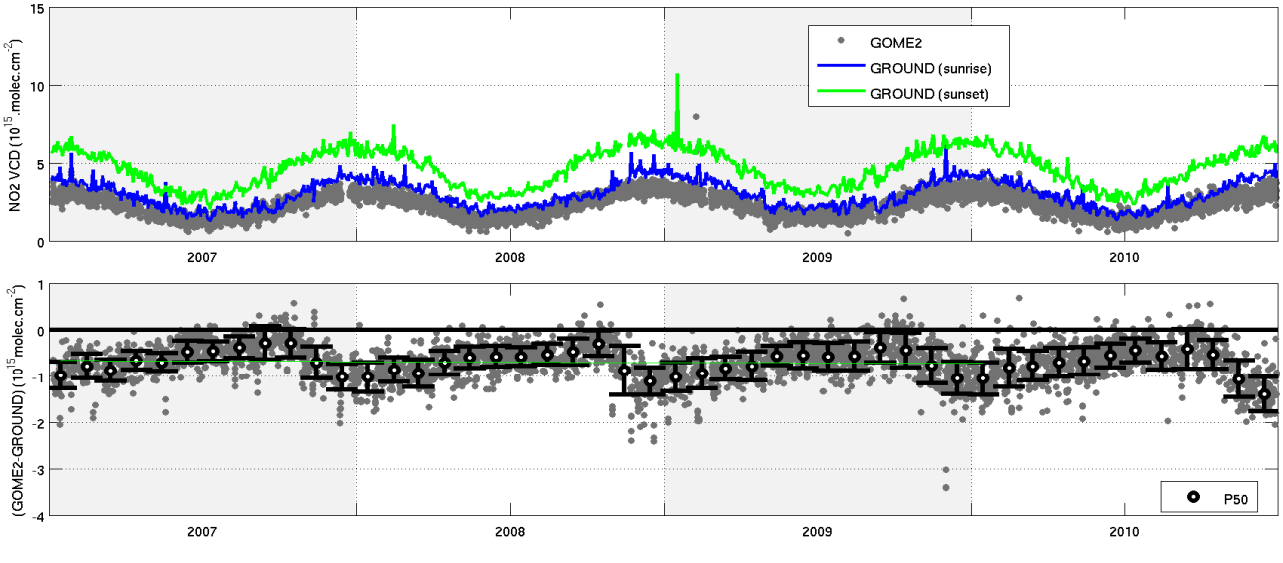

GOME2 OFL $GDP_{43a}nd_{44}$	UVVIS (Source: NDACC)	Method: zovp pixels vs. Twilights
Source: GOME2 OFL $GDP_{43a}nd_{44}$ NO2 VCD	Source: NDACC	Global agreement: -0.7 ± 0.4 (10^{15}mol.cm^{-2})
8037 pixels in 1430 days (04/01/2007 - 07/02/2011)	3163 values in 1590 days (19/07/2006 - 31/12/2010)	Linear drift: -0.02*t - 0.66 (10^{15}mol.cm^{-2}/year) , ϕ = 0.684

	JAN	FEB	MAR	APR	MAY	JUN	JUL	AUG	SEP	OCT	NOV	DEC
2007	-1.0 ± 0.3	-0.8 ± 0.3	-0.9 ± 0.2	-0.7 ± 0.2	-0.7 ± 0.2	-0.5 ± 0.2	-0.5 ± 0.2	-0.4 ± 0.2	-0.3 ± 0.4	-0.3 ± 0.3	-0.7 ± 0.3	-1.0 ± 0.3
2008	-1.0 ± 0.3	-0.9 ± 0.3	-0.9 ± 0.3	-0.7 ± 0.3	-0.6 ± 0.2	-0.6 ± 0.2	-0.6 ± 0.2	-0.5 ± 0.2	-0.5 ± 0.3	-0.3 ± 0.3	-0.9 ± 0.5	-1.1 ± 0.3
2009	-1.0 ± 0.3	-0.9 ± 0.3	-0.8 ± 0.2	-0.8 ± 0.3	-0.6 ± 0.2	-0.6 ± 0.3	-0.6 ± 0.3	-0.6 ± 0.3	-0.4 ± 0.3	-0.4 ± 0.4	-0.8 ± 0.4	-1.0 ± 0.4
2010	-1.1 ± 0.4	-0.8 ± 0.4	-0.8 ± 0.3	-0.7 ± 0.3	-0.7 ± 0.3	-0.6 ± 0.3	-0.5 ± 0.3	-0.6 ± 0.3	-0.4 ± 0.4	-0.5 ± 0.3	-1.1 ± 0.4	-1.4 ± 0.4

Figure 3.1.3. Same as **Figure 3.1.2.** but over the NDACC station of Lauder (New Zealand, 45°S), measured by GOME-2 (GDP 4.3/4.4) and by the UVVIS spectrometer operated by NIWA.

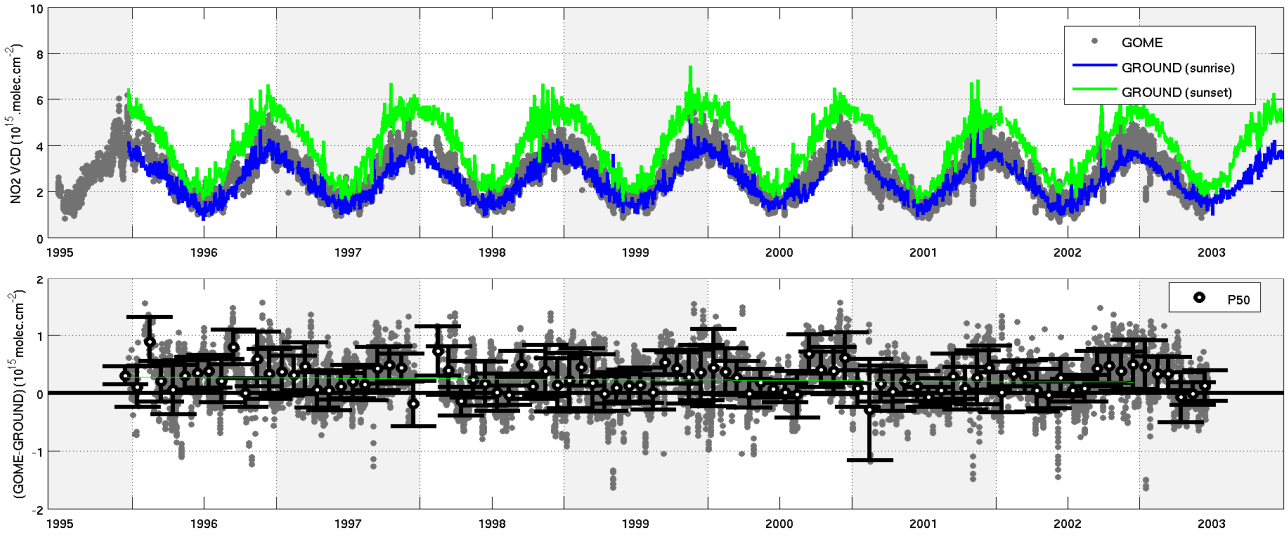

GOME OFL GDP 4.1	UVVIS (Source: NDACC)	Method: zovp pixels vs. Twilights
Source: GOME OFL GDP 4.1 O3 VCD	Source: NDACC	Global agreement: 0.2 ± 0.4 (10^{15}mol.cm^{-2})
18898 pixels in 2502 days (28/06/1995 - 22/06/2003)	8551 values in 4326 days (22/12/1995 - 31/12/2007)	Linear drift: -0.01*t + 0.29 (10^{15}mol.cm^{-2}/year) , ϕ = -0.007

	JAN	FEB	MAR	APR	MAY	JUN	JUL	AUG	SEP	OCT	NOV	DEC
1995	-	-	-	-	-	-	-	-	-	-	-	0.3 ± 0.2
1996	0.1 ± 0.3	0.9 ± 0.4	0.2 ± 0.4	0.1 ± 0.4	0.3 ± 0.3	0.3 ± 0.3	0.4 ± 0.3	0.2 ± 0.4	0.8 ± 0.3	0.0 ± 0.2	0.6 ± 0.5	0.3 ± 0.4
1997	0.4 ± 0.4	0.3 ± 0.3	0.5 ± 0.4	0.1 ± 0.3	0.0 ± 0.3	0.1 ± 0.2	0.2 ± 0.3	0.2 ± 0.3	0.4 ± 0.4	0.5 ± 0.3	0.4 ± 0.2	-0.2 ± 0.4
1998	-	0.7 ± 0.4	0.4 ± 0.4	-0.1 ± 0.3	0.2 ± 0.3	0.2 ± 0.4	0.0 ± 0.3	-0.0 ± 0.2	0.5 ± 0.2	0.1 ± 0.2	0.4 ± 0.4	0.1 ± 0.5
1999	0.2 ± 0.5	0.5 ± 0.3	0.2 ± 0.5	-0.0 ± 0.3	0.1 ± 0.3	0.1 ± 0.3	0.1 ± 0.3	0.0 ± 0.3	0.5 ± 0.2	0.4 ± 0.3	0.3 ± 0.5	0.4 ± 0.5
2000	0.4 ± 0.7	0.4 ± 0.4	0.3 ± 0.3	-0.0 ± 0.3	0.2 ± 0.2	0.1 ± 0.2	0.0 ± 0.2	-0.0 ± 0.4	0.7 ± 0.3	0.4 ± 0.3	0.4 ± 0.4	0.6 ± 0.4
2001	0.1 ± 0.3	-0.3 ± 0.9	0.2 ± 0.3	0.0 ± 0.3	0.2 ± 0.2	0.1 ± 0.3	-0.1 ± 0.2	0.0 ± 0.2	0.3 ± 0.4	0.1 ± 0.4	0.3 ± 0.5	0.4 ± 0.4
2002	0.0 ± 0.3	0.3 ± 0.2	0.3 ± 0.3	0.0 ± 0.4	-0.0 ± 0.2	0.3 ± 0.3	0.0 ± 0.2	0.1 ± 0.2	0.4 ± 0.3	0.5 ± 0.3	0.4 ± 0.3	0.5 ± 0.4
2003	0.5 ± 0.5	0.3 ± 0.3	0.3 ± 0.3	-0.1 ± 0.4	-0.0 ± 0.2	0.1 ± 0.3	-	-	-	-	-	-

Figure 3.1.4. Same as **Figure 3.1.2.** but here the SAOZ UVVIS NO_2 column data measured at Kerguelen are compared to ERS-2 GOME-1 NO_2 column data over 1995-2003 processed with the offline GDP version 4.1.

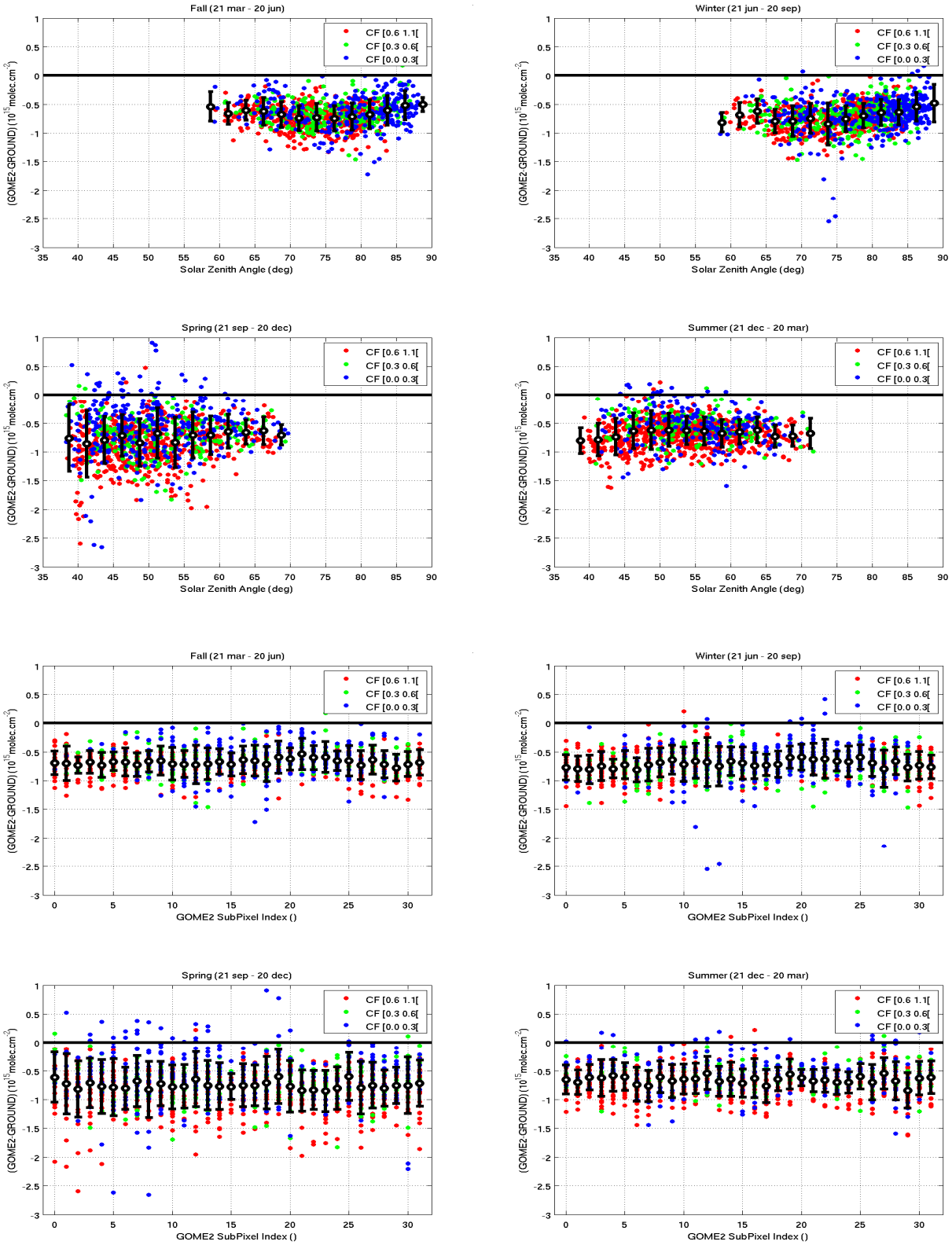

Figure 3.1.5. - Absolute difference between GOME-2 GDP 4.3/4.4 and NDACC UVVIS NO_2 vertical column at Kerguelen, represented as a function of the GOME-2 solar zenith angle (four upper plates), the GOME-2 sub pixel index (four lower plates) from East (0) to West (32), and the season (Fall-Winter-Spring-Summer sequence). The colour code represents the class of fractional cloud cover (CF).

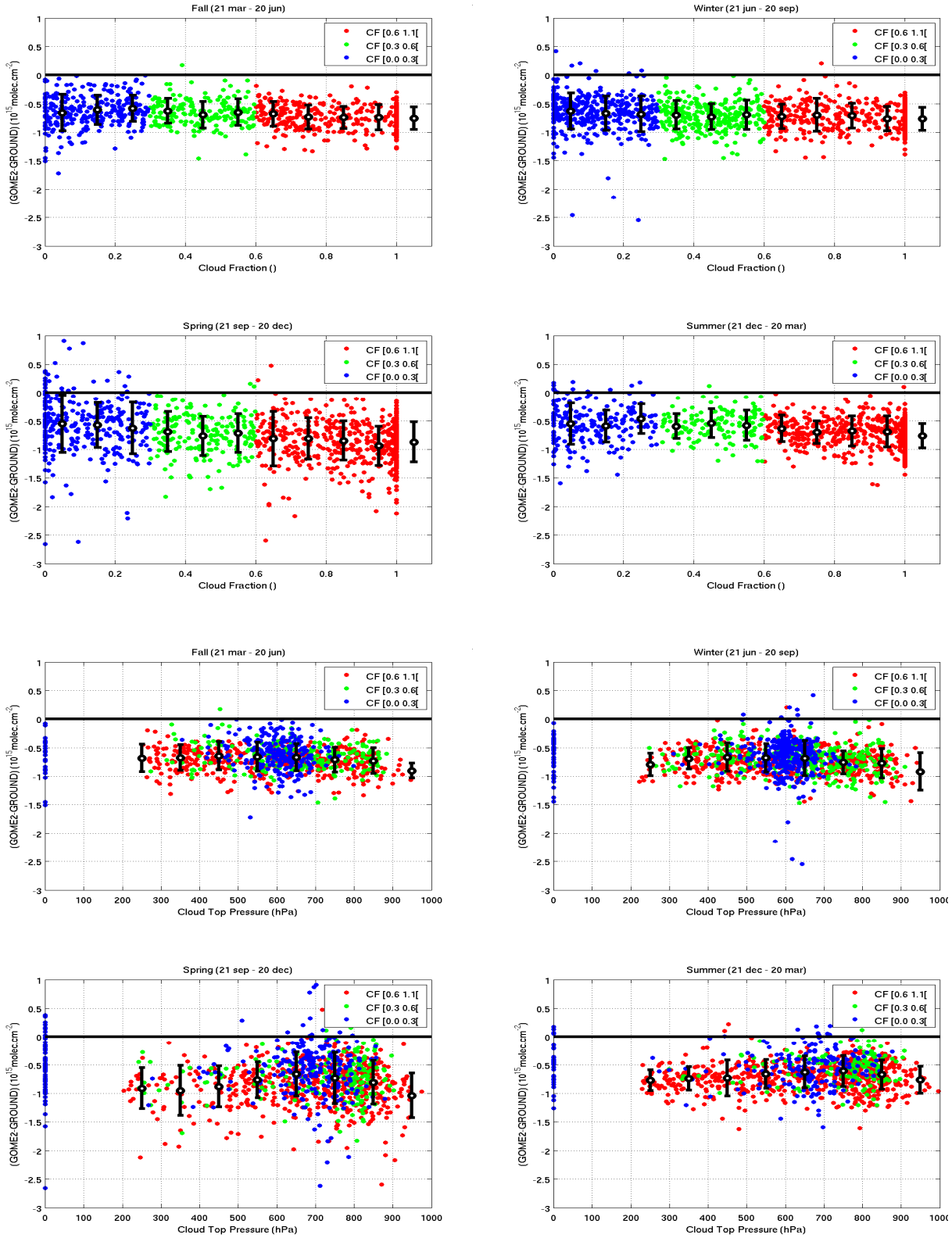

Figure 3.1.6. - Same as **Figure 3.1.5.**, but as a function of the GOME-2 fractional cloud cover (CF, four upper plates, and also colour code), the GOME-2 cloud top pressure (CTP, four lower plates), and the season (Fall-Winter-Spring-Summer sequence).

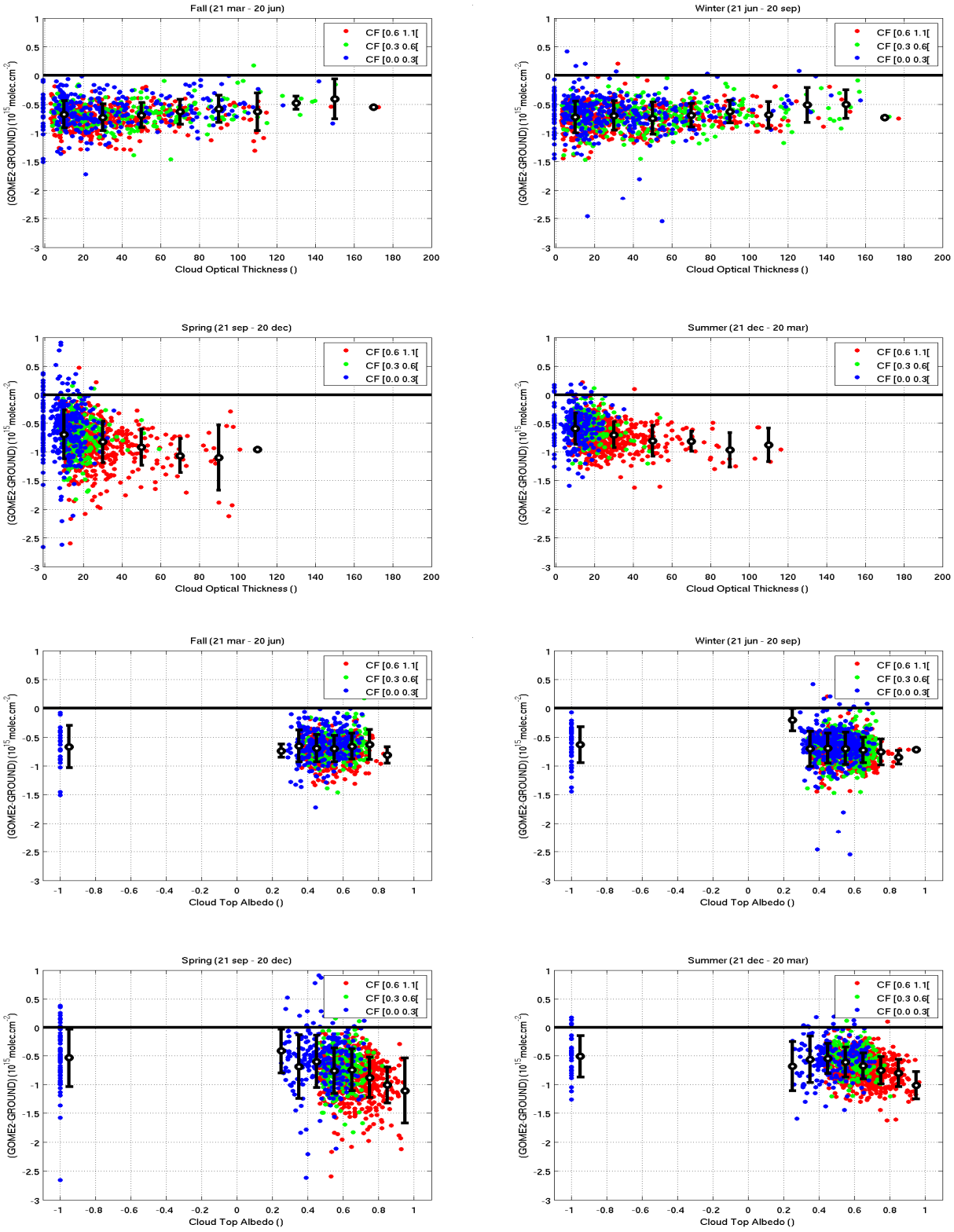

Figure 3.1.7. - Same as **Figure 3.1.5.**, but as a function of the GOME-2 cloud optical thickness (COT, four upper plates) and the GOME-2 cloud top albedo (CTA, four lower plates).

Arctic and Antarctic stations: Comparisons with ground-based UVVIS data of GOME-2 GDP 4.3/4.4 NO_2 column data at high latitudes are illustrated in Figure 3.1.8. and Figure 3.1.9. at NDACC Arctic stations, and in Figure 3.1.10. to Figure 3.1.11. at NDACC Antarctic stations. Compared to the format of Figure 3.1.2., which holds for low and middle latitudes, figures at polar stations include an additional curve, in red: the sunrise UVVIS observations adjusted to the 10:00 mean solar local time. Adjusted data ("adjSR" in the graphs and tables) are those used for the calculation of absolute differences between GOME-2 and UVVIS observations. The photochemical adjustment is calculated with the IASB-BIRA stacked box photochemical model PSCBOX (Errera and Fonteyn, 2000) initialised with 3D-CTM SLIMCAT output (Chipperfield, 1999). The photochemical model has been validated through intercomparison exercises with other existing models (Hendrick et al., 2000, 2006). The comparison method has been used successfully for GOME-1 long-term validation and for SCIAMACHY validation (see e.g. VAL_INITIAL_2007).

Like at Southern middle latitudes, GOME-2 and UVVIS instruments capture similarly seasonal, monthly and day-to-day changes in total NO_2 in polar areas. Quantitatively, the comparison at the Arctic site of Ny-Ålesund (Figure 3.1.8.) shows a good agreement of a few 10^{14} molec.cm^{-2} in March-April, comparable to the agreement of 2 10^{14} molec.cm^{-2} observed with GOME-1 (VAL_INITIAL_2007) and to the bias estimate of the ground-based data. In August and September the agreement is within ±5 10^{14} molec.cm^{-2}, with a larger variability from year to year. The scatter of absolute differences varies from 2 to 4 10^{14} molec.cm^{-2} from one year to another; however, since a similar increase can be noticed in the sunrise-to-sunset difference reported by the UVVIS instrument, it is reasonable to attribute year-to-year variations of the agreement mainly to atmospheric effects rather than to an increase of the GOME-2 errors.

Comparisons at stations located around the **Arctic polar circle**, like Sodankylä in Finland (Figure 3.1.9.), show no long-term degradation of the agreement with time, but rather an annual cycle and year-to-year variability of this agreement. Part of this annual and inter-annual variability might be explained by remaining uncertainties in our treatment of the diurnal cycle during polar day. The photochemical adjustment is calculated for a nadir-viewing satellite. This simplification works pretty well for instruments with a 960-km swath width like GOME-1 and SCIAMACHY, for which the off-nadir scan angle remains moderate, but it does not take into account properly the large solar local time variations along the measured optical path in the GOME-2 case of wide off-nadir scan angles (up to approximately 56.6° for the nominal swath width of 1920 km). Not significant at low latitudes, the effect reaches a maximum in polar areas where both the direct (incoming sunlight) and scattered parts of the GOME-2 optical path cross a large range of solar zenith angle.

Figure 3.1.10. and Figure 3.1.11. show comparison of GOME-2 NO_2 column data with NDACC UVVIS data at the **Antarctic stations** of Arrival Heights and Rothera, respectively. The first GOME-2 data recorded at the end of the polar night (August at Rothera and September at Arrival Heights), in the denoxified polar vortex, agree to within ±2 10^{14} molec.cm^{-2} with ground-based measurements at the two stations. Note that this really good agreement would exceed 100% if expressed in percentage relative difference, which justifies the use of absolute differences. A small negative offset of about -0.4 to -0.6 10^{14} molec.cm^{-2} can be observed in March and April, thus in fall. In summer, around the Antarctic polar circle, several tracks of GOME-2 total NO_2 data appear in the time series. They reflect the different daily overpasses of the sites by GOME-2, each with a different solar local time. Around summer solstice, one of the GOME-2 tracks is close to the unadjusted UVVIS measurements, suggesting that the GOME-2 optical path crosses mainly twilight air masses measured under midnight sun. Comparisons of such data conclude to a good agreement of a few 10^{14} molec.cm^{-2}. Other tracks are closer to the adjusted sunrise observations, suggesting that these tracks are based on GOME-2 data acquired in the mid-morning. As in the Arctic, the large scatter of the GOME-2 data around the mean tracks is likely due to the wide off-nadir scan angles which, at high latitudes, make the GOME-2 optical path crosses a wide range of local solar time. Figure 3.1.11. also shows that most of GOME-2 NO_2 column data at solstice range within the realistic interval of 4 to 6 10^{15} molec.cm^{-2}, predicted by photochemical models.

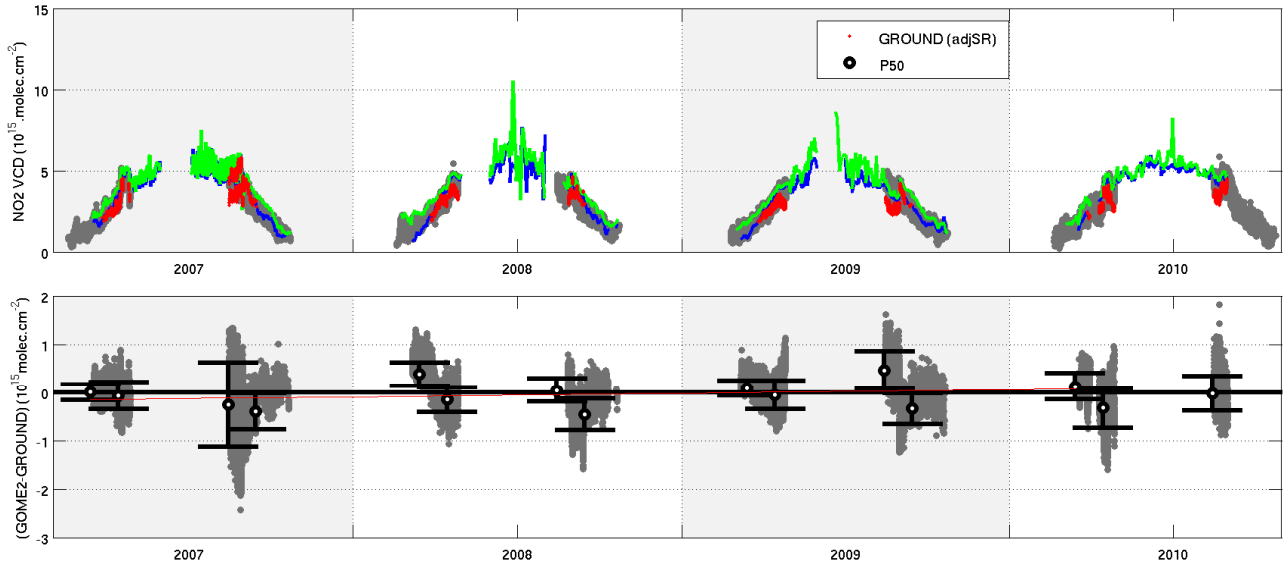

GOME2 OFL GDP 4.3.and.4.4	UVVIS (Source: calval)	Method: zovp pixels vs. Twilights (photochem. corrected)
Source: GOME2 OFL GDP 4.3.and.4.4 NO2 VCD	Source: calval	Global agreement: -0.1 ± 0.4 (10^{15}mol.cm^{-2})
78565 pixels in 522 days (18/02/2007 - 24/10/2010)	1387 values in 703 days (17/03/2007 - 31/08/2010)	Linear drift: 0.08*t - 0.17 (10^{15}mol.cm^{-2}/year) , rp = 0.261

	JAN	FEB	MAR	APR	MAY	JUN	JUL	AUG	SEP	OCT	NOV	DEC
2007	-	-	0.0 ± 0.2	-0.1 ± 0.3	-	-	-	-0.3 ± 0.9	-0.4 ± 0.4	-	-	-
2008	-	-	0.4 ± 0.2	-0.2 ± 0.3	-	-	-	0.0 ± 0.2	-0.5 ± 0.3	-	-	-
2009	-	-	0.1 ± 0.2	-0.1 ± 0.3	-	-	-	0.5 ± 0.4	-0.3 ± 0.3	-	-	-
2010	-	-	0.1 ± 0.3	-0.3 ± 0.4	-	-	-	-0.0 ± 0.4	-	-	-	-

Figure 3.1.8. - Same as **Figure 3.1.2.**, but at the NDACC Arctic station of Ny-Ålesund (Spitsbergen, 78°N) with the UVVIS instrument operated by IUP/U. Bremen. Absolute differences are calculated using ground-based UVVIS data adjusted with a photochemical box model to the local solar time of the GOME-2 measurement ('adjSR' in red).

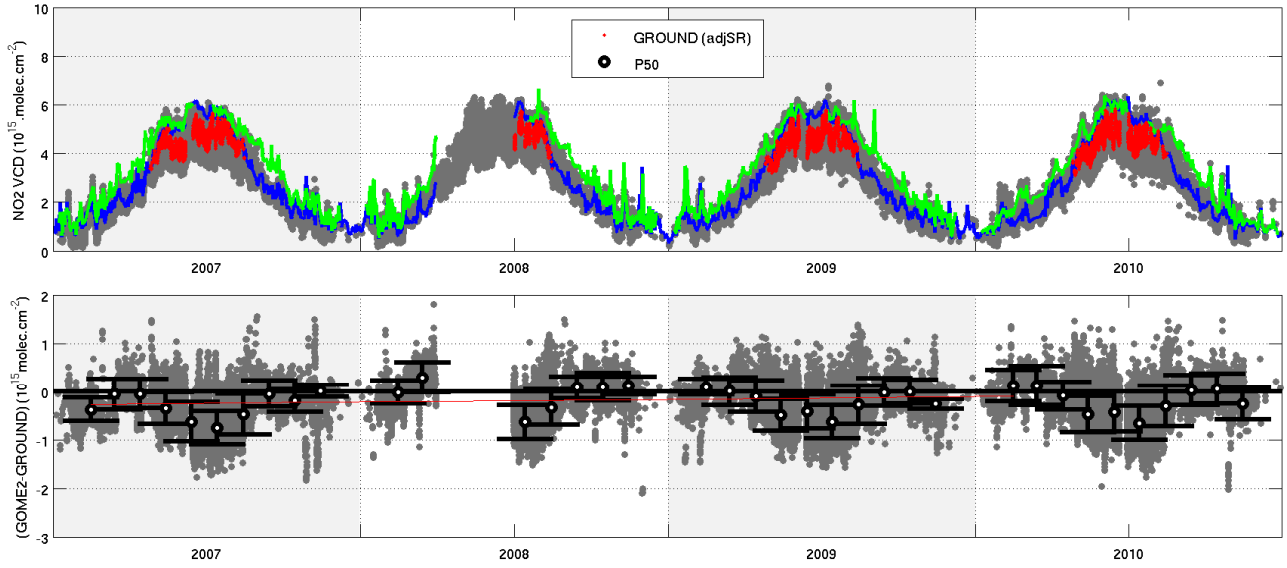

GOME2 OFL GDP 4.3.and.4.4	UVVIS (Source: calval)	Method: zovp pixels vs. Twilights (photochem. corrected)
Source: GOME2 OFL GDP 4.3.and.4.4 NO2 VCD	Source: calval	Global agreement: -0.3 ± 0.4 (10^{15}mol.cm^{-2})
76011 pixels in 1353 days (05/01/2007 - 07/02/2011)	2426 values in 1335 days (01/01/2007 - 31/12/2010)	Linear drift: 0.05*t - 0.28 (10^{15}mol.cm^{-2}/year) , rp = 0.186

	JAN	FEB	MAR	APR	MAY	JUN	JUL	AUG	SEP	OCT	NOV	DEC
2007	-	-0.4 ± 0.2	-0.1 ± 0.3	-0.1 ± 0.3	-0.4 ± 0.3	-0.6 ± 0.4	-0.8 ± 0.3	-0.5 ± 0.4	-0.0 ± 0.3	-0.2 ± 0.2	0.0 ± 0.1	-
2008	-	-0.0 ± 0.2	0.3 ± 0.3	-	-	-	-0.6 ± 0.4	-0.3 ± 0.4	0.1 ± 0.2	0.1 ± 0.3	0.1 ± 0.2	-
2009	-	0.1 ± 0.2	0.0 ± 0.3	-0.1 ± 0.3	-0.5 ± 0.3	-0.4 ± 0.4	-0.6 ± 0.3	-0.3 ± 0.4	-0.0 ± 0.3	-0.0 ± 0.2	-0.3 ± 0.1	-
2010	-	0.1 ± 0.3	0.1 ± 0.4	-0.1 ± 0.3	-0.5 ± 0.4	-0.4 ± 0.4	-0.7 ± 0.3	-0.3 ± 0.4	0.0 ± 0.3	0.1 ± 0.3	-0.3 ± 0.3	-

Figure 3.1.9. - Same as **Figure 3.1.2.**, but at the NDACC Arctic station of Sodankylä (Finland, 67°N) with the SAOZ UVVIS instrument operated by CNRS/LATMOS at FMI-ARC.

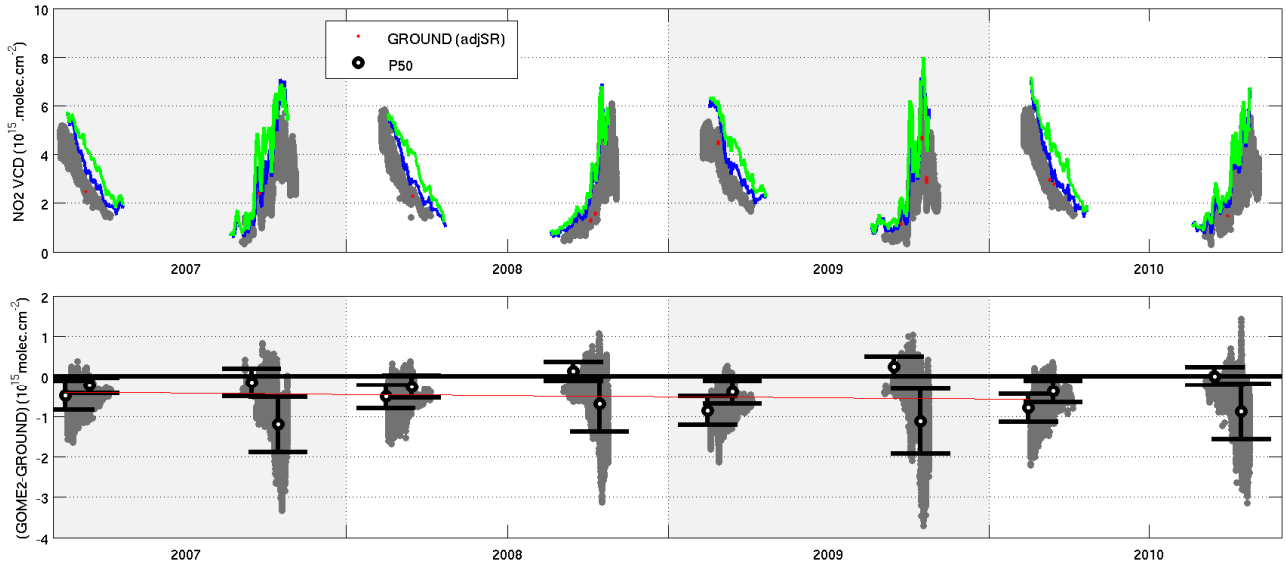

GOME2 OFL GDP 4.3.and.4.4	UVVIS (Source: NDACC)	Method: zovp pixels vs. Twilights (photochem. corrected)
Source: GOME2 OFL GDP 4.3.and.4.4 NO2 VCD	Source: NDACC	Global agreement: -0.9 ± 0.6 (10^{15}mol.cm^{-2})
51353 pixels in 457 days (09/02/2007 - 11/02/2011)	1053 values in 521 days (17/02/2007 - 25/10/2010)	Linear drift: -0.06*t - 0.39 (10^{15}mol.cm^{-2}/year) , rp = -0.132

	JAN	FEB	MAR	APR	MAY	JUN	JUL	AUG	SEP	OCT	NOV	DEC
2007	-	-0.5 ± 0.4	-0.2 ± 0.2	-	-	-	-	-	-0.2 ± 0.3	-1.2 ± 0.7	-	-
2008	-	-0.5 ± 0.3	-0.3 ± 0.3	-	-	-	-	-	0.1 ± 0.2	-0.7 ± 0.7	-	-
2009	-	-0.9 ± 0.3	-0.4 ± 0.3	-	-	-	-	-	0.2 ± 0.2	-1.1 ± 0.8	-	-
2010	-	-0.8 ± 0.4	-0.4 ± 0.3	-	-	-	-	-	0.0 ± 0.2	-0.9 ± 0.7	-	-

Figure 3.1.10. - Same as **Figure 3.1.2.**, but at the NDACC Antarctic station of Arrival Heights (78°S) with the UVVIS DOAS instrument operated by NIWA.

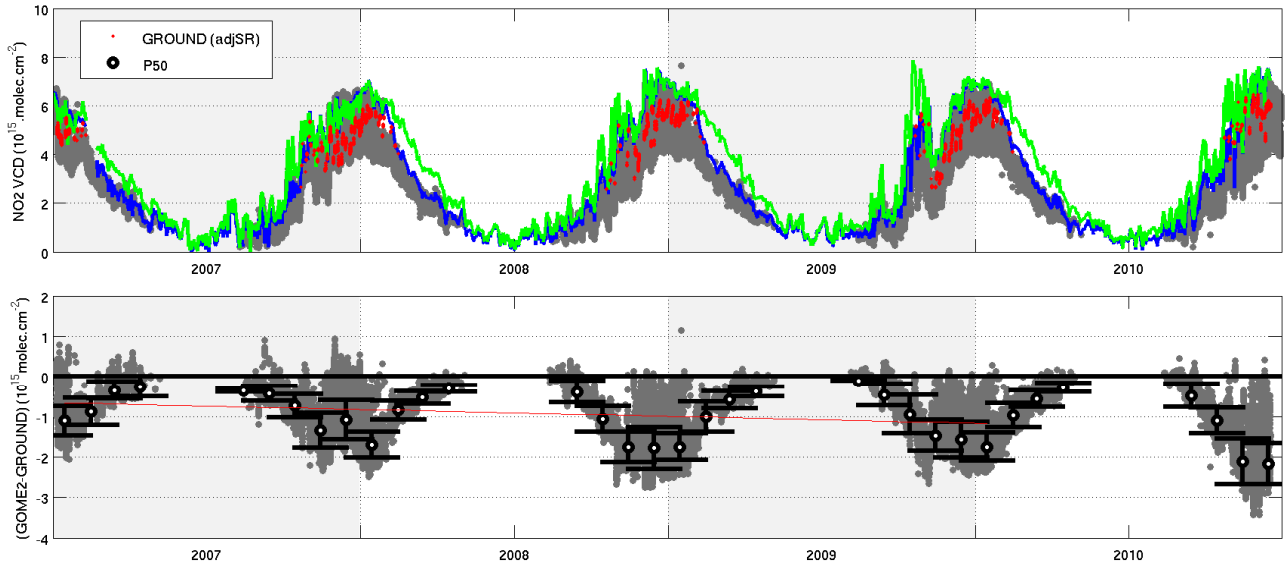

GOME2 OFL GDP 4.3.and.4.4	UVVIS (Source: calval)	Method: zovp pixels vs. Twilights (photochem. corrected)
Source: GOME2 OFL GDP 4.3.and.4.4 NO2 VCD	Source: calval	Global agreement: -1.1 ± 0.7 (10^{15}mol.cm^{-2})
52027 pixels in 1046 days (05/01/2007 - 07/02/2011)	2758 values in 1402 days (01/01/2007 - 17/12/2010)	Linear drift: -0.17*t - 0.66 (10^{15}mol.cm^{-2}/year) , rp = -0.291

	JAN	FEB	MAR	APR	MAY	JUN	JUL	AUG	SEP	OCT	NOV	DEC
2007	-1.1 ± 0.4	-0.9 ± 0.3	-0.3 ± 0.2	-0.3 ± 0.3	-	-	-	-0.3 ± 0.0	-0.4 ± 0.2	-0.7 ± 0.3	-1.3 ± 0.4	-1.1 ± 0.5
2008	-1.7 ± 0.3	-0.8 ± 0.2	-0.5 ± 0.2	-0.3 ± 0.1	-	-	-	-	-0.4 ± 0.3	-1.1 ± 0.3	-1.8 ± 0.4	-1.8 ± 0.5
2009	-1.8 ± 0.3	-1.0 ± 0.4	-0.6 ± 0.2	-0.4 ± 0.1	-	-	-	-0.1 ± 0.0	-0.5 ± 0.3	-0.9 ± 0.5	-1.5 ± 0.4	-1.6 ± 0.4
2010	-1.8 ± 0.3	-1.0 ± 0.3	-0.6 ± 0.2	-0.3 ± 0.1	-	-	-	-	-0.5 ± 0.3	-1.1 ± 0.3	-2.1 ± 0.6	-2.2 ± 0.5

Figure 3.1.11. - Same as Figure 3.1.2., but at the NDACC Antarctic station of Rothera (68°S, Antarctic Peninsula) with the UVVIS SAOZ instrument operated by BAS-NERC.

Figure 3.1.12. shows comparisons in the **equatorial zone**, at the NDACC station of Mérida (8°N). Mid-morning GOME-2 and sunrise UVVIS data agree quite well, usually within a few 10^{14} molec.cm^{-2}. The day-to-day variability of total NO_2 captured by GOME-2 is somewhat noisier than that captured by the ground-based UVVIS. The less frequent overpass of equatorial stations by GOME-2 limits the occurrence of comparison pairs, as seen in the figure. Hence the significance of statistical estimates of the agreement between GOME-2 and ground-based observations is subject to caution.

At **tropical stations** of the NDACC, we observe a small negative bias of GOME-2 data with respect to NDACC/UVVIS observations. At the stations of Izaña on Tenerife Island in the Atlantic Ocean (Figure 3.1.13.), Saint-Denis on Reunion Island in the Indian Ocean (Figure 3.1.15.), and Bauru in Brazil in the vicinity of Sao Paulo (Figure 3.1.16.), the monthly mean agreement ranges to within 0 and -7 10^{14} molec.cm-2. At Mauna Loa in Hawaii (Figure 3.1.14.), the underestimation ranges between -3 and -10 10^{14} molec.cm-2, that is, a negative offset about 2-3 10^{14} molec.cm-2 larger than at other tropical stations. For the three mostly clean-air sites (Izaña, Mauna Loa, and Saint-Denis), the standard deviation of the agreement is about 3 10^{14} molec.cm^{-2}. It is much noisier at Bauru (about 9 10^{14} molec.cm^{-2}), reflecting influences of the pollution emitted by the megacity of Sao Paulo. These influences appear despite several precautions. First, pollution events in ground-based SAOZ data have been filtered out. Second, thanks to the optical path matching selection technique, the comparison addresses only GOME-2 air masses located above the Atlantic Ocean and not air masses encompassing Sao Paulo. Neglecting these precautions produce comparison results affected by a strong bias and by a noise exceeding 1.5 10^{15} molec.cm^{-2}.

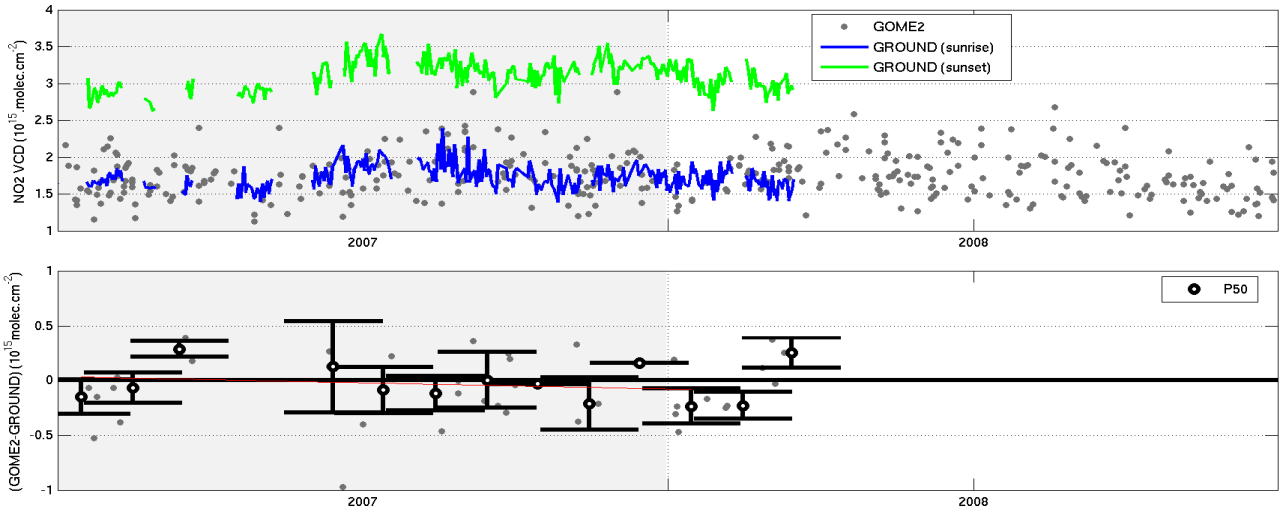

GOME2 OFL GDP 4.3			UVVIS (Source: calval)					Method: zovp pixels vs. Twilights				
Source: GOME2 OFL GDP 4.3 NO2 VCD			Source: calval					Global agreement: -0.1 ± 0.3 (10^{15}mol.cm^{-2})				
516 pixels in 400 days (05/01/2007 - 06/12/2009)			516 values in 292 days (01/01/2007 - 16/03/2008)					Linear drift: -0.11*t + 0.03 (10^{15}mol.cm^{-2}/year) , rp = -0.241				
	JAN	FEB	MAR	APR	MAY	JUN	JUL	AUG	SEP	OCT	NOV	DEC
2007	-0.2 ± 0.2	-0.1 ± 0.1	0.3 ± 0.1	-	-	0.1 ± 0.4	-0.1 ± 0.2	-0.1 ± 0.2	-0.0 ± 0.3	-0.0 ± 0.0	-0.2 ± 0.2	0.2 ± 0.0
2008	-0.2 ± 0.2	-0.2 ± 0.1	0.2 ± 0.1	-	-	-	-	-	-	-	-	-

Figure 3.1.12. - Same as Figure 3.1.2., but at the NDACC station of Mérida (Venezuela, 8°N) with the UVVIS DOAS instrument operated by IUP/U. Bremen.

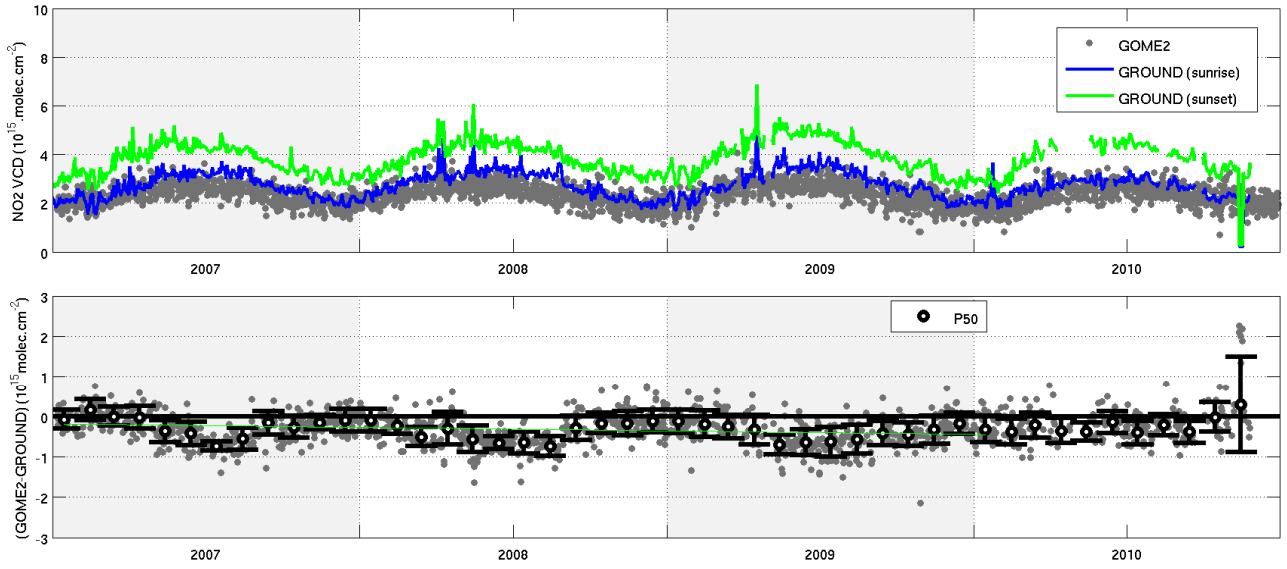

GOME2 OFL $GDP_{43a}nd_{44}$	UVVIS (Source: calval)	Method: zovp pixels vs. Twilights
Source: GOME2 OFL $GDP_{43a}nd_{44}$ NO2 VCD	Source: calval	Global agreement: -0.3 ± 0.4 (10^{15}mol.cm^{-2})
3209 pixels in 1325 days (06/01/2007 - 11/02/2011)	2869 values in 1488 days (19/07/2006 - 25/11/2010)	Linear drift: -0.09*t - 0.15 (10^{15}mol.cm^{-2}/year) , ϕ = 0.663

	JAN	FEB	MAR	APR	MAY	JUN	JUL	AUG	SEP	OCT	NOV	DEC
2007	-0.1 ± 0.2	0.2 ± 0.3	-0.0 ± 0.2	-0.0 ± 0.3	-0.4 ± 0.3	-0.4 ± 0.3	-0.7 ± 0.1	-0.6 ± 0.3	-0.2 ± 0.3	-0.3 ± 0.3	-0.2 ± 0.2	-0.1 ± 0.3
2008	-0.1 ± 0.3	-0.2 ± 0.2	-0.5 ± 0.2	-0.3 ± 0.4	-0.6 ± 0.3	-0.7 ± 0.2	-0.7 ± 0.3	-0.7 ± 0.2	-0.3 ± 0.3	-0.2 ± 0.3	-0.2 ± 0.3	-0.1 ± 0.3
2009	-0.1 ± 0.3	-0.2 ± 0.3	-0.3 ± 0.3	-0.3 ± 0.4	-0.7 ± 0.2	-0.6 ± 0.3	-0.6 ± 0.4	-0.6 ± 0.4	-0.4 ± 0.3	-0.5 ± 0.3	-0.3 ± 0.3	-0.2 ± 0.3
2010	-0.3 ± 0.3	-0.4 ± 0.3	-0.2 ± 0.3	-0.4 ± 0.3	-0.4 ± 0.2	-0.1 ± 0.3	-0.4 ± 0.3	-0.2 ± 0.3	-0.4 ± 0.3	-0.0 ± 0.4	0.3 ± 1.2	-

Figure 3.1.13. - Same as Figure 3.1.2., but at the NDACC northern subtropical station of Izaña (Tenerife, Spain, 28°N) with the UVVIS DOAS instrument operated by INTA.

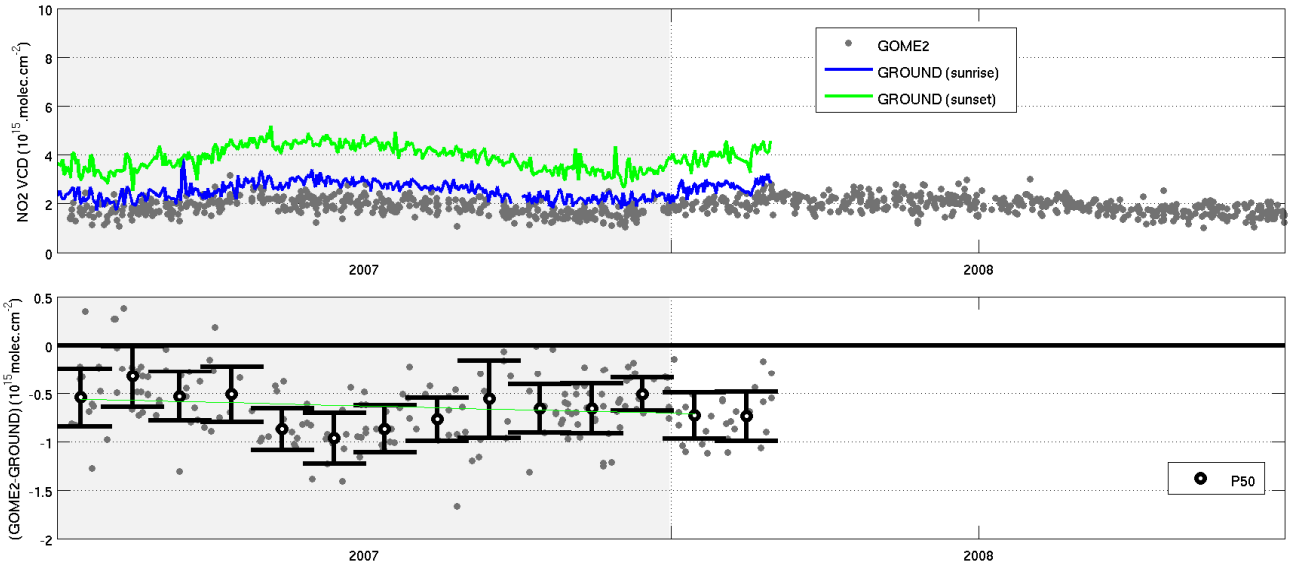

GOME2 OFL $GDP_{43a}nd_{44}$	UVVIS (Source: NDACC)	Method: zovp pixels vs. Twilights
Source: GOME2 OFL $GDP_{43a}nd_{44}$ NO2 VCD	Source: NDACC	Global agreement: -0.7 ± 0.3 (10^{15}mol.cm^{-2})
2003 pixels in 1066 days (08/01/2007 - 07/02/2011)	1093 values in 562 days (19/07/2006 - 29/02/2008)	Linear drift: -0.15*t - 0.49 (10^{15}mol.cm^{-2}/year) , ϕ = 0.496

	JAN	FEB	MAR	APR	MAY	JUN	JUL	AUG	SEP	OCT	NOV	DEC
2007	-0.5 ± 0.3	-0.3 ± 0.3	-0.5 ± 0.3	-0.5 ± 0.3	-0.9 ± 0.2	-1.0 ± 0.3	-0.9 ± 0.2	-0.8 ± 0.2	-0.6 ± 0.4	-0.7 ± 0.3	-0.7 ± 0.3	-0.5 ± 0.2
2008	-0.7 ± 0.2	-0.7 ± 0.3	-	-	-	-	-	-	-	-	-	-

Figure 3.1.14. - Same as Figure 3.1.2., but at the NDACC northern tropical station of Mauna Loa (Hawaii, 20°N) with the UVVIS DOAS instrument operated by NIWA.

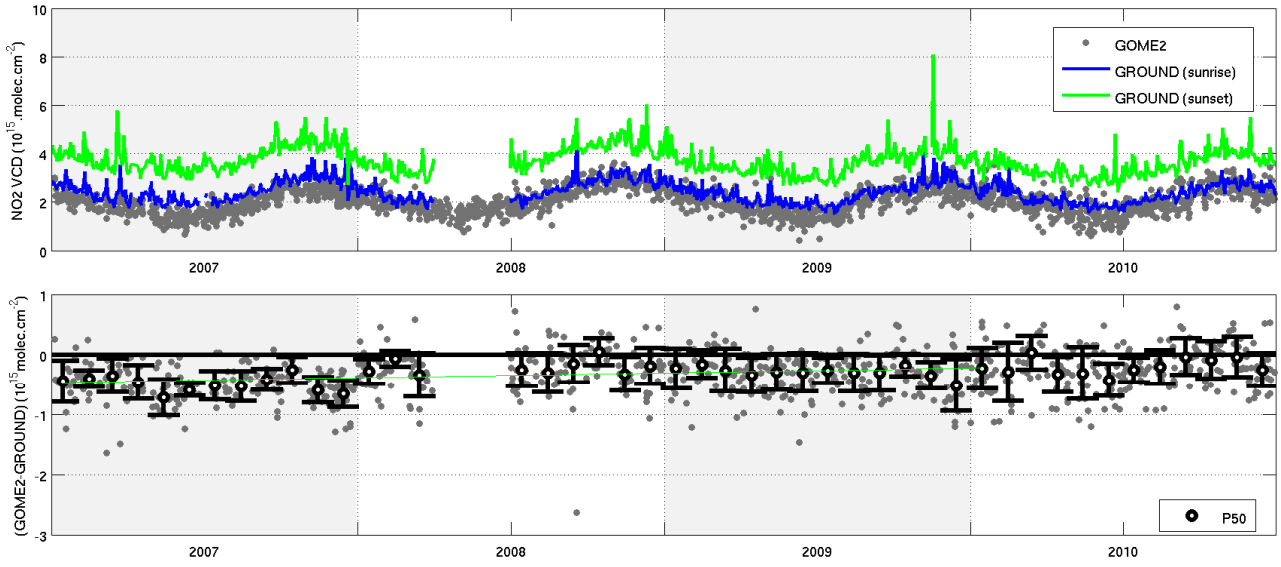

GOME2 OFL $GDP_{43a}nd_{44}$	UVVIS (Source: calval)	Method: zovp pixels vs. Twilights
Source: GOME2 OFL $GDP_{43a}nd_{44}$ NO2 VCD	Source: calval	Global agreement: -0.3 ± 0.3 (10^{15}mol.cm^{-2})
2039 pixels in 1099 days (05/01/2007 - 07/02/2011)	2939 values in 1489 days (19/07/2006 - 31/12/2010)	Linear drift: 0.08*t - 0.50 (10^{15}mol.cm^{-2}/year) , ϕ = 0.335

	JAN	FEB	MAR	APR	MAY	JUN	JUL	AUG	SEP	OCT	NOV	DEC
2007	-0.4 ± 0.3	-0.4 ± 0.1	-0.4 ± 0.3	-0.5 ± 0.3	-0.7 ± 0.3	-0.6 ± 0.1	-0.5 ± 0.2	-0.5 ± 0.3	-0.4 ± 0.2	-0.3 ± 0.2	-0.6 ± 0.2	-0.7 ± 0.2
2008	-0.3 ± 0.2	-0.1 ± 0.1	-0.3 ± 0.4	-	-	-	-0.3 ± 0.3	-0.3 ± 0.3	-0.2 ± 0.3	0.0 ± 0.2	-0.3 ± 0.3	-0.2 ± 0.3
2009	-0.2 ± 0.3	-0.2 ± 0.2	-0.3 ± 0.4	-0.3 ± 0.3	-0.3 ± 0.3	-0.3 ± 0.3	-0.3 ± 0.2	-0.3 ± 0.3	-0.3 ± 0.3	-0.2 ± 0.2	-0.4 ± 0.2	-0.5 ± 0.4
2010	-0.2 ± 0.3	-0.3 ± 0.5	0.0 ± 0.3	-0.3 ± 0.3	-0.3 ± 0.4	-0.4 ± 0.3	-0.3 ± 0.2	-0.2 ± 0.3	-0.0 ± 0.3	-0.1 ± 0.3	-0.0 ± 0.3	-0.3 ± 0.3

Figure 3.1.15. - Same as Figure 3.1.2., but at the NDACC southern tropical station of Saint-Denis (Reunion Island, 21°S) with the UVVIS SAOZ instrument operated by CNRS/LATMOS at U. Réunion/LACY.

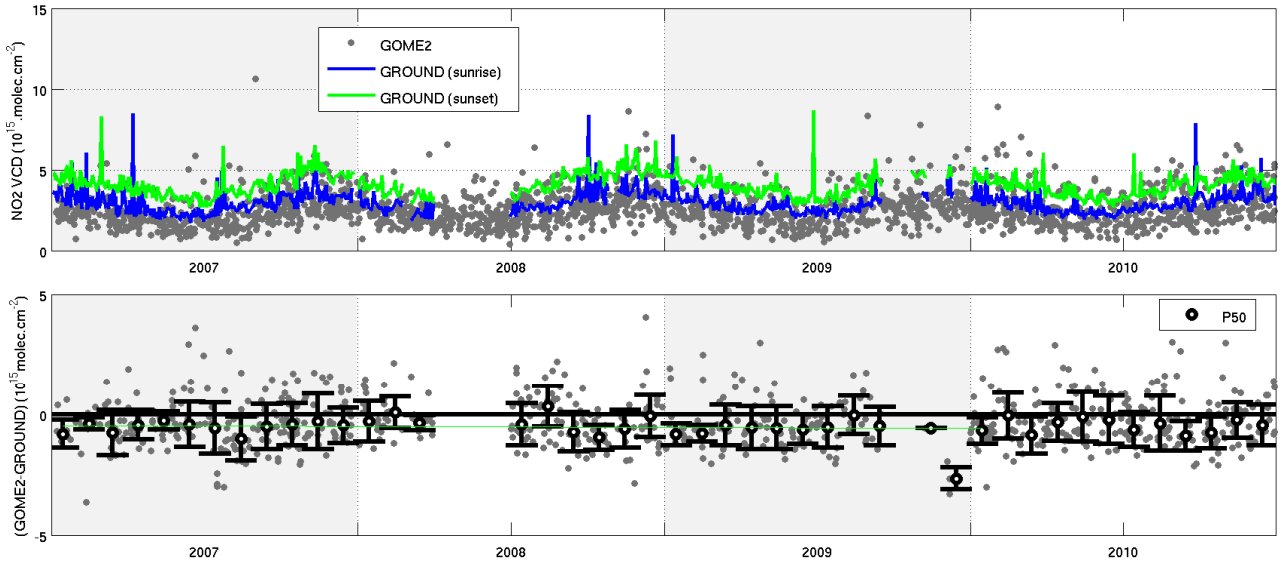

GOME2 OFL $GDP_{43a}nd_{44}$	UVVIS (Source: calval)	Method: zovp pixels vs. Twilights
Source: GOME2 OFL $GDP_{43a}nd_{44}$ NO2 VCD	Source: calval	Global agreement: -0.5 ± 0.9 (10^{15}mol.cm^{-2})
2077 pixels in 1113 days (06/01/2007 - 11/02/2011)	2628 values in 1371 days (19/07/2006 - 31/12/2010)	Linear drift: -0.04*t - 0.45 (10^{15}mol.cm^{-2}/year) , ϕ = 0.057

	JAN	FEB	MAR	APR	MAY	JUN	JUL	AUG	SEP	OCT	NOV	DEC
2007	-0.8 ± 0.6	-0.4 ± 0.2	-0.8 ± 0.9	-0.4 ± 0.6	-0.3 ± 0.4	-0.4 ± 0.9	-0.6 ± 1.1	-1.0 ± 0.9	-0.5 ± 0.9	-0.4 ± 0.9	-0.3 ± 1.2	-0.5 ± 0.7
2008	-0.3 ± 0.8	0.1 ± 0.7	-0.4 ± 0.3	-	-	-	-0.4 ± 0.9	0.3 ± 0.9	-0.7 ± 0.8	-1.0 ± 0.5	-0.6 ± 0.8	-0.1 ± 0.9
2009	-0.8 ± 0.5	-0.8 ± 0.3	-0.4 ± 0.8	-0.6 ± 0.9	-0.6 ± 0.9	-0.6 ± 0.6	-0.5 ± 0.9	-0.0 ± 0.8	-0.5 ± 0.8	-	-0.6 ± 0.0	-2.7 ± 0.5
2010	-0.7 ± 0.5	-0.1 ± 0.9	-0.9 ± 0.8	-0.3 ± 0.8	-0.1 ± 1.0	-0.2 ± 1.0	-0.6 ± 0.7	-0.4 ± 1.1	-0.9 ± 0.6	-0.8 ± 0.7	-0.2 ± 0.7	-0.4 ± 0.9

Figure 3.1.16. - Same as Figure 3.1.2., but at the NDACC southern tropical station of Bauru (Brazil, 22°S) with the UVVIS SAOZ instrument operated by CNRS/LATMOS at UNESP.

B.3.3 Stratospheric validation over polluted areas: Pilot study at O.H.P.

In this section we report progress with the validation of GOME-2 stratospheric NO_2 data over polluted areas. The NDACC station at the Observatoire de Haute Provence (O.H.P., 44°N, 6°E) in Southern France is equipped by CNRS/LATMOS with a SAOZ UVVIS instrument measuring stratospheric NO_2 and by IASB-BIRA with a MAX-DOAS instrument measuring tropospheric NO_2. This station offers interesting characteristics that make it a good candidate as a pilot site. Although the station is located in the clean environment of the Alpes de Haute Provence, GOME-2 ground pixels intersecting SAOZ optical paths can encompass areas affected by pollution from the valleys of Rhone and Durance in France and Po in Italy. The station itself experiences from time to time high NO_2 concentrations transported to the site, which is measured by the MAX-DOAS. Looking at all GOME-2 data collocated with SAOZ observations, it is difficult to draw any quantitative conclusion: indeed, in case of tropospheric pollution the vertical weighting functions of the two types of measurement (nadir-viewing GOME-2 against zenith-sky SAOZ) is so different that the meaning of the comparison is corrupted by extremely large vertical smoothing errors. However, assuming that most of the pollution if contained in the first lowest kilometers above the surface, we can nevertheless filter out pollution events by a cloud-slicing method screening GOME-2 data according to the fractional cloud cover.

Figure 3.1.17. depicts the difference between GOME-2 and SAOZ data as a function of the GOME-2 fractional cloud cover. A threshold appears around 25% of cloud fraction, beyond which the large disagreement of about 2-4 10^{15} molec/cm^2 drops suddenly to more acceptable values of a few 10^{14} molec/cm^2, values comparable to those observed at clean-air stations. A similar behavior is observed when the agreement is presented as a function of the GOME-2 solar zenith angle (Figure 3.1.18.) and the GOME-2 GDP 4.2 NO_2 tropospheric column (Figure 3.1.19.) validated in the next section.

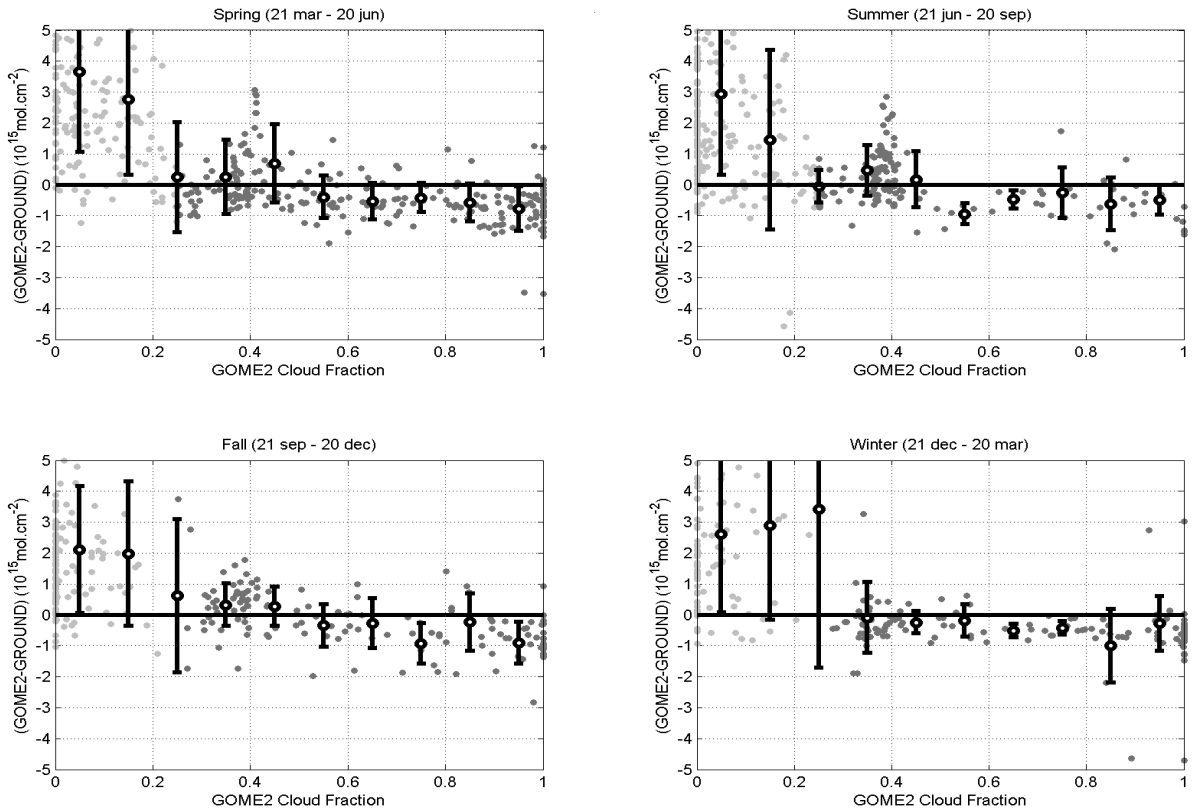

Figure 3.1.17. - Absolute difference between GOME-2 and ground-based SAOZ NO_2 vertical column over the NDACC Alpine station of OHP, as a function of the GOME-2 cloud fraction. The four seasons are separated.

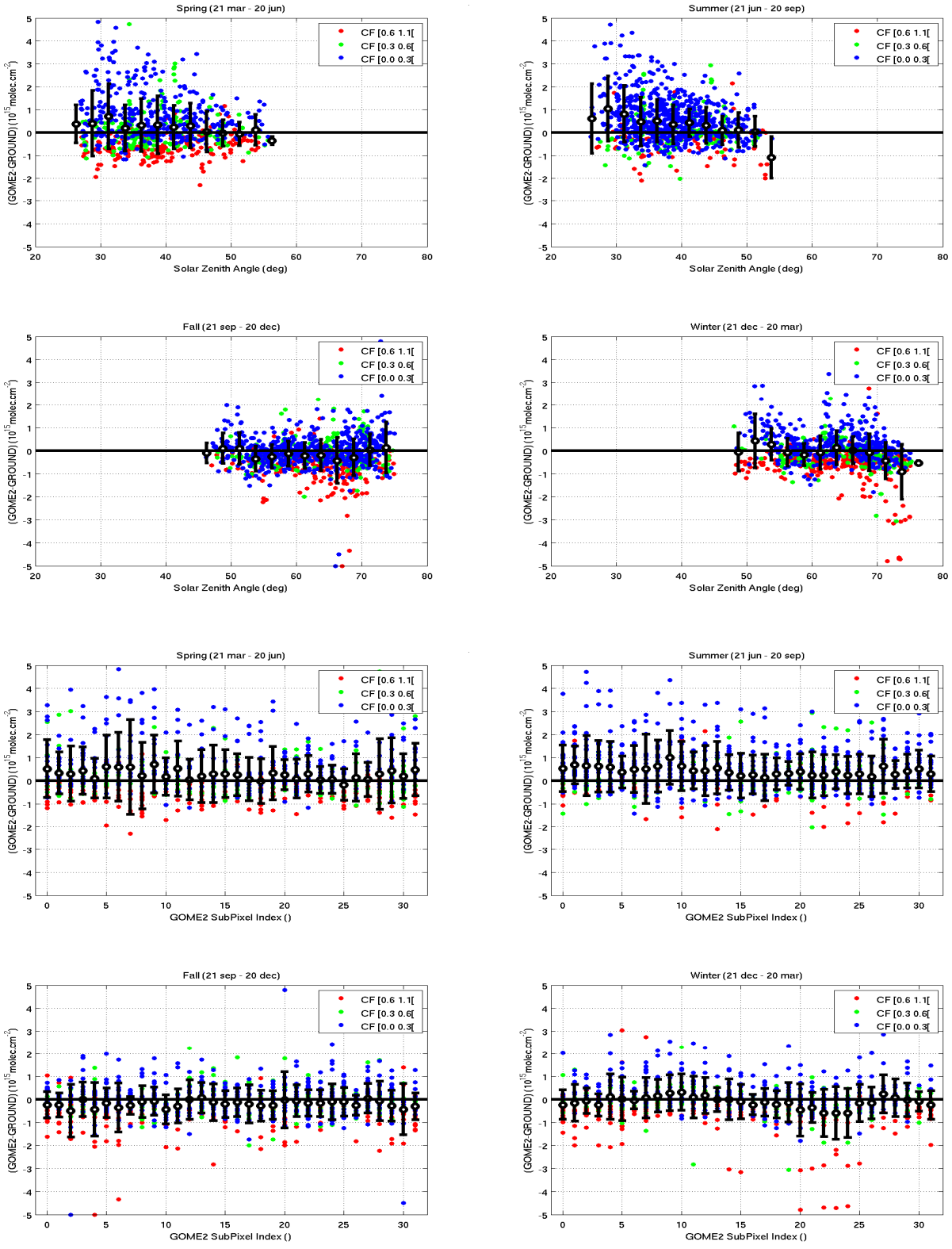

Figure 3.1.18. - Same as Figure 3.1.17., but as a function of the GOME-2 solar zenith angle (four upper plates) and the GOME-2 sub pixel index (four lower plates) from East (0) to West (32), and with colour code corresponding to three cloud fraction ranges.

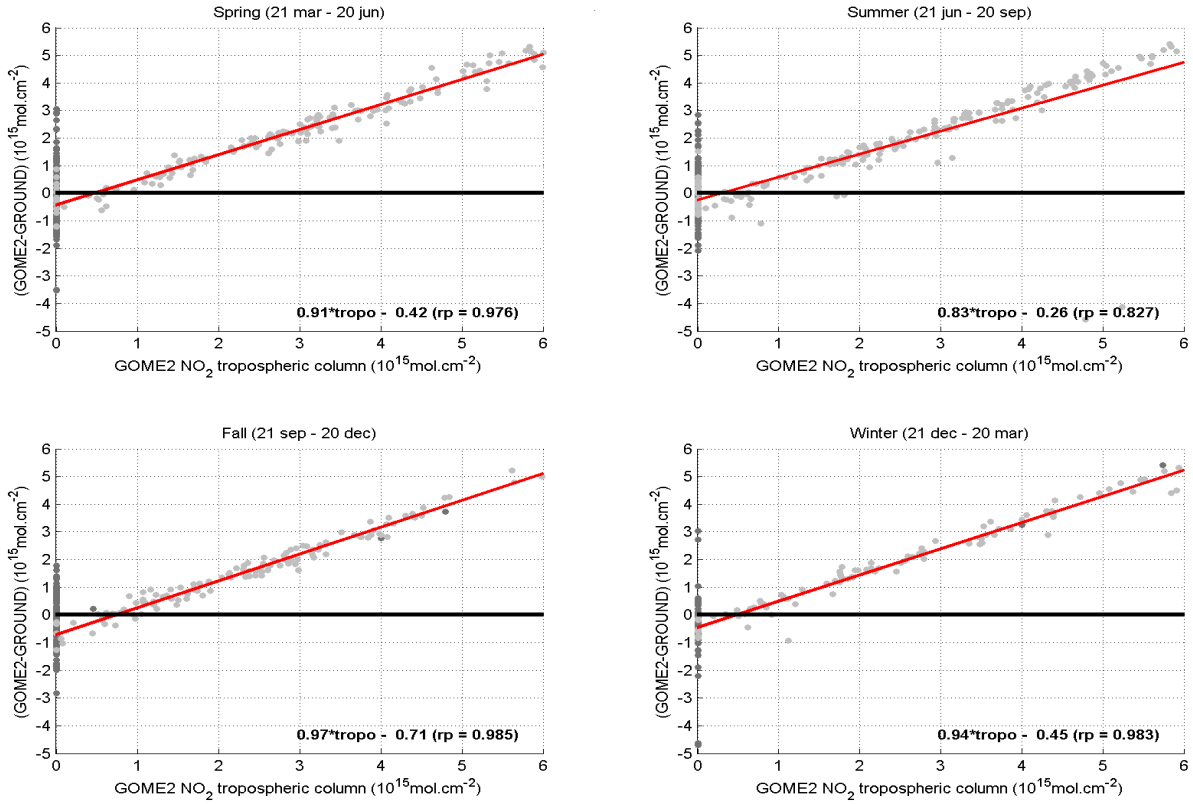

Figure 3.1.19. - Same as Figure 3.1.17., but as a function of the GOME-2 GDP 4.3 NO_2 tropospheric column.

As noted in the case of pollution-free comparisons at the Southern middle latitude stations of Kerguelen and Lauder, the very weak dependence of the agreement on the solar zenith angle (Figure 3.1.18., upper graphs) and on the sub pixel index (Figure 3.1.18., lower graphs) indicates that the photochemical time difference between cloudy GOME-2 data and twilight measurements is handled appropriately. The difference between cloud-free GOME-2 total columns and NDACC stratospheric columns is supposed to be an estimate of the tropospheric column. The compacity of the linear regression between GOME-2 tropospheric columns from one part, and this difference between GOME-2 and NDACC values from the other part, indicates the good consistency of two different processing channels of GDP 4.3/4.4.

Applying a filter on GOME-2 data based on the threshold value of 25% of the cloud cover, we can compare partly cloudy GOME-2 and SAOZ NO_2 column time series as in Figure 3.1.20. The quantitative agreement ranges from -5 to +7 10^{14} molec/cm^2, that is, within the 10% range in all months except in April and May, with a yearly median agreement of 0 ± 7 10^{14} molec/cm^2.

Similar results are illustrated hereafter for the NDACC middle latitude stations of Harestua in Norway (Figure 3.1.21.), Bremen in Germany (Figure 3.1.22.), and Issyk-Kul in Kyrgyzstan (Figure 3.1.23.), where the yearly median agreement is 2 ± 5 10^{14} molec/cm^2, 3 ± 8 10^{14} molec/cm^2, and 0 ± 4 10^{14} molec/cm^2, respectively.

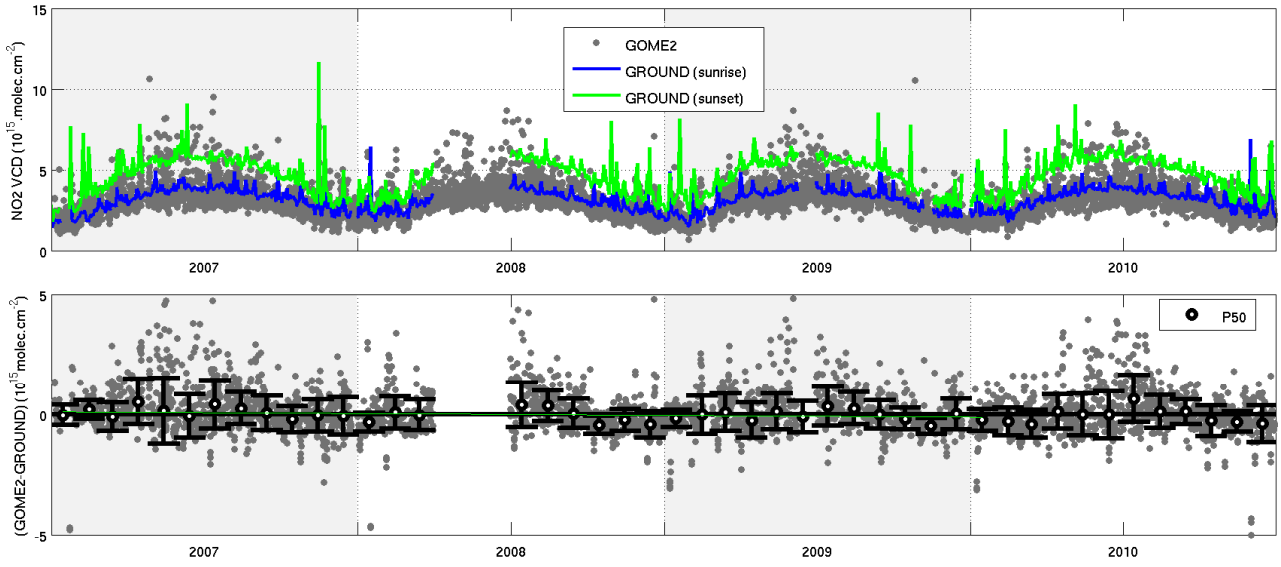

GOME2 OFL $GDP_{43a}nd_{44}$	UVVIS (Source: calval)	Method: zovp pixels vs. Twilights
Source: GOME2 OFL $GDP_{43a}nd_{44}$ NO2 VCD	Source: calval	Global agreement: -0.0 ± 0.7 (10^{15}mol.cm^{-2})
7751 pixels in 1441 days (05/01/2007 - 07/02/2011)	2904 values in 1462 days (19/07/2006 - 31/12/2010)	Linear drift: -0.08*t + 0.14 (10^{15}mol.cm^{-2}/year) , ϕ = 0.188

	JAN	FEB	MAR	APR	MAY	JUN	JUL	AUG	SEP	OCT	NOV	DEC
2007	-0.0 ± 0.4	0.2 ± 0.4	-0.1 ± 0.6	0.5 ± 0.9	0.1 ± 1.4	-0.1 ± 0.9	0.4 ± 1.0	0.2 ± 0.7	0.0 ± 0.7	-0.2 ± 0.5	-0.1 ± 0.7	-0.1 ± 0.8
2008	-0.3 ± 0.4	0.1 ± 0.7	-0.0 ± 0.6	-	-	-	0.4 ± 0.9	0.3 ± 0.6	0.0 ± 0.6	-0.4 ± 0.4	-0.2 ± 0.5	-0.4 ± 0.5
2009	-0.2 ± 0.4	-0.0 ± 0.8	0.1 ± 0.8	-0.3 ± 0.7	0.1 ± 0.7	-0.1 ± 0.6	0.3 ± 0.8	0.2 ± 0.7	-0.0 ± 0.6	-0.2 ± 0.4	-0.5 ± 0.3	0.0 ± 0.6
2010	-0.2 ± 0.5	-0.3 ± 0.6	-0.4 ± 0.6	0.1 ± 0.7	-0.0 ± 0.9	-0.0 ± 1.0	0.7 ± 1.0	0.1 ± 0.7	0.1 ± 0.5	-0.3 ± 0.6	-0.3 ± 0.4	-0.4 ± 0.8

Figure 3.1.20. - Same as **Figure 3.1.2.**, but at the NDACC Alpine station of OHP (Southern France, 44°N) with the UVVIS SAOZ instrument operated by CNRS/LATMOS.

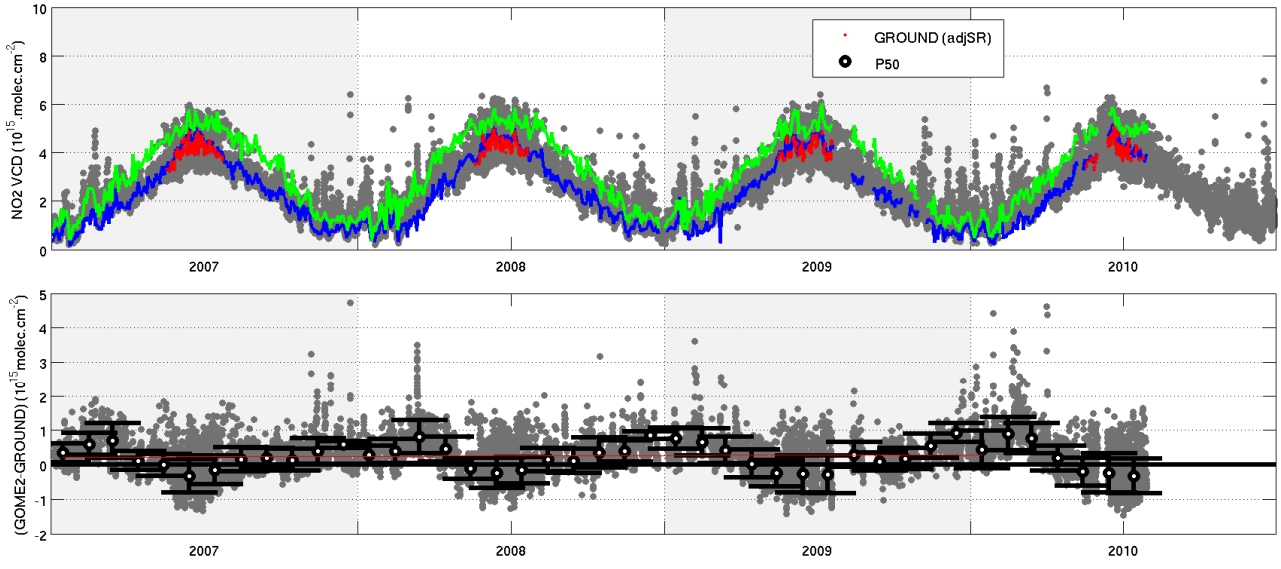

GOME2 OFL GDP 4.3.and.4.4	UVVIS (Source: NDACC)	Method: zovp pixels vs. Twilights (photochem. corrected)
Source: GOME2 OFL GDP 4.3.and.4.4 NO2 VCD	Source: NDACC	Global agreement: 0.2 ± 0.5 (10^{15}mol.cm^{-2})
25500 pixels in 1452 days (05/01/2007 - 11/02/2011)	2071 values in 1080 days (01/01/2007 - 30/07/2010)	Linear drift: 0.02*t + 0.22 (10^{15}mol.cm^{-2}/year) , rp = 0.064

	JAN	FEB	MAR	APR	MAY	JUN	JUL	AUG	SEP	OCT	NOV	DEC
2007	0.3 ± 0.3	0.6 ± 0.3	0.7 ± 0.5	0.1 ± 0.3	-0.0 ± 0.3	-0.3 ± 0.5	-0.2 ± 0.4	0.2 ± 0.4	0.2 ± 0.3	0.1 ± 0.3	0.4 ± 0.4	0.6 ± 0.1
2008	0.3 ± 0.3	0.4 ± 0.4	0.8 ± 0.5	0.5 ± 0.4	-0.1 ± 0.3	-0.2 ± 0.4	-0.2 ± 0.4	0.2 ± 0.3	0.1 ± 0.4	0.3 ± 0.4	0.4 ± 0.3	0.9 ± 0.1
2009	0.8 ± 0.3	0.7 ± 0.4	0.4 ± 0.4	0.0 ± 0.4	-0.2 ± 0.4	-0.3 ± 0.5	-0.3 ± 0.5	0.3 ± 0.4	0.1 ± 0.3	0.2 ± 0.3	0.5 ± 0.3	0.9 ± 0.3
2010	0.4 ± 0.5	0.9 ± 0.5	0.8 ± 0.4	0.2 ± 0.4	-0.2 ± 0.4	-0.2 ± 0.6	-0.3 ± 0.5	-	-	-	-	-

Figure 3.1.21. - Same as **Figure 3.1.2.**, but at the NDACC station of Harestua (Southern Norway, 60°N) with the UVVIS DOAS instrument operated by IASB-BIRA. Sunrise data adjusted to white night conditions are plotted in red.

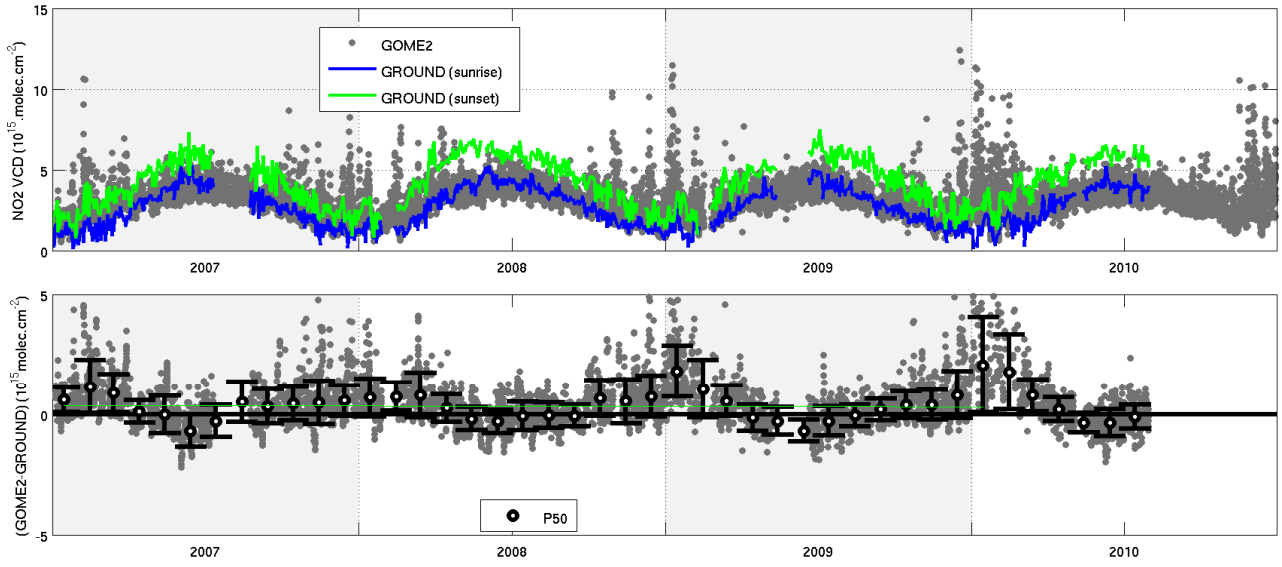

GOME2 OFL $GDP_{43a}nd_{44}$	UVVIS (Source: calval)	Method: zovp pixels vs. Twilights
Source: GOME2 OFL $GDP_{43a}nd_{44}$ NO2 VCD	Source: calval	Global agreement: 0.3 ± 0.8 (10^{15}mol.cm^{-2})
13595 pixels in 1449 days (05/01/2007 - 11/02/2011)	2282 values in 1246 days (19/07/2006 - 31/07/2010)	Linear drift: -0.02*t + 0.37 (10^{15}mol.cm^{-2}/year) , ϕ = 0.651

	JAN	FEB	MAR	APR	MAY	JUN	JUL	AUG	SEP	OCT	NOV	DEC
2007	0.6 ± 0.5	1.1 ± 1.1	0.9 ± 0.8	0.1 ± 0.5	-0.0 ± 0.8	-0.7 ± 0.7	-0.3 ± 0.7	0.5 ± 0.8	0.3 ± 0.7	0.4 ± 0.7	0.5 ± 0.9	0.6 ± 0.6
2008	0.7 ± 0.8	0.7 ± 0.6	0.8 ± 0.9	0.3 ± 0.6	-0.2 ± 0.5	-0.3 ± 0.5	-0.1 ± 0.6	-0.0 ± 0.5	-0.1 ± 0.5	0.7 ± 0.8	0.5 ± 0.9	0.7 ± 0.8
2009	1.8 ± 1.1	1.0 ± 1.2	0.6 ± 0.6	-0.1 ± 0.5	-0.3 ± 0.6	-0.7 ± 0.5	-0.3 ± 0.6	-0.1 ± 0.4	0.2 ± 0.5	0.4 ± 0.6	0.4 ± 0.6	0.8 ± 1.0
2010	2.1 ± 2.0	1.8 ± 1.6	0.8 ± 0.7	0.2 ± 0.5	-0.4 ± 0.4	-0.4 ± 0.6	-0.1 ± 0.5	-	-	-	-	-

Figure 3.1.22. - Same as **Figure 3.1.2.**, but at the NDACC station of Bremen (Germany, 53°N) with the UVVIS DOAS instrument operated by IFE/IUP.

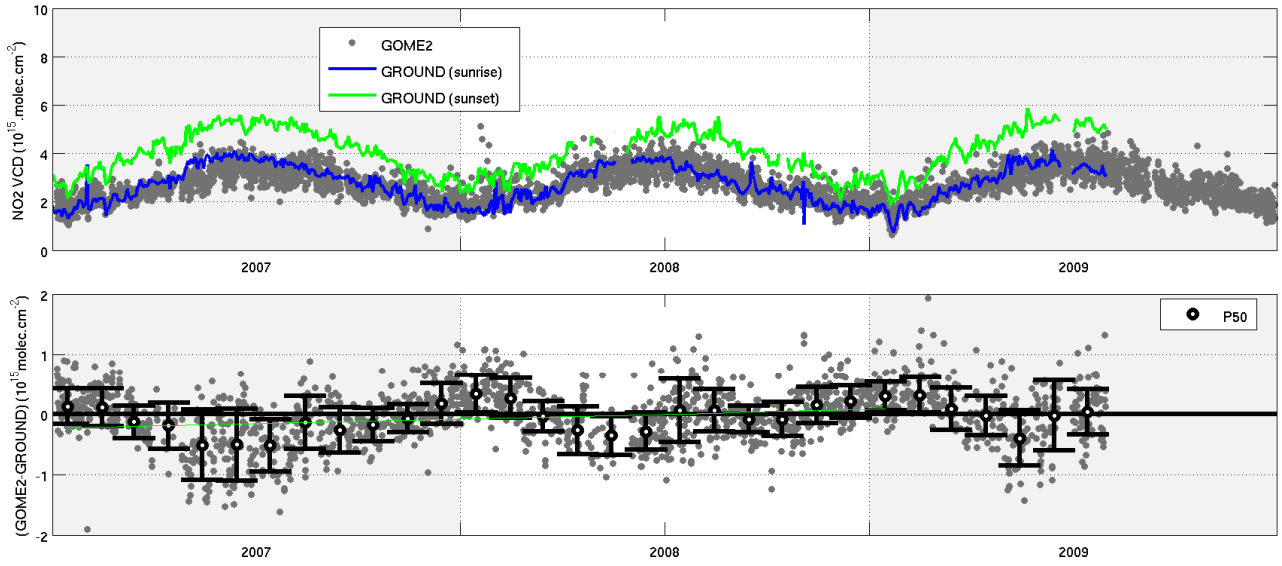

GOME2 OFL $GDP_{43a}nd_{44}$	UVVIS (Source: NDACC)	Method: zovp pixels vs. Twilights
Source: GOME2 OFL $GDP_{43a}nd_{44}$ NO2 VCD	Source: NDACC	Global agreement: -0.0 ± 0.4 (10^{15}mol.cm^{-2})
6843 pixels in 1389 days (05/01/2007 - 12/02/2011)	1894 values in 1041 days (19/07/2006 - 31/07/2009)	Linear drift: 0.16*t - 0.31 (10^{15}mol.cm^{-2}/year) , ϕ = 0.675

	JAN	FEB	MAR	APR	MAY	JUN	JUL	AUG	SEP	OCT	NOV	DEC
2007	0.1 ± 0.3	0.1 ± 0.3	-0.1 ± 0.3	-0.2 ± 0.4	-0.5 ± 0.6	-0.5 ± 0.6	-0.5 ± 0.4	-0.1 ± 0.4	-0.3 ± 0.4	-0.2 ± 0.3	-0.1 ± 0.2	0.2 ± 0.3
2008	0.3 ± 0.3	0.3 ± 0.3	-0.0 ± 0.3	-0.3 ± 0.4	-0.4 ± 0.3	-0.3 ± 0.3	0.1 ± 0.5	0.1 ± 0.4	-0.1 ± 0.2	-0.1 ± 0.3	0.1 ± 0.3	0.2 ± 0.3
2009	0.3 ± 0.2	0.3 ± 0.3	0.1 ± 0.4	-0.0 ± 0.3	-0.4 ± 0.5	-0.0 ± 0.6	0.0 ± 0.4	-	-	-	-	-

Figure 3.1.23. - Same as **Figure 3.1.2.**, but at the NDACC station of Issyk-Kul (Kyrgyzstan, 43°N) with the UVVIS DOAS instrument operated by KSNU.

B.4 Direct comparison of tropospheric vertical column densities

The direct comparison of GOME-2 tropospheric NO_2 with correlative sources is under progress. The development of the methodology and the techniques for the comparison with ground-based correlative data is under progress, and BIRA-IASB performed comparison with MAX-DOAS measurements at OHP, spanning three year of GOME-2 observations.

B.4.1 Comparison with MAX-DOAS observations at OHP

Some preliminary comparisons of tropospheric NO_2 vertical column have been performed by comparing GOME-2 data (from March 2007 to March 2010, GDP 4.3-4.4) to tropospheric columns measured from the ground using a Multi-Axis DOAS instrument. BIRA-IASB is conducting MAX-DOAS observations at the Observatoire de Haute Provence (OHP) in Southern France (43.94°N, 5.71°E) since 2005. Data retrieved at this location are used to test and set up a method for the comparison/validation of tropospheric GOME-2 tropospheric NO_2 retrievals. In this section, the MAX-DOAS technique is first shortly reviewed; secondly, the MAX-DOAS instrument at OHP is presented, and finally the comparison with satellite data is reported.

B.4.1.1 Description of the MAX-DOAS technique

The Multi-Axis DOAS (MAX-DOAS) is a recently developed remote sensing technique allowing the determination of the vertically resolved abundance of atmospheric trace species by use of their structured absorption bands in the UV and visible spectral regions (Heckel et al., 2005, Honninger et al., 2004, Wagner et al., 2004, Wittrock et al., 2004). It is based on an extension of the zenith-sky DOAS technique commonly used for stratospheric monitoring e.g. as part of the Network for the Detection of Atmospheric Composition Change (NDACC), Roscoe et al., 1999, Van Daele et al., 2005)

As the zenith sky instruments, the MAX-DOAS instruments collect scattered light from the zenith direction during twilight (being sensitive to the stratospheric content) but in addition during the day, off-axis measurements are performed by scanning multiple line-of-sight (LOS) angles from the horizon to the zenith, which increases the measurement sensitivity towards absorbers present close to the surface. Indeed, since photon scattering largely occurs below the tropopause, the photons collected from different elevations angles have essentially the same stratospheric path but a different light path in the troposphere. The smaller the elevation angle, the longer is the length of the light path in the free troposphere and in the boundary layer. Tropospheric and stratospheric amount can be separated and converted into vertical column densities (VCD).

The retrieval of the vertical columns is a two step process, involving first a DOAS fitting (Platt, 1994) that generate a so-called differential slant column density (DSCD) from spectrum measured at each elevation and secondly the simulation of the optical average enhancement undergone by the photons. This latter, commonly named air mass factor (AMF), is calculated by means of a radiative transfer model and applied to the SCD to derive the vertical column density: VCD = SCD/AMF.

In the DOAS retrieval, each spectrum is analysed with respect to a reference spectrum (generally a zenith spectra around noon, at the minimum solar zenith angle (SZA), in order to minimize the path in the atmosphere and thus trace gases absorption) and a least square fitting is applied in a selected wavelength region, including signatures of NO_2, O_3, H_2O, O_4, the Ring effect and generally a second NO_2 cross-section to account for the temperature dependence.

As in the case of satellite measurements, the radiative transfer model must be initialised with the precise wavelength and geometry of the measurement, and proper information on the state of the atmosphere, as the

pressure and temperature profiles, the concentration profile of relevant absorbers (as O_3 and NO_2), an a priori concentration profile of the target molecule, surface albedo, and aerosol load at the time of the measurement.

Radiative transfer model used by different MAX-DOAS (and zenith sky DOAS) users have been compared in Hendrick et al. (2006) and in Wagner et al. (2007), showing good consistency when the same initialisation and assumptions are made, e.g. on a-priori profiles. The first exercise involves comparison of simulated NO_2 and HCHO SCD, while in the second, altitude dependent box-AMF and radiances are computed for different wavelengths and aerosols scenarios. Convergence between the models reaches ~5% for both exercises.
Information on atmospheric aerosols can be gained from MAX-DOAS measurements themselves, through analysis of absorbers having a known vertical profile. In the UV/Vis the most suitable trace gas for aerosols retrieval is the oxygen collision pair O_4, which displays numerous absorption bands and is easy to detect with the DOAS technique (Wagner et al., 2004). The O_4 concentration is proportional to the square of the O_2 concentration and it is characterized by a scale height of ~ 4km. Therefore the maximum information is obtained in a layer close to the surface, which also corresponds to the bulk altitude of boundary layer aerosols. Wagner et al., 2004 and Friess et al., 2006 showed that several types of information on aerosol can be inferred by MAX-DOAS measurements of the optical depth of O_4 and from the variation of the intensity of diffuse skylight measured at different viewing directions and wavelengths.

In the following analyses, we stick to a simplified geometrical approach to the tropospheric NO_2 retrieval. Assuming that the NO_2 layer is located below the mean scattering altitude, the tropospheric NO_2 vertical column can be derived applying the following approximation where a geometrical AMF is considered:

$$VC_{trop} = \frac{SCD_{off-axis} - SCD_{zenith}}{\sin^{-1}(LOS) - 1} \qquad (6)$$

This approach is based on two assumptions: first that the stratospheric absorption is similar in the horizon-viewing and zenith-sky direction of the same scan, and therefore cancels, and second, that for the 2 highest off-axis viewing angles (generally around 15° and 30°), the geometric light path enhancement is a good approximation in the boundary layer. In order to test the validity of these assumptions, the results from the two elevation angles are compared and only measurements where the tropospheric columns agree within 10% are retained. This approach ensures that measurement points strongly affected by clouds or horizontal inhomogeneities are eliminated.

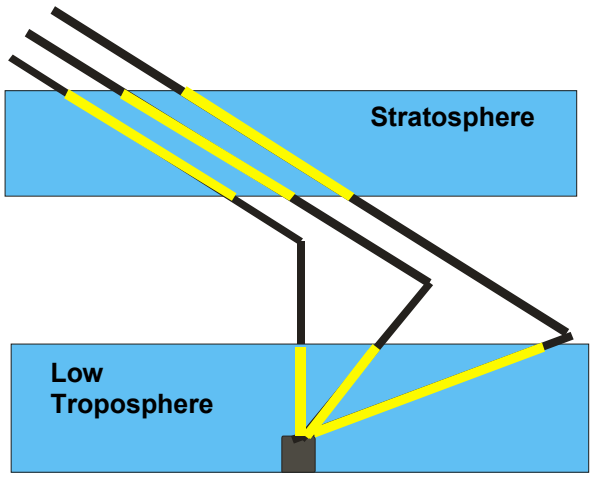

Figure 4.1.1 - Sketch of the MAX-DOAS geometry and the conditions for the application of the geometrical approximation: last scattering altitude above the NO_2 layer and same stratospheric path for consecutives zenith and off-axis elevations.

This method has been used to obtain tropospheric NO_2 columns from MAX-DOAS measurements performed during the DANDELIONS campaigns, comparing the results to OMI satellite retrievals (Brinksma et al.,

2008, and Celarier et al., 2008). An overview of the validity of the geometrical approach is given in figure 2 for several days during the 2006 DANDELIONS campaign, where the tropospheric columns obtained from the Bremen MAX-DOAS instrument by applying the geometrical approximation and by applying their BREAM[1] optimal estimation profile retrieval algorithm (Wittrock, 2006). Good agreement is found between the two methods, supporting the use of the simple geometrical approximation for retrieving the tropospheric columns.

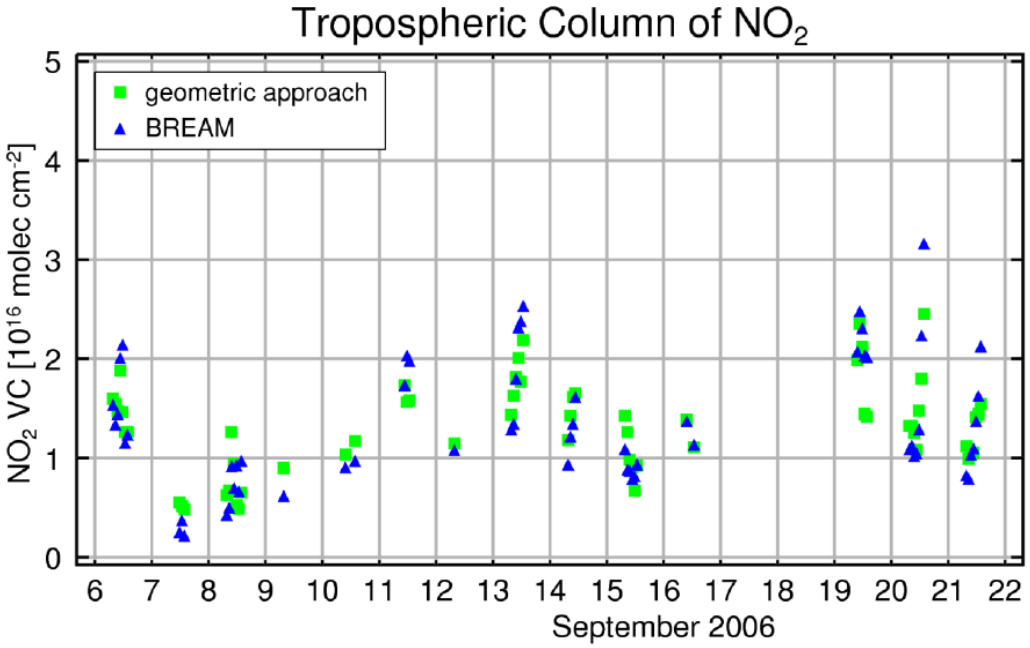

Figure 4.1.2 - Time series of tropospheric NO_2 VCD obtained from the Bremen MAX-DOAS instrument, when applying the geometrical approximation (green) and when using the BREAM optimal estimation method (blue), during part of the DANDELIONS campaign in 2006. Courtesy of F. Wittrock, IFE/IUP/U. Bremen.

In order to further assess the errors related to the use of the geometrical approximation, sensitivity tests have been computed by BIRA-IASB, comparing the geometrical AMF to AMF calculated with the radiative transfer model UVspec/DISORT (Mayer and Kylling, 2005; Hendrick et al., 2006). Simulations results are presented and discussed in the next section for the specific case of the OHP MAX-DOAS instrument.

B.4.1.2 MAX-DOAS retrievals/results at OHP

BIRA-IASB is operating a MAX-DOAS instrument at OHP (43.94°N, 5.71°E) since 2005. OHP is a primary station of the international Network for the Detection of Atmospheric Composition Change (NDACC), a contributing network of WMO's Global Atmosphere Watch (GAW). The station alternates between background and polluted conditions (essentially due to transport from polluted neighbourhoods), providing interesting test cases for GOME-2 sensitivity to tropospheric NO_2. As aforementioned, the station also reports the stratospheric column amount of ozone and NO_2 (stratospheric reference provided by SAOZ instrument operated by CNRS at OHP since 1992), as well as ancillary data as vertical distribution of temperature and ozone (balloons, lidars), ultraviolet radiation, and aerosols.

The MAX-DOAS instrument at OHP is a grating spectrometer, covering the 330-390nm range and collecting photons from 3° elevations to the zenith; more information on the instrument is given in Table 4.1.

[1] BREAM: Bremian Advanced MAX-DOAS retrieval algotihm.

OHP MAX-DOAS	
Spectrometer	Jobin-Yvon Triax 180
Detector (and T°)	Hamamatsu (1024) at -40°C
Grating	1800 grooves/mm
Resolution	0.7 nm
Wavelength Range	330-390nm
Azimuth direction	Can be adjusted
Viewing geometry	3,6,10,18,90° : from 2005 to june 2007 3-6[1] 6-16[2],20,25,30,90° since june 2007

Table 4.1 - Description of the OHP MAX-DOAS instrument.

The differential slant columns densities (DSCD) are obtained applying the DOAS technique in the 367-387 nm wavelength range and including several other absorbers, like ozone, O_4, Ring. NO_2 tropospheric columns are obtained from the differential slant columns densities as described in the previous section, by applying the geometrical approximation. Only columns retrieved at 30° elevation and that differ less than 10 % to columns obtained from 16° are considered, in order to ensure the validity of the approximation (upper part of the figure 4.1.5).

In order to estimates the errors relative to the geometrical approximation, radiative transfer model simulations have been performed for several aerosols conditions, albedo, NO_2 vertical distribution and geometry (azimuth angle, elevation angle, SZA), as summarized in Table 4.2 hereafter.

Surface albedo	5%, 10%
SZA	20°, 30°, 40°, 60°, 70°, 80°
Wavelength	374nm
Azimuth angle	0°, 90°, 130°, 180°, 230°, 270°
Elevation angle	15°, 30°, 90°
Aerosols	• Constant extinction within 0 and 1km and zero above • asymmetry factor = 0.68 (urban type), • very small absorption, in order to have single scattering albedo = 1

Table 4.2 - Description of the parameters tested within the radiative transfer model simulations.

Example of results for an a-priori profile of NO_2 constant and confined in the boundary layer (assumed to have a thickness of 1 km), an albedo of 5% and 180° of relative azimuth angle are presented in Figure 4.1.3 for several SZA, elevations and aerosols loads. The results are expressed as the ratio of the differential AMF calculated with the radiative transfer model ($AMFdiff_{RTM}=AMF_{RTM}(elev) - AMF_{RTM}(zen)$) to the differential geometrical AMF ($AMFdff_{geom}$).

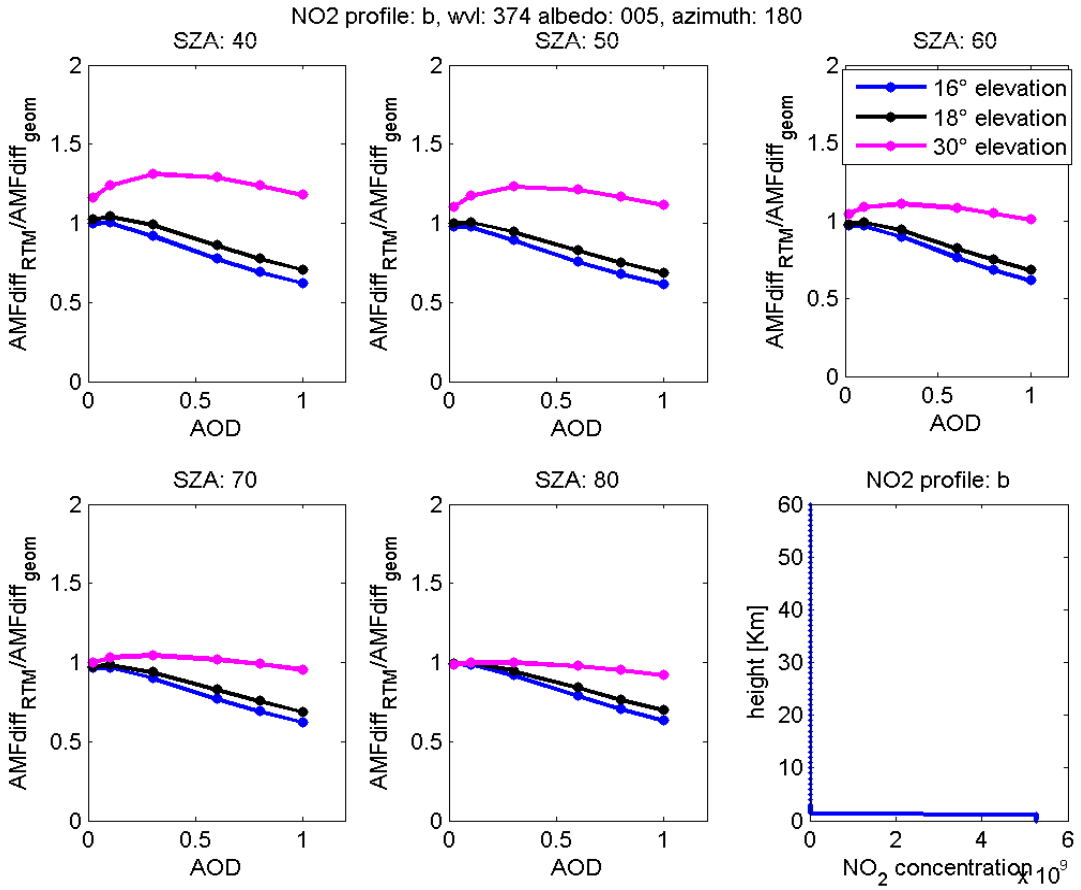

Figure 4.1.3 - Error on the NO_2 vertical column when applying the geometrical approximation, as function of the aerosol load expressed through the aerosols optical depth (AOD) at ground, for an NO_2 profile homogeneously mixed in the first km of the atmosphere.

Indeed:

$$VCD_{underestimation} = \frac{VCD_{geometric}}{VCD_{RTM}} = \frac{AMFdiff_{RTM}}{AMFdiff_{geometric}} = \frac{AMF_{off-axis} - AMF_{zenith}}{\sin^{-1}(LOS) - 1} \qquad (7)$$

This expression represents the systematic error on the NO_2 VCD when applying the geometrical approximation, as a function of the aerosol load. For small SZA (up to 65°) and almost all aerosols optical depth (AOD), the VCD retrieved with the geometrical approximation at 30° elevation, is over-estimating the real column, while applying the approximation at 16° or 18° elevation, is underestimating the column. At higher SZA the different behaviour between the two elevations is less pronounced. The large contrast between 30° and 16° results is ensuring that the data contaminated by aerosols are excluded after the filtering of 10% difference of the tropospheric columns retrieved at these two elevations.

Several tests have been made changing the albedo and the a-priori NO_2 profile shape (i.e. including free tropospheric and/or stratospheric background). No qualitative behaviour differences neither large quantitative difference is found with respect to the attitude presented in Figure 4.1.3. Several studies have also been performed changing the azimuthal directions; the results for 30° elevation, several solar zenith angle (SZA) and the 6 azimuth angles are presented in the figure 4.1.4 showing that the general findings of over-estimation are valid for all the tested cases, except when pointing in the sun direction (relative azimuth from zero up to around 30° azimuth). In that case, the geometric approximation applied to 30° elevation (also true for 16° elevation, not shown here) under-estimates the true columns for a SZA up to 70°.

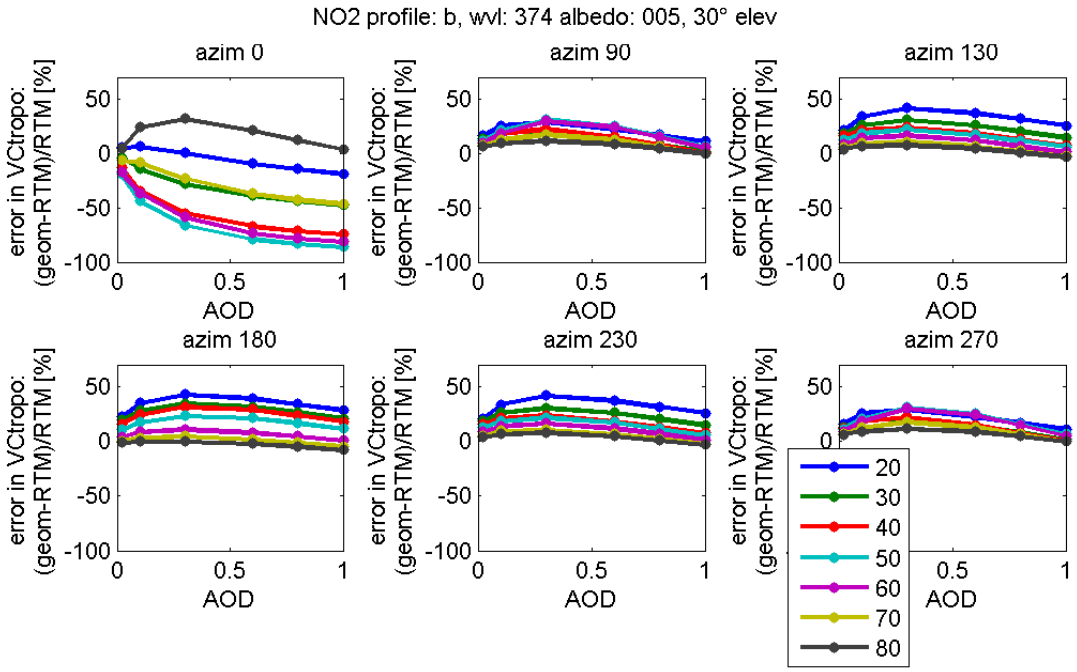

Figure 4.1.4 - Errors in percent on the NO_2 tropospheric VCD for different aerosols loads and geometries, when retrieving the columns using a simple geometrical approximation from 30° elevation instead of radiative transfer model calculations. The different subplots are the results for different azimuth values, and results for SZA from 20° to 80° are plotted in different colours. An NO_2 profile constant in the first km and zero above has been used, as well as aerosols proprieties described in table 4.3.

It should be mentioned, that when pointing in the sun direction (Figure 4.1.5) the behaviour of the under-estimation from columns retrieved at 30° and 16° with the geometrical approximation is similar up to 70° SZA, and those data will not be excluded after the filtering.

According to these (limited) tests, one concludes that errors on the geometrical approximation are minimized under moderate aerosol contents when measurements are conducted at medium SZA and at azimuth close to 90°.

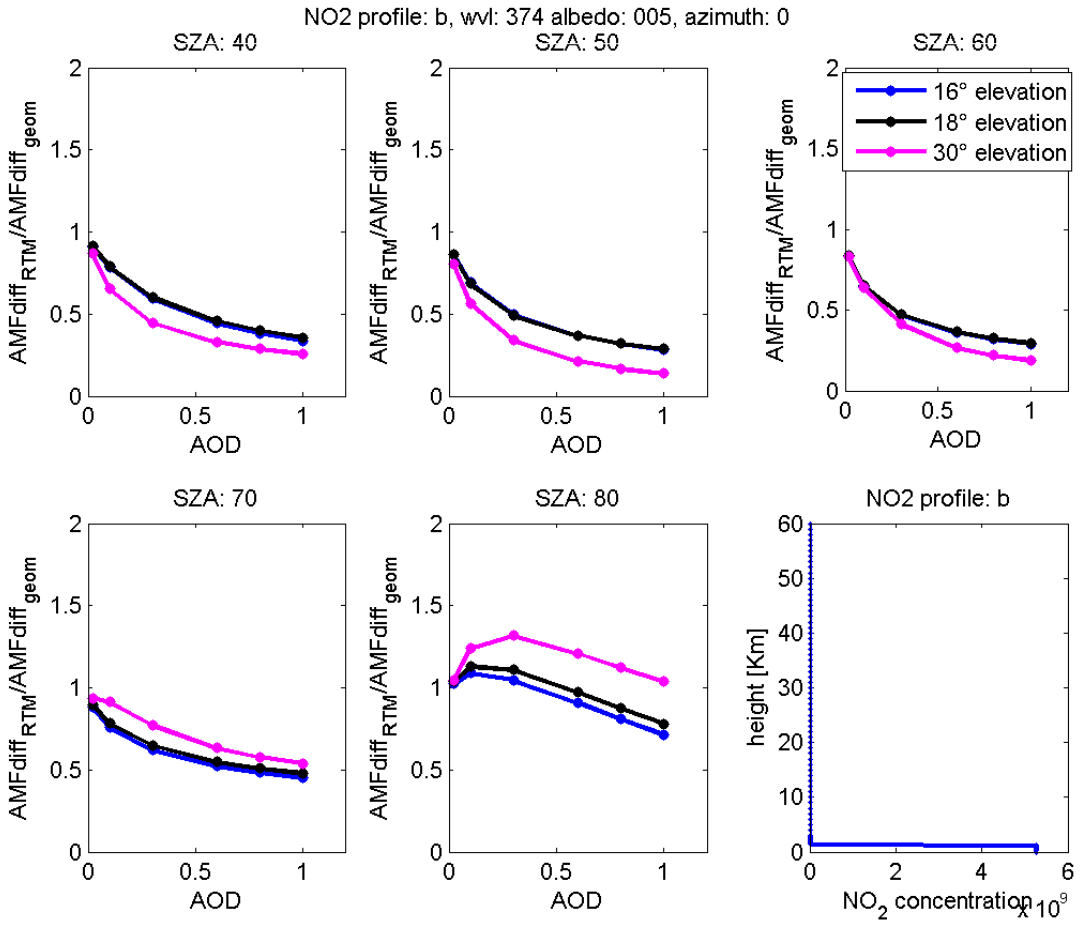

Figure 4.1.5 - Under-estimation of the vertical column when applying the geometrical approximation as function of aerosol load expressed through the aerosols optical depth (AOD) at ground, for an NO_2 profile homogeneously mixed in the first km of the atmosphere.

Based on these simulation results and measurements of the aerosol optical depth (AOD) available at 440nm from the CIMEL instrument operated at OHP (PI: Philippe Goloub from Lille), we have estimated the size of the uncertainty on our tropospheric NO_2 columns due to aerosol load. Figure 4.1.6 summarizes the evolution of the resulting errors $(V_g - V_{RTM})/V_{RTM}$ for the columns obtained at 30° elevation. Over the whole time period (June 2007 to March 2010), the mean error is of 8.5 % (± 8.6% for VCDs retrieved at 30°elevation) and of -11% (± 10%for VCDs retrieved at 16° elevation). If we consider only the points in a time interval of 2 hours around 9h30 (the GOME-2 overpass time), the mean error due to the geometrical approximation is of -3% ±4.8%.

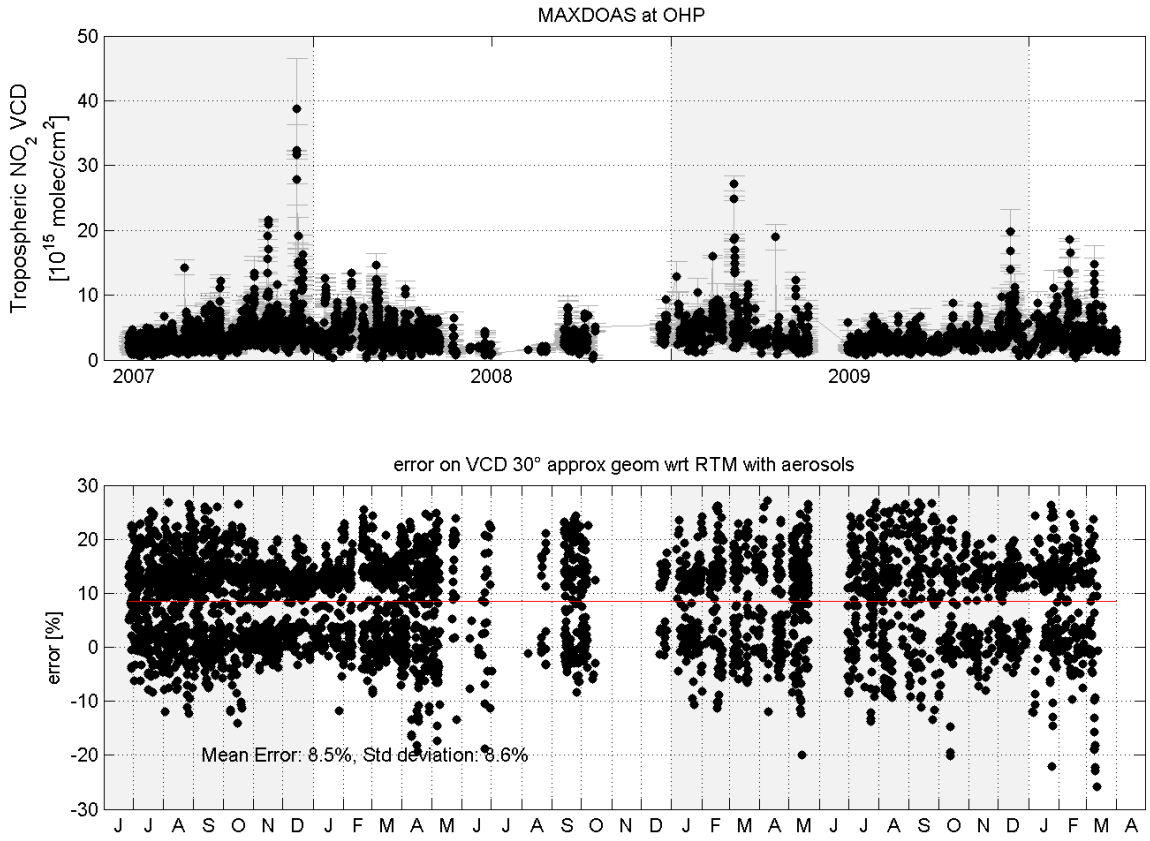

Figure 4.1.6 - OHP MAX-DOAS time series from June 2007 to March 2010 of tropospheric NO_2 VCD retrieved with the geometrical approximation, and the respective errors estimated from radiative transfer modelling and aerosols content estimation from CIMEL data at OHP.

So far, the NO_2 DSCD were retrieved with an NO_2 cross section measured at 220°K (Vandaele et al., 1998), as done in the GOME-2 retrieval. The MAX-DOAS VCDs were then corrected for the temperature dependence of the NO_2 cross-section. A correction factor dependent on the tropospheric NO_2 temperature was applied after the DSCD retrieval, as done for the GOME-2 GDP product version 4.3, using the method developed by Boersma et al. (2004).

A variation of 0.25% per degree Kelvin was found to be the representative for the NO_2 cross-section (Vandaele et al., 1998, at 220K and 294K) temperature dependence in the 364-384nm range, and for the OHP MAX-DOAS resolution.

The correction factor α_L was thus applied to the MAX-DOAS tropospheric VCD:

$$\mathrm{VCD}_{\mathrm{Temp\_corr}} = \frac{1}{\alpha_L} VCD \qquad (9)$$

with

$$\alpha_L = 1 + 0.0025(T_0 - T_L) \qquad (10)$$

where T_0 is the temperature of the NO_2 cross-section used in the DOAS fit (220K) and T_L is the temperature of the NO_2 layer. The temperature information was obtained from the NCEP data measured at OHP, and the mean value within the first 1.5km was considered to be representative of the tropospheric temperature.

Without correction, fluctuations in the atmospheric temperatures induce errors represented in Figure 4.1.7. For the selected time period, an average error of ~20% was found.

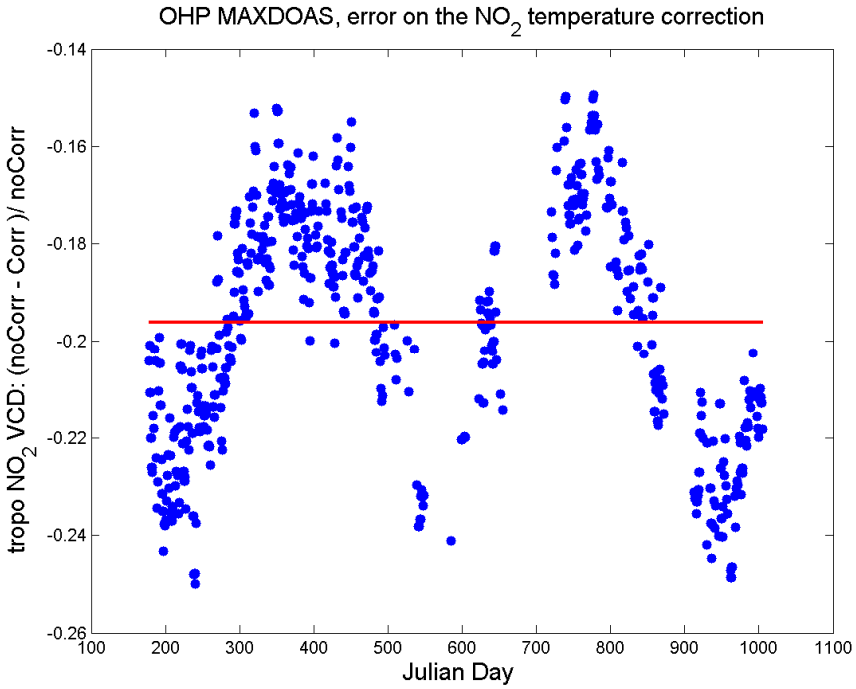

Figure 4.1.7 - OHP MAX-DOAS percentual error between not applying and applying the temperature correction (equation 9) of the NO_2 cross-section based on the NCEP data (Julian day since January 2007).

A second approach, more appropriate when dealing with tropospheric columns and using directly a room temperature NO_2 cross-section in the DSCD retrievals, is used from October 2009 on. The time series of the monthly means for the different approaches are reported in figure 4.1.8, as well as their differences in percent. A mean difference of ~7.5 % is found compared to the previous correction, and of ~23% compared to using a cross-section at 220°K. In the following sections, when comparing with the satellite retrieval (that also correct for the temperature dependence of the NO_2 cross-section) the black curve will be used (the so-called room temperature), but we should remember that the true column is probably somewhere between the black and the red curves.

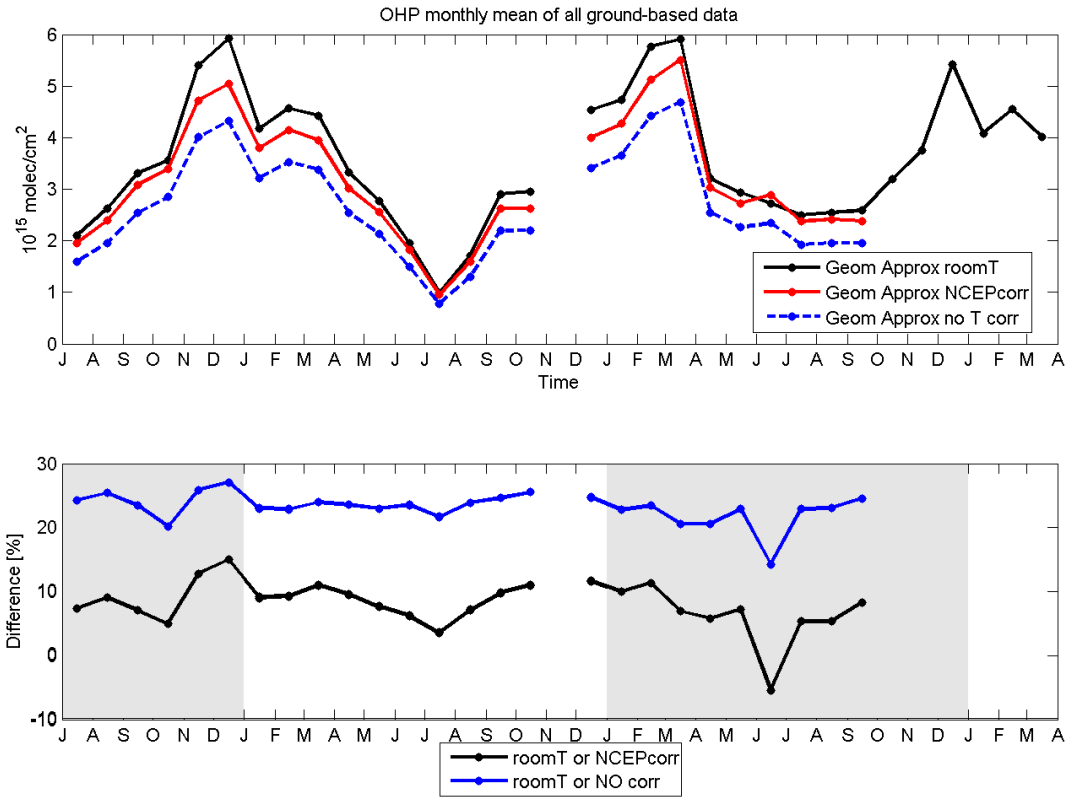

Figure 4.1.8 - OHP MAX-DOAS tropospheric NO_2 columns time series since July 2007 for the different choices of correction of the NO_2 cross-section temperature dependence, and the differences between the methods, in percent.

B.4.1.3 Satellite data over OHP and comparison with MAX-DOAS data

The tropospheric NO_2 columns obtained from the MAX-DOAS data at OHP during the period from June 2007 to March 2010 are interpolated at the GOME-2 overpass time, and the two datasets are compared in Figure 4.1.9. Only GOME-2 cloud free data (in fact, the selection has been done not on the cloud threshold, but selecting data having a tropospheric flag indicating polluted conditions, a meaningful tropospheric retrieval and intensity weighted cloud fraction less than 50%) within a 100km radius above OHP are retained.

Figure 4.1.10 shows the same results by means of a scatter plot, adding some statistical information as the correlation coefficient R and the slope of a linear regression analysis. A relatively large scatter is found in the correlation plot, with a correlation coefficient of about 0.67 and a slope of 0.8±0.04 for a linear regression fit. These results (with GDP version 4.3) are similar to those reported with GDP 4.1, in version 1_0 of this report (VAL_ORR-A3_2008, covering 6 month of data) and version 2_0 (VAL_ORR-B_2008 with dataset of one year (June 2007-June 2008)). The results of the comparisons are of the same order than before (correlation coefficient around 0.66-0.65) but with a slightly smaller slope (0.8 instead of around 0.98-1±0.09). This can be due both to the updated version of the GOME-2 product (GDP 4.3 is now correcting for the temperature dependence of the NO_2 cross-section while version 4.1 was not), and partially to the change in the temperature correction method in the ground-based data (mean difference of ~7.5 %, see previous section).

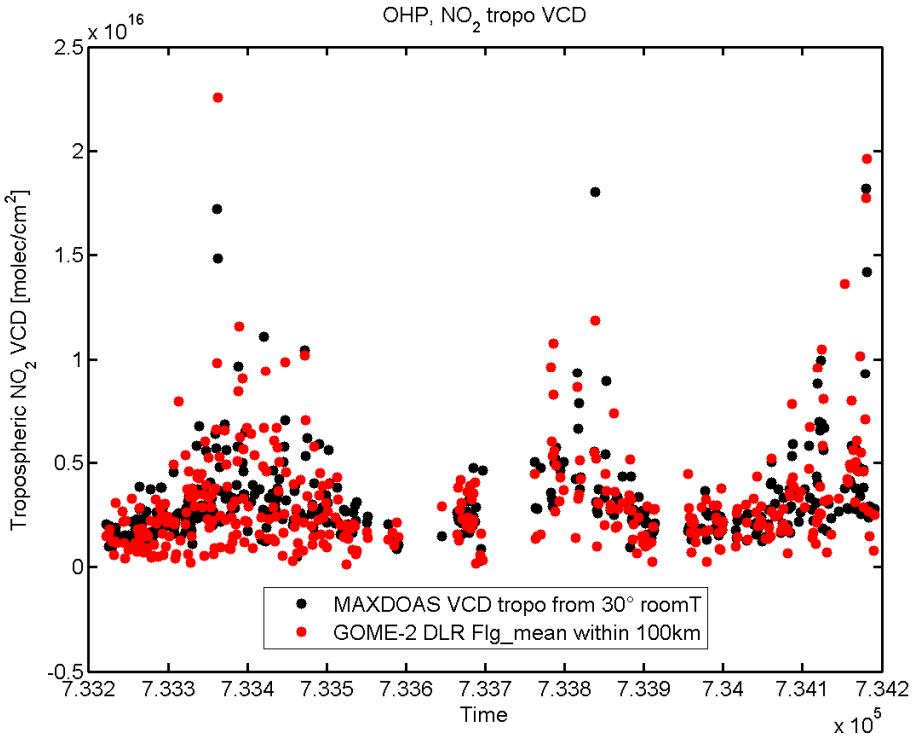

Figure 4.1.9 - Time series of the MAX-DOAS and the GOME-2 GDP tropospheric NO_2 VCD (mean value of all the pixels within 100km around OHP, after flag selection). Period: June 2007 to March 2010.

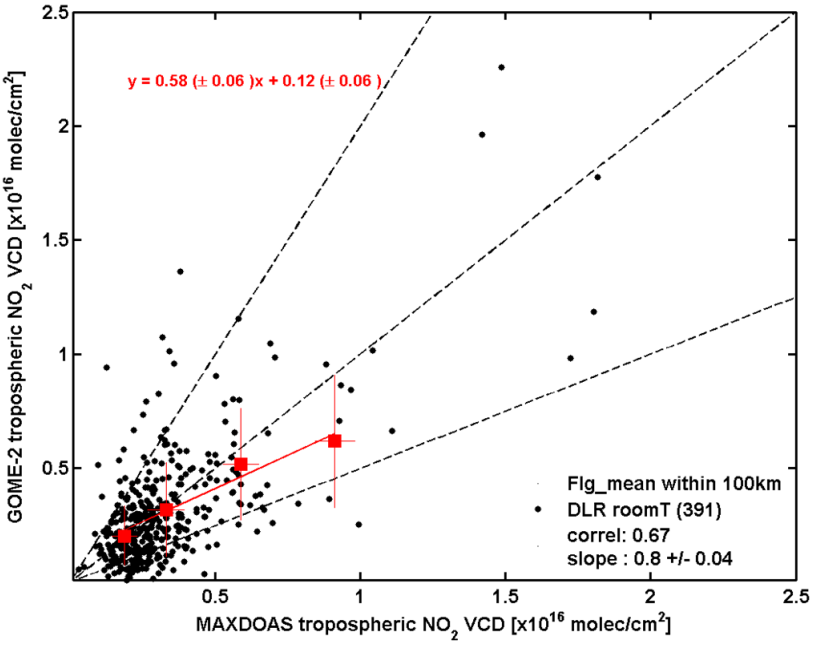

Figure 4.1.10 - Scatter plot of the MAX-DOAS and the GOME-2 GDP tropospheric NO_2 VCD (mean value of all the pixels within 100km around OHP, after flag selection). The black points are all the data, while the red squares are the average in bins of 0.25×10^{16}molec/cm². Information about the correlation coefficient and the slope of the linear regression line are given in the legend, while the equation of the regression line for the averaged data are in red on the top of the figure.

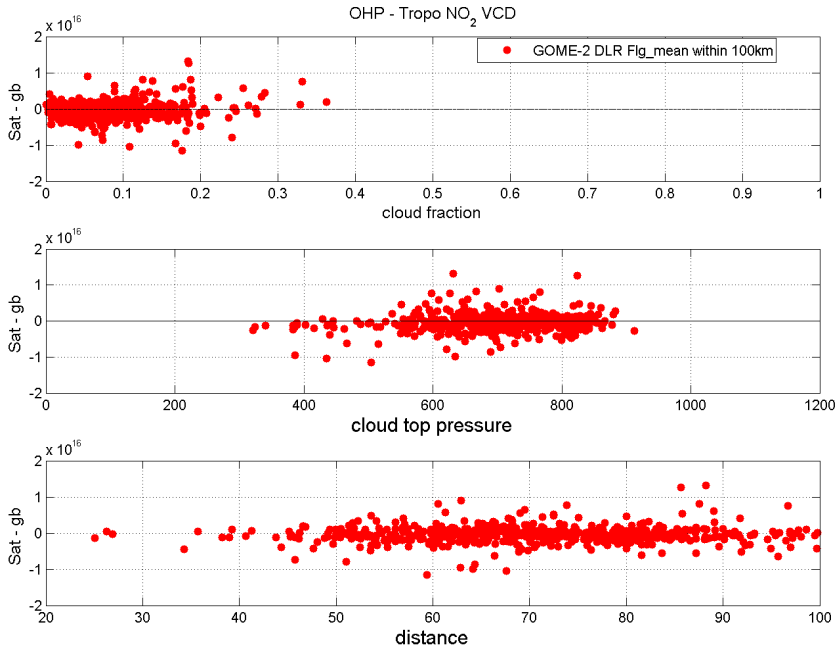

Figure 4.1.11 - Plot of the differences between GOME-2 GDP VCD (mean value of all the pixels within 100km around OHP, after flag selection) and MAX-DOAS tropospheric NO_2, with respect to GOME-2 cloud fraction and cloud top pressure.

Other options of pixel selection have been tested: (i) averaging the ground-based data instead of performing an interpolation at the time of the satellite overpass, (ii) the impact of the choice of the GOME-2 pixels selection (looking to the closest pixel or by taking the mean value of all the pixels within 100km), and (iii) the influence of including or not the back scan pixels in the comparison have been tested. No significant statistical difference is found over the time period studied.

The distribution of difference between the satellite and the ground-based tropospheric data is also investigated in order to verify the behaviour with respect to cloud fraction and height. The results are presented in figure 4.1.11. No anomaly appears, giving confidence in the GOME-2 GDP tropospheric NO_2 retrieval performed up to a cloud fraction of ~35%.

The monthly mean values and their absolute and relative differences have also been studied. The resulting plot for OHP for the period June 2007 to March 2010 is presented in figure 4.1.12. We can see that the seasonal variation is observed similarly by both the MAX-DOAS and the GOME-2 instruments. The differences are generally within ±0.5 10^{15} molec/cm², i.e. within ±50% in relative. Differences of up to 1.8 are observed only occasionally10^{15} molec/cm², like in December 2008 and January 2009. During that period, however, the comparison suffers from a lack of points coming from a ground-based instrumental problem; in October and November 2008 no points (or almost none) are available, and the instrument was fixed and restarted in December 2008.

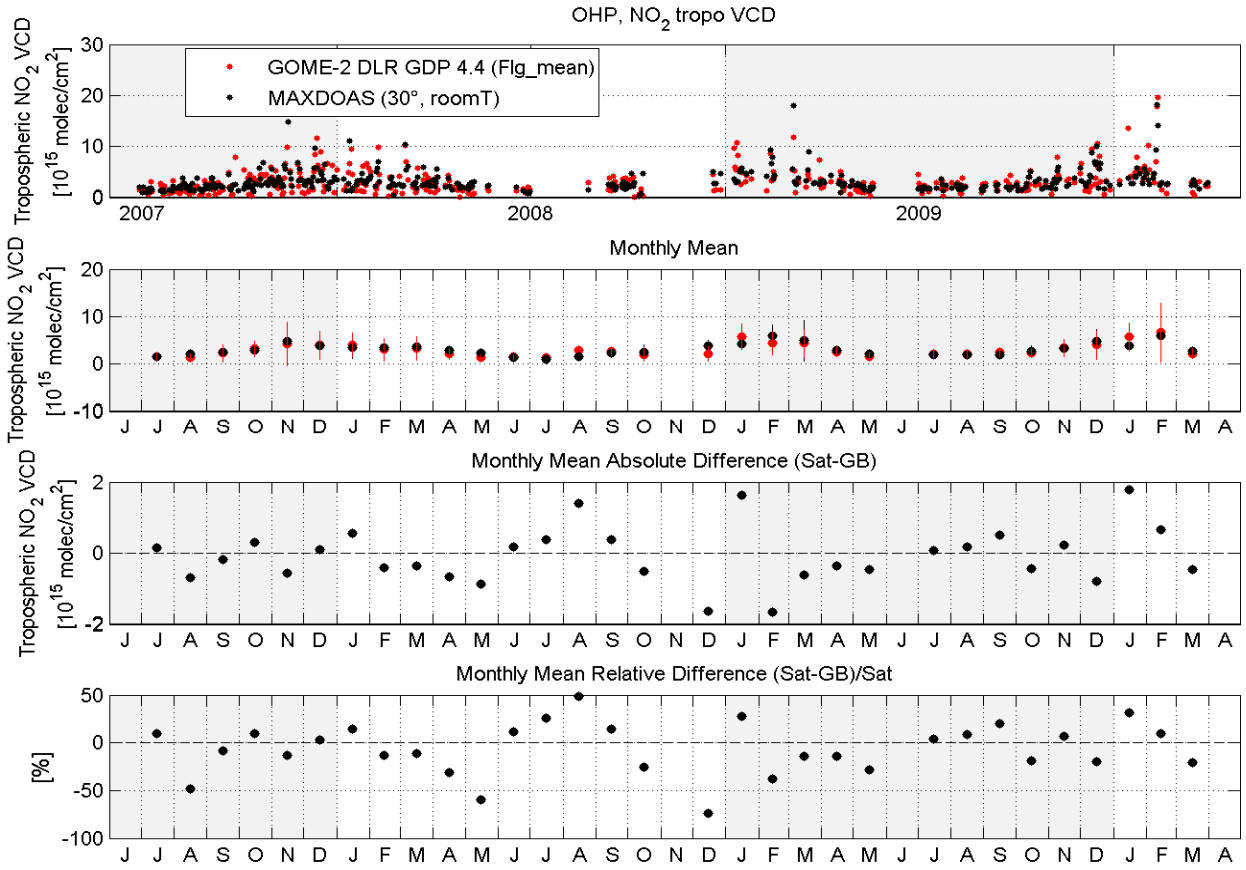

Figure 4.1.12 – Comparison of the time series of the MAX-DOAS and the GOME-2 GDP tropospheric NO_2 VCD (mean value of all the pixels within 100km around OHP, after flag selection) from June 2007 to March 2010. The first subplot represent the time-series (as in figure 4.1.9), the second subplot shows the monthly mean values (with the standard deviation of the points as error bar), and the third and fourth subplots are the absolute and relative difference of the monthly means.

The good global agreement is also highlighted through the correlation plot of the monthly means (see figure 4.1.13): a correlation coefficient of 0.82 and a slope of a linear regression fit of 0.96 are obtained.

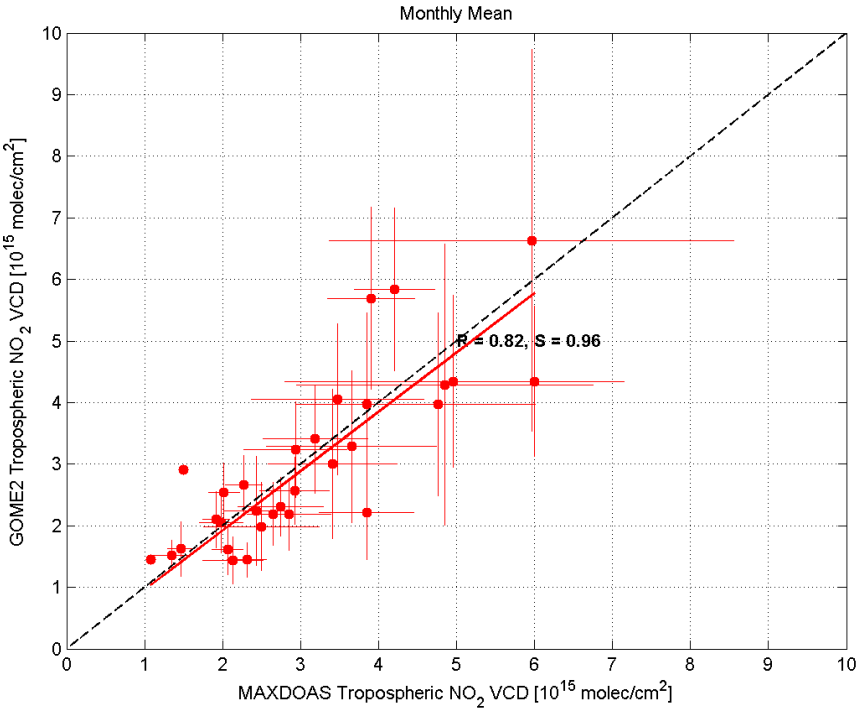

Figure 4.1.13 - Scatter plot of the monthly means MAX-DOAS and GOME-2 GDP tropospheric NO_2 VCD.

For illustration, the same kind of comparison has been computed using OMI NASA/KNMI (AVDC, collection3) data (Bucsela et al., 2006) above OHP. Results of this comparison are presented in figure 4.1.14 and 4.1.15: a similar dispersion in the comparison between the ground-based MAX-DOAS and the satellite data is found, even with larger scatter in the OMI data compared to GOME-2 results. It has to be remembered that OMI do not measure at the same moment of the day than GOME-2, so the two satellite datasets can not be compared directly. However the MAX-DOAS is a good link between them as it measures all along the day, and the data are interpolated at each satellite overpass time (the MAX-DOAS time series in figure 4.1.12 and 4.1.14 are thus not identical neither). Moreover, some differences in the capture of the NO_2 variability from the two satellite instruments can probably be related to the way the selection of the satellite pixels has been done, including the choice of the cloud selection as well as the distance and average criterion, capturing differently the spatial variability. This additional illustration shows that GOME-2 can reproduce the tropospheric NO_2 content at OHP, at least as well as other operational products as OMI NASA/KNMI (AVDC).

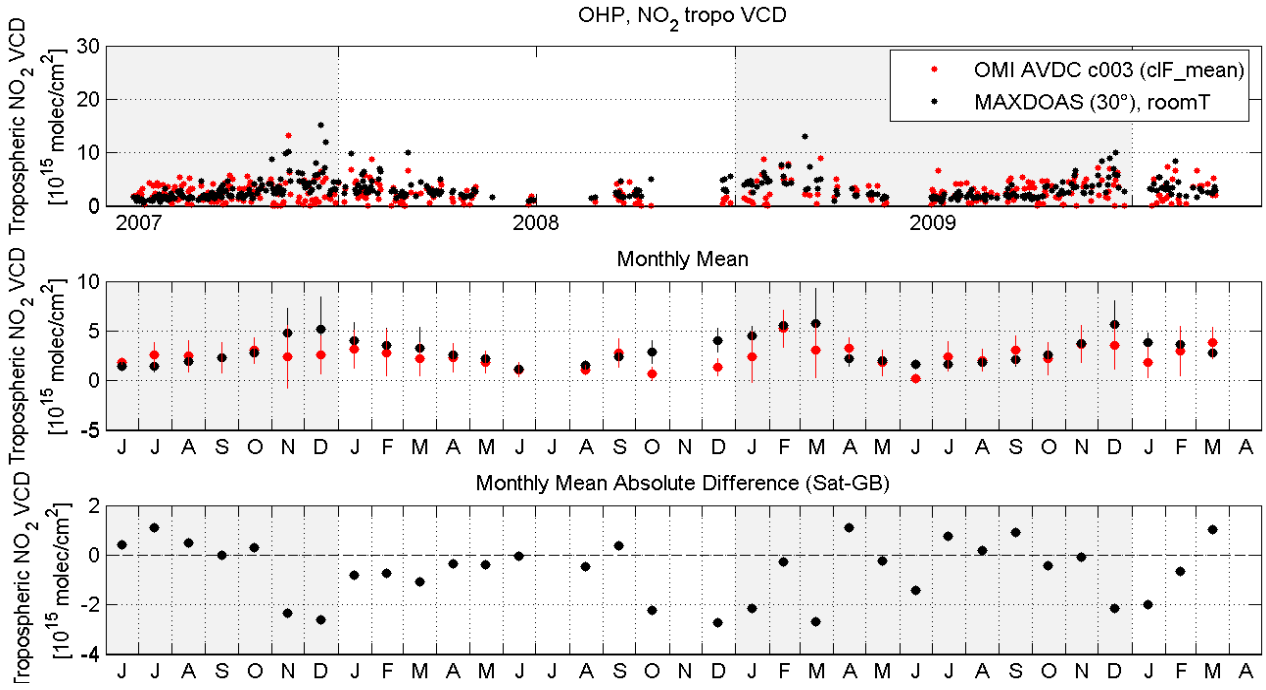

Figure 4.1.14 – As in figure 4.1.12, but for the MAX-DOAS and the OMI NASA/KNMI (AVDC, collection3) tropospheric NO_2 VCD (closest point within 50km around OHP, for cloud free data).

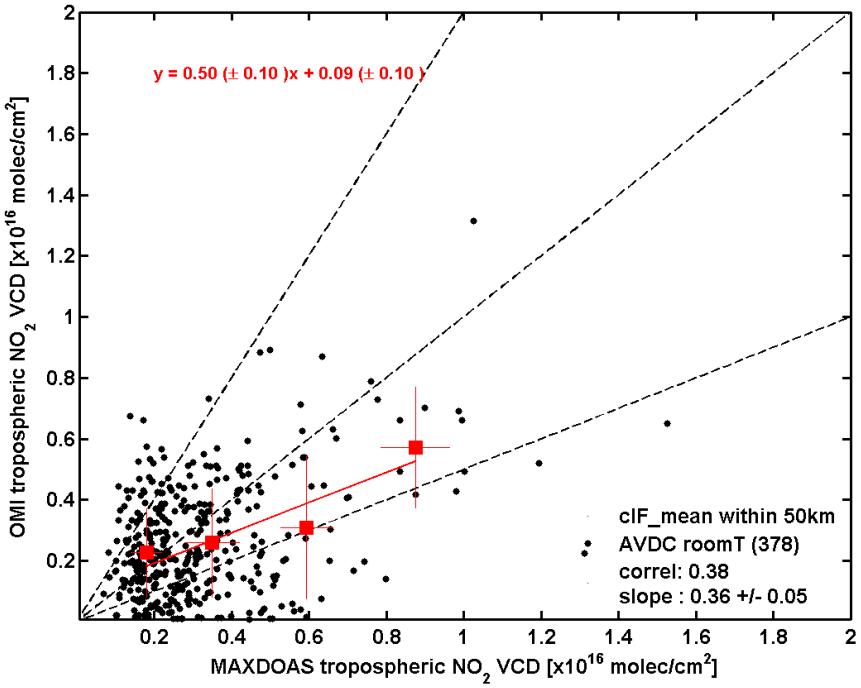

Figure 4.1.15 - Scatter plot of the MAX-DOAS and the OMI NASA/KNMI (AVDC) tropospheric NO_2 VCD (closest point within 50km around OHP, for cloud free data). The black points are all the data, while the red squares are the average in bins of $0.25x10^{16}$molec/cm². Information about the correlation coefficient and the slope of the linear regression line are given in the legend, while the equation of the regression line for the averaged data are in red on the top of the figure.

B.4.2 Comparison with MAX-DOAS observations at Beijing

A MAX-DOAS instrument has been installed by BIRA-IASB in Beijing from June 2008 to April 2009, in the context of the AMFIC[2] project (www.amfic.eu). This location is a very interesting place, in much more polluted conditions compared to the above-described situation at OHP (~ one order of magnitude higher for NO_2) but is also much more affected by aerosols.

The MAX-DOAS instrument in Beijing is a grating spectrometer, covering the UV and VIS range and collecting photons from the horizon to the zenith; more information on the instrument is given in Table 4.2. A detailed description of the instrument can be found in Clémer et al., 2009.

Beijing MAX-DOAS (Visible and UV respectively)	
Spectrometer	ORIEL MS127 and ORIEL MS260 imaging spectrometer
Detector (and T°)	Camera CCD Princeton Instruments/Roper Scientific 1340x100 pixels and 2048x512 pixels, back illuminated, cooled around -50°C
Grating	600 and 1200 grooves/mm
Resolution	1 and 0.45 nm
Wavelength Range	400-700nm 300-390nm
Azimuth direction	Pointing North (-180°)
Viewing geometry	0,2,4,6,8,10,12,15,30 and zenith

Table 4.2.1 - Description of the Beijing MAX-DOAS instrument.

The differential slant columns densities (DSCD) of NO_2 are obtained applying the DOAS technique in the visible (421-470 nm) range and including several other absorbers, like ozone, O_4, Glyoxal and Ring. So far, NO_2 tropospheric columns are obtained from the differential slant columns densities by applying the geometrical approximation, as done at OHP. Only columns retrieved at 30° elevation and that differ less than 30 % to columns obtained from 15° are considered, in order to ensure the validity of the approximation.

In the case of Beijing, the satellite data have been kept only for pixels within 50km, instead of 100km as around OHP. This choice is related to the specific topography around the city: Beijing is surrounded in the north and in the west by mountains (see figures 4.2.1 and 4.2.2). The NO_2 field is thus expected to change very rapidly from the city to the mountains area, as can be seen e.g. in figure 4.2.2, and taking 100km would include satellite pixels over the cleaner mountain region. 50 km seems thus a good compromise between the representativity and the number of pixels.

The time series and the monthly mean are presented in figure 4.2.3, while the scatter plot, the correlation and the slope of a linear regression fit are presented in figure 4.2.4. Figure 4.2.5 shows the correlation plot of the monthly mean values.

[2] AMFIC : Air quality Monitoring and Forecasting In China

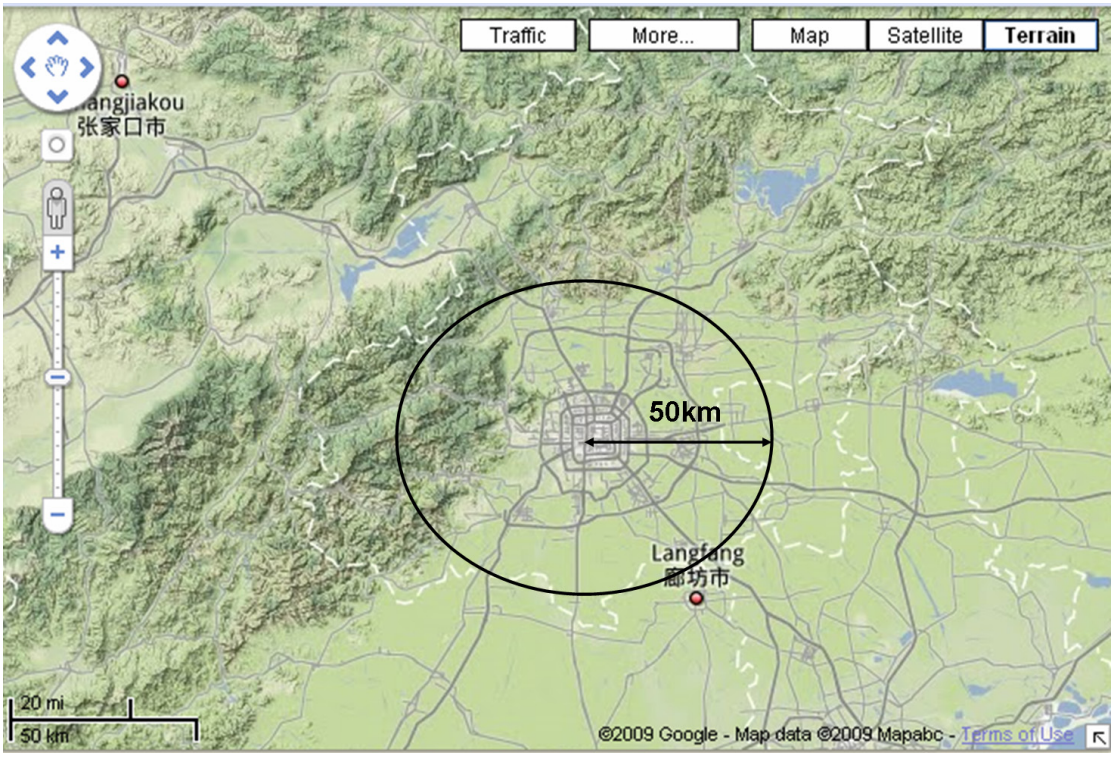

Figure 4.2.1 – Overview of the topography and the roads around Beijing.

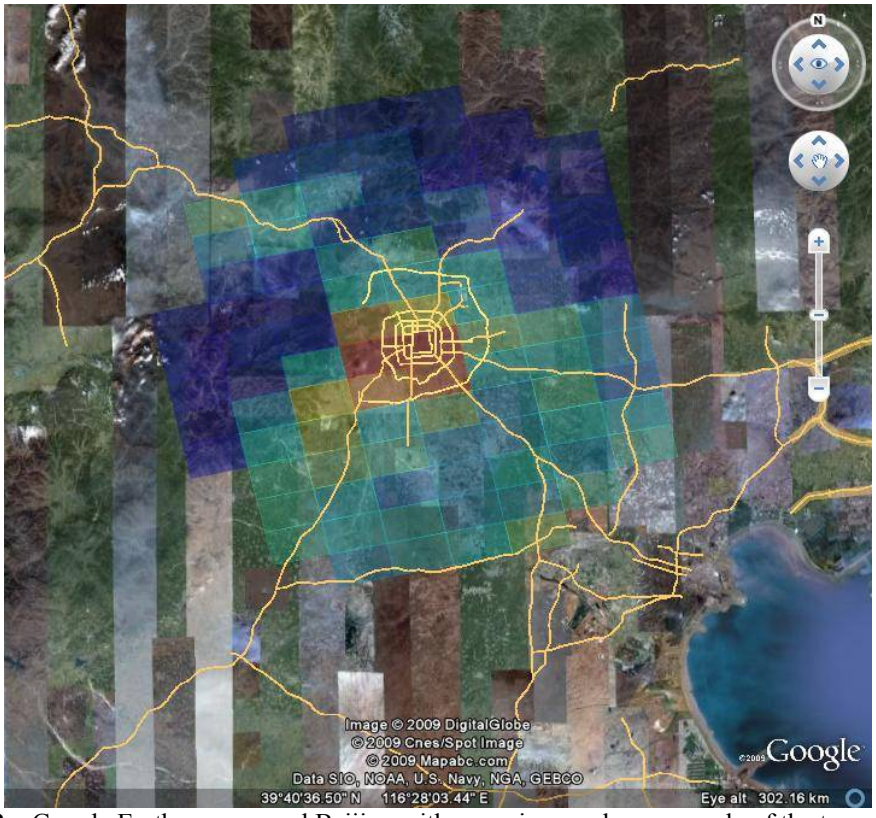

Figure 4.2.2 – Google Earth map around Beijing with, superimposed, an example of the tropopsheric NO_2 gradients as seen by OMI on one day in July 2008.

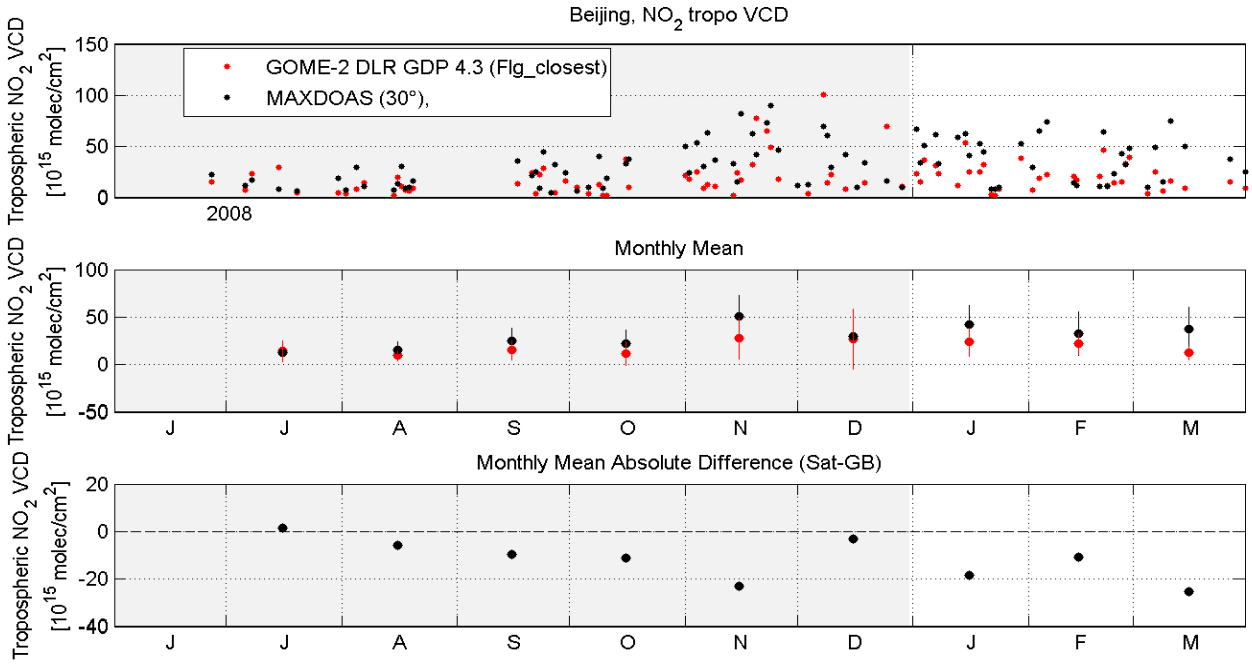

Figure 4.2.3 – As in figure 4.2.12, but for the MAX-DOAS and the GOME-2 GDP tropospheric NO_2 VCD (closest pixel within 50km around Beijing, after flag selection) from June 2008 to end March 2009.

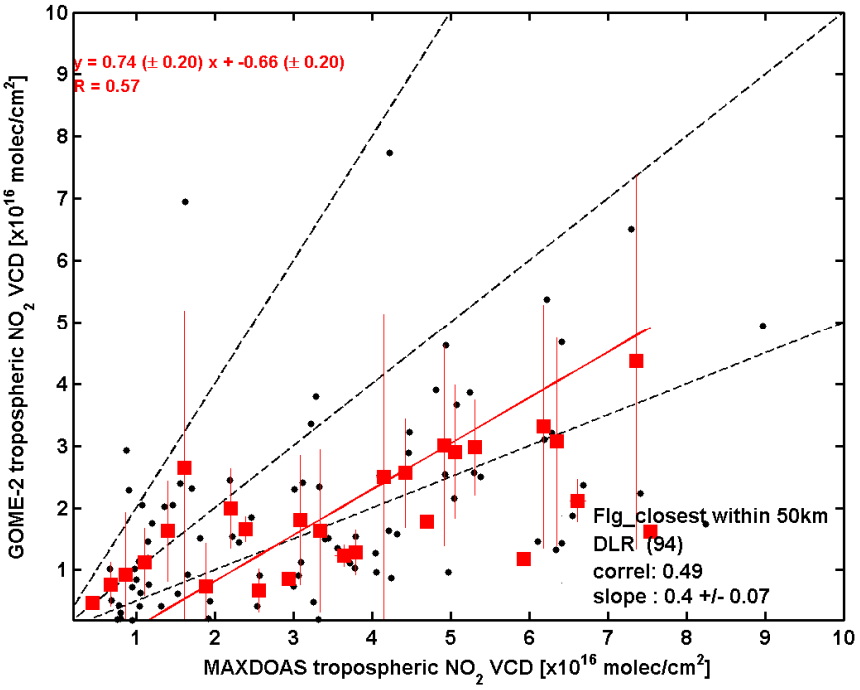

Figure 4.2.4 - Scatter plot of the MAX-DOAS and the GOME-2 GDP tropospheric NO_2 VCD (closest pixel within 50km around Beijing, after flag selection). Information about the correlation coefficient and the slope of the linear regression line are given in the legend.

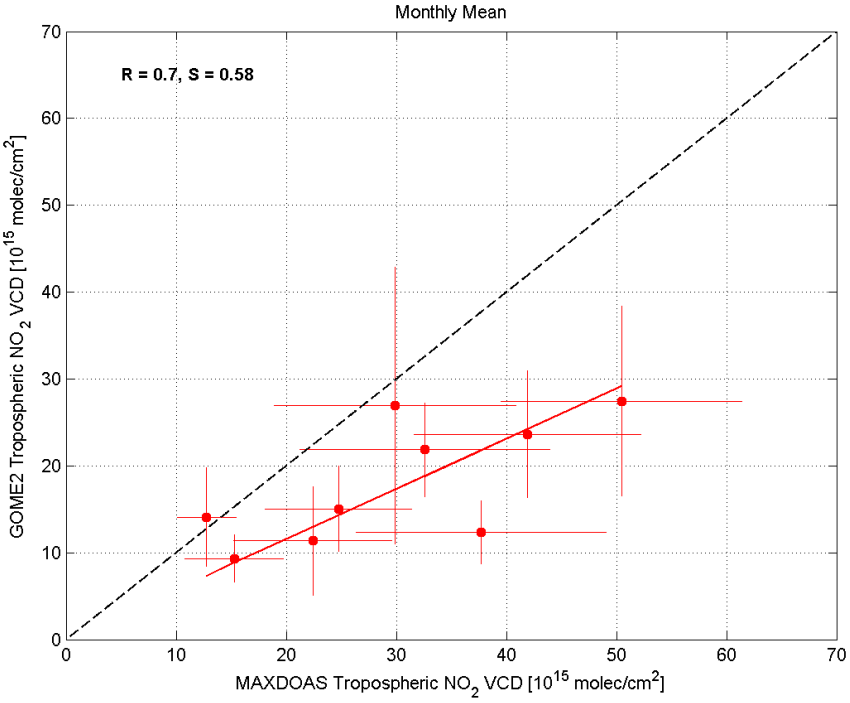

Figure 4.2.5 - Scatter plot of the monthly means MAX-DOAS and GOME-2 GDP tropospheric NO_2 VCD.

From these figures we can see that the seasonal variations in Beijing are reproduced by both instruments and that there is a bias of around 10-20 $\cdot 10^{15}$. Compared to OHP, the differences between the satellite and the ground-based instrument are much larger (up to one order of magnitude), the satellite seeing less NO_2 than the MAX-DOAS. Part of the differences can be explained by the fact that the MAX-DOAS is installed in the city centre of Beijing, and is thus directly sampling the local pollution, that the satellite can not catch.
Furthermore, due to an instrumental problem with the MAX-DOAS in Beijing during the summer 2008, a small number of points are present when the tropospheric NO_2 is lower, and the statistical significance is thus not comparable between the period of low NO_2 (the summer) and of high NO_2 (from October to February).
It should also be mentioned that the columns obtained from the MAX-DOAS are preliminary data, obtained applying the geometrical approximation, but that a more sophisticated retrieval scheme is under development at BIRA, which takes into account the aerosols. An overview of this retrieval scheme is given in a following section (page 60). As Beijing has much larger aerosols loads compared to OHP, the correction of the aerosols is much more important, both for the MAX-DOAS and the satellite retrievals, increasing the uncertainties on the tropospheric NO_2 columns. The presence of large aerosol loads can also reduce the sensibility of the satellite retrieval to the tropospheric content (opacity).

Table 4.2.2 summarizes the results obtained for different selection criterion.

	Closest pixel within flagged data around 50km	Mean of pixels within flagged data around 50km
Interpolation of ground-based data	All points: R = 0.49 S = 0.4±0.07 Bins of trop. Columns: R = 0.57 y = 0.74 x -0.66 Monthly means: R = 0.7 S = 0.58	All points: R = 0.56 S = 0.42±0.06 Bins of trop. Columns: R = 0.56 y = 0.72 x -0.69 Monthly means: R = 0.82 S = 0.54

Table 4.2.2 - Correlation and slope information for different choices of ground-based and GOME-2 (GDP 4.3) pixels selections.

A similar behaviour is obtained when comparing the MAX-DOAS data to the OMI NASA/KNMI (AVDC, collection3) data (Bucsela et al., 2006) above Beijing, as showed in figures 4.2.6, 4.2.7 and 4.2.8:

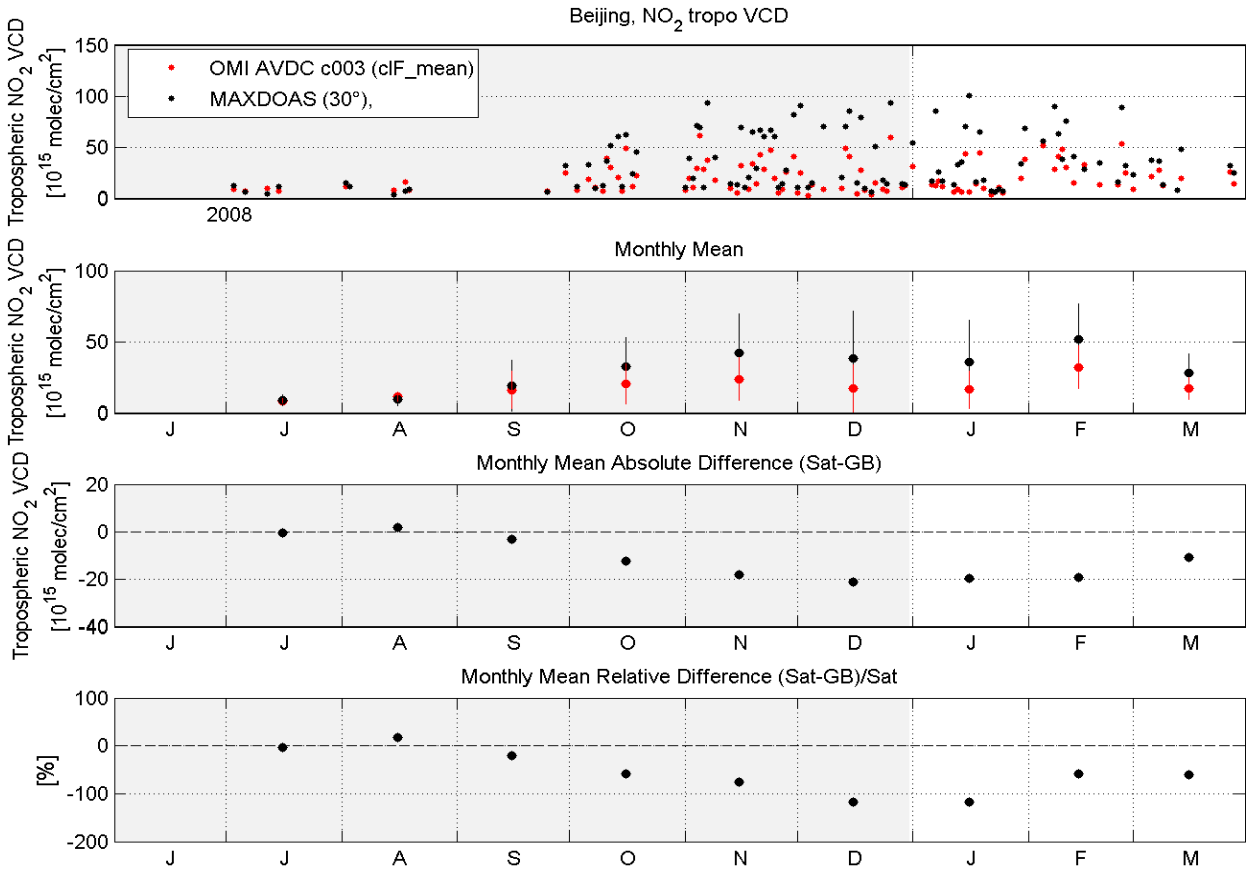

Figure 4.2.6 – As in figure 4.2.11, but for the MAX-DOAS and the OMI NASA/KNMI (AVDC collection3) tropospheric NO_2 VCD (closest point within 50km around OHP, for cloud free data) from June 2008 to March 2009.

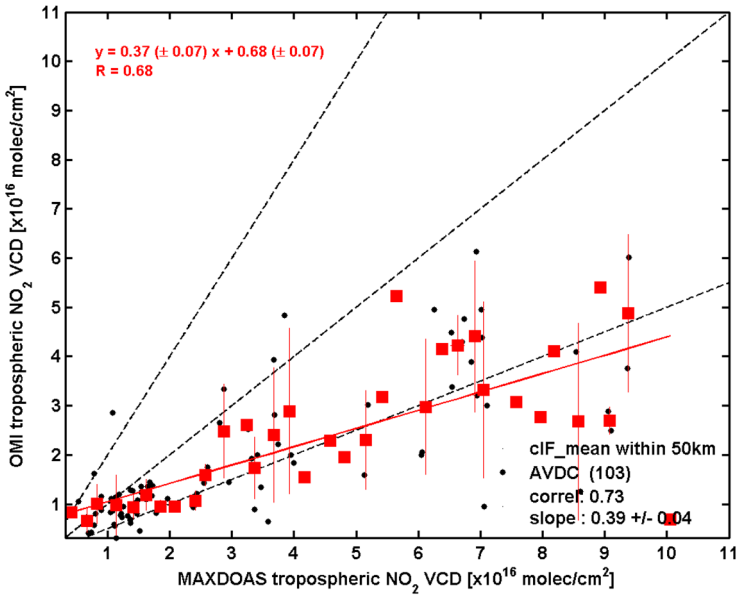

Figure 4.2.7 - Scatter plot of the MAX-DOAS and the OMI NASA/KNMI (AVDC collection3) tropospheric NO_2 VCD (closest point within 50km around OHP, for cloud free data). Information about the correlation coefficient and the slope of the linear regression line are given in the legend.

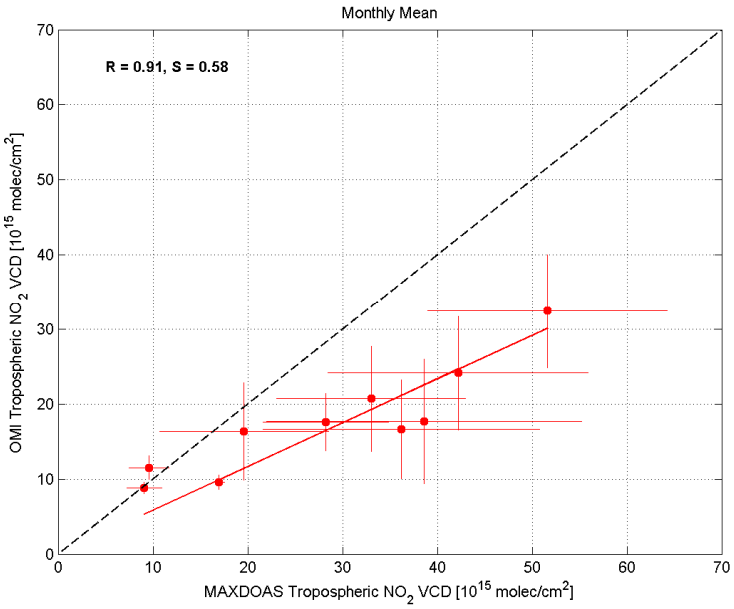

Figure 4.2.8 - Scatter plot of the monthly means MAX-DOAS and OMI NASA/KNMI (AVDC collection3) tropospheric NO_2 VCD.

This additional illustration shows that the comparison and validation with remote-sensing ground-based instruments, such as the MAX-DOAS, is not an easy task around Beijing and the difference of sensibility (due to the location) and the uncertainties in both retrievals leads to much larger differences than in the pilot study around OHP. Additional ground-based MAX-DOAS in other locations are needed to extend the comparison with different pollution cases, in order to cover different NO_2 scenarios, and conclude on the efficiency of the MAX-DOAS for the validation of satellite measurements. However, in order to better understand the quality of the tropospheric NO_2 product of GOME-2 GDP, an additional study involving other satellite products around OHP and Beijing is presented in the following section.

B.5 Comparisons with other satellites tropospheric products

In order to better understand the quality of the GOME-2 GDP tropospheric NO_2 product, an additional study involving other satellite products around OHP and Beijing is presented here.
The following figures (5.1.1 to 5.1.3) present the time series of the monthly mean tropospheric NO_2 retrieved from GOME-2 (GDP and TEMIS products) and from SCIAMACHY (TEMIS product) around OHP (within 100 and 50km) and Beijing (around 50km) from January 2007 to March 2010. The ground-based MAX-DOAS time-series are super-imposed in black in order to make the link with the previous figures of sections B.4.2 and B.4.2. Each figure contains 2 subplots, representing 2 ways of selecting the satellite data: either taking the mean value of only the tropospheric flagged data (as showed in sections B.4.2 and B.4.2), either doing a selection on the cloud fraction (<20%). These two selections do not always give the same results and we have thus chosen to show both cases, the first one being the best selection for each product (tropospheric flag ok) and the second one in order to make a selection that is much equivalent as possible for all the 3 products.

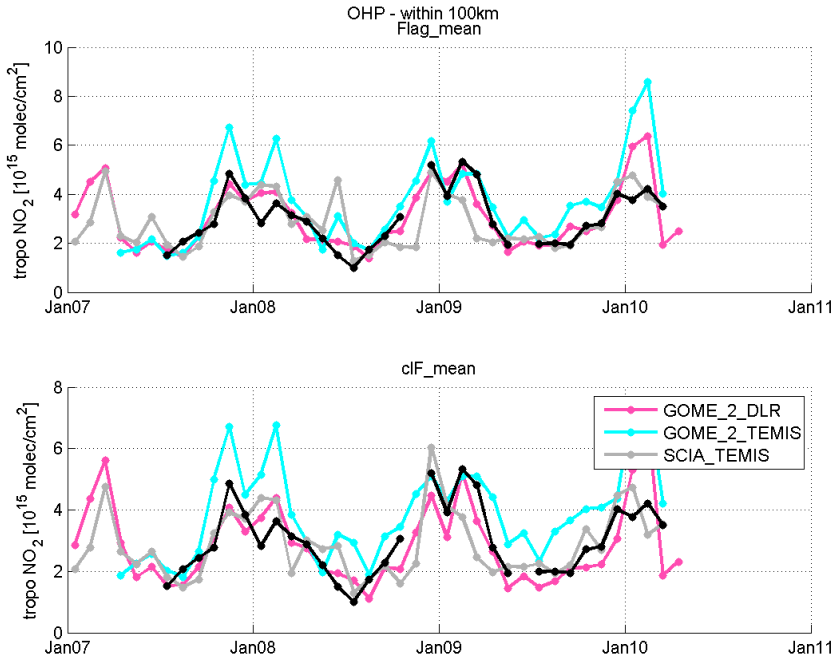

Figure 5.1.1 – Time-series of the monthly means tropospheric NO_2 VCD from January 2007 to March 2010, including GOME-2 data from GDP (magenta curve), GOME-2 data from TEMIS product (cyan curve) and SCIAMACHY data from TEMIS product (grey curve) within 100km of OHP station. MAX-DOAS data (black curve) are also super-imposed.

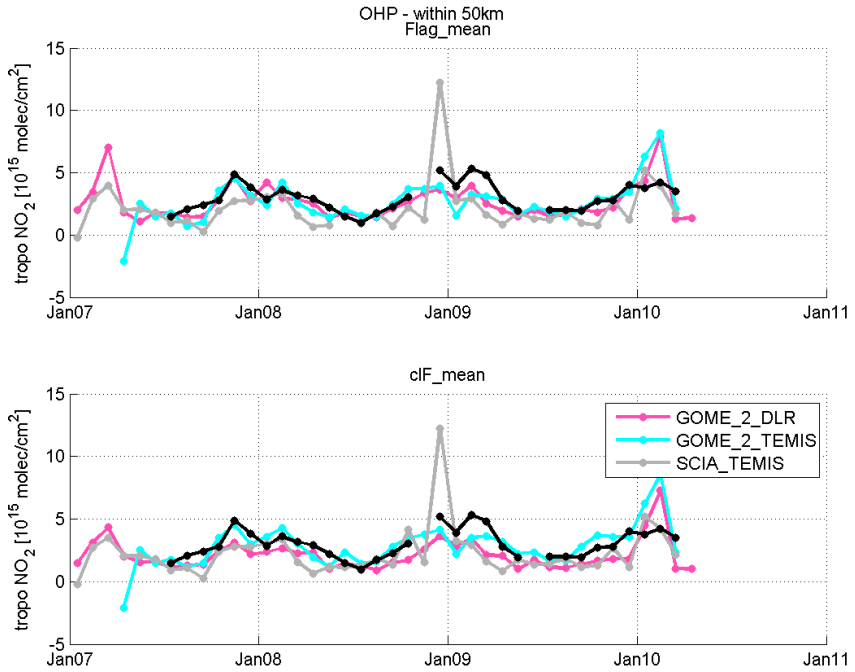

Figure 5.1.2 – Time-series of the monthly means tropospheric NO_2 VCD from January 2007 to March 2010, including GOME-2 data from GDP (magenta curve), GOME-2 data from TEMIS product (cyan curve) and SCIAMACHY data from TEMIS product (grey curve) within 50km of OHP station. MAX-DOAS data (black curve) are also superimposed.

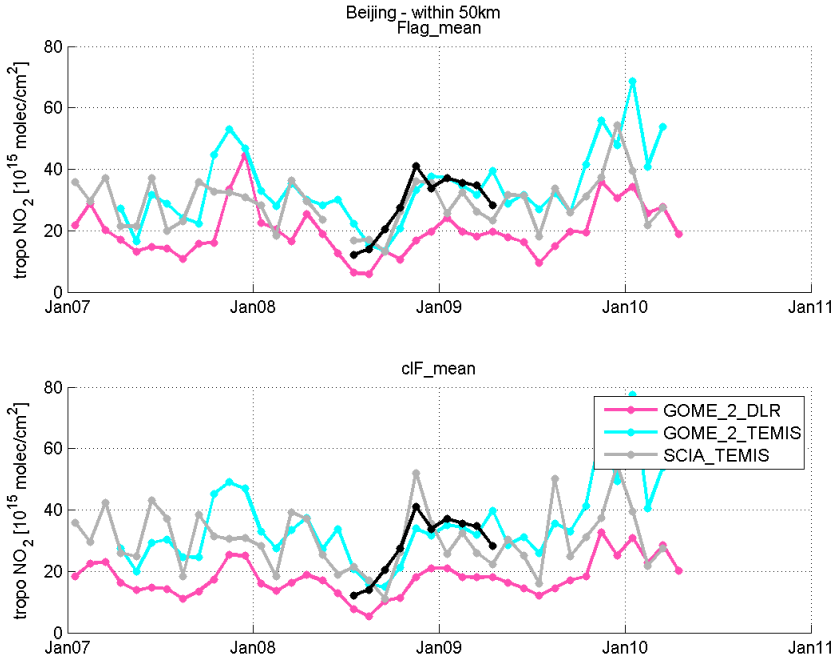

Figure 5.1.3 – Time-series of the monthly means tropospheric NO_2 VCD from January 2007 to March 2010, including GOME-2 data from GDP (magenta curve), GOME-2 data from TEMIS product (cyan curve) and SCIAMACHY data from TEMIS product (grey curve) within 50km of Beijing station. MAX-DOAS data (black curve) are also superimposed.

From these figures, we can see that GOME-2 GDP is in a general good agreement with GOME-2 and SCIAMACHY TEMIS products around OHP and Beijing, reproducing the seasonal variations, but that there are some differences. In Beijing (figure 5.1.3) the GDP product is always smaller than the ground-based and than the TEMIS product, highlighting that it is not just the differences between the two type of measurements, as thought in section B.4.3, but that the choices for the retrieval settings (see table 5.1 for an overview of the differences) plays a large role in Beijing. Moreover, in figure 5.1.1 GOME-2 TEMIS is higher that the other 2 products, and than the ground-based; this is not the case anymore when reducing the radius to 50km around OHP (figure 5.1.2). In order to quantify these deviations, the relative and absolute differences are showed in figure 5.1.4 for OHP (left) and for Beijing (right), both keeping only data within 50km. The differences between the GOME-2 products (red curves) is fluctuating above OHP but is systematic above Beijing. In order to better understand the source of these differences, an "end-to-end" comparison is performed in figure 5.1.5 for OHP (left) and for Beijing (right), comparing also the tropopsheric slant columns and the stratospheric columns.

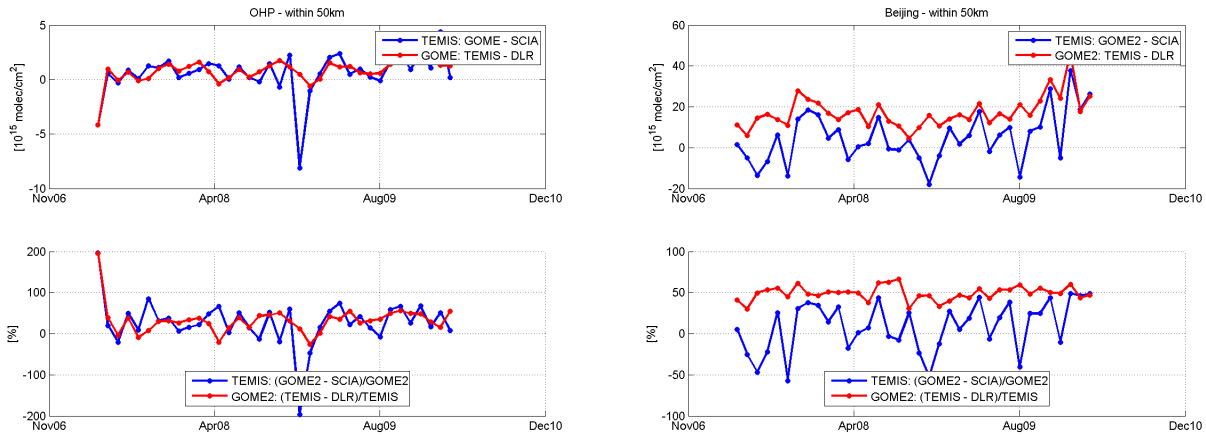

Figure 5.1.4 – Time-series of the relative and absolute differences between the 2 TEMIS products (blue curve) and the 2 GOME-2 products (red curve) around OHP (left) and Beijing (right).

	SCIAMACHY (TEMIS)	**GOME-2 (TEMIS)**	**GOME-2 (GDP)**
SCD retrieval	DOAS retrieval within 426.5-451.5nm	DOAS retrieval within 425-450nm	DOAS retrieval within 425-450nm (GDP 4.3/4.4)
Stratospheric correction	Assimilated NO_2 stratospheric SCD with the TM4 chemistry-transport model	Assimilated NO_2 stratospheric SCD with the TM4 chemistry-transport model	Spatial filtering/ masking of polluted areas
AMF calculation	DAK RTM	DAK RTM	LIDORT RTM
NO_2 a-priori profile	Daily profiles (TM4)	Daily profiles (TM4)	Monthly mean profiles (MOZART-2)
Cloud treatment	Correction based on FRESCO+ cloud retrieval scheme	Correction based on FRESCO cloud retrieval scheme	Correction based on OCRA/ ROCCIN cloud retrieval scheme
Aerosols	Implicitly corrected by cloud treatment		
Albedo	GOME/TOMS database		

Table 5.1 - Main differences between the different satellite tropospheric NO_2 retrievals.

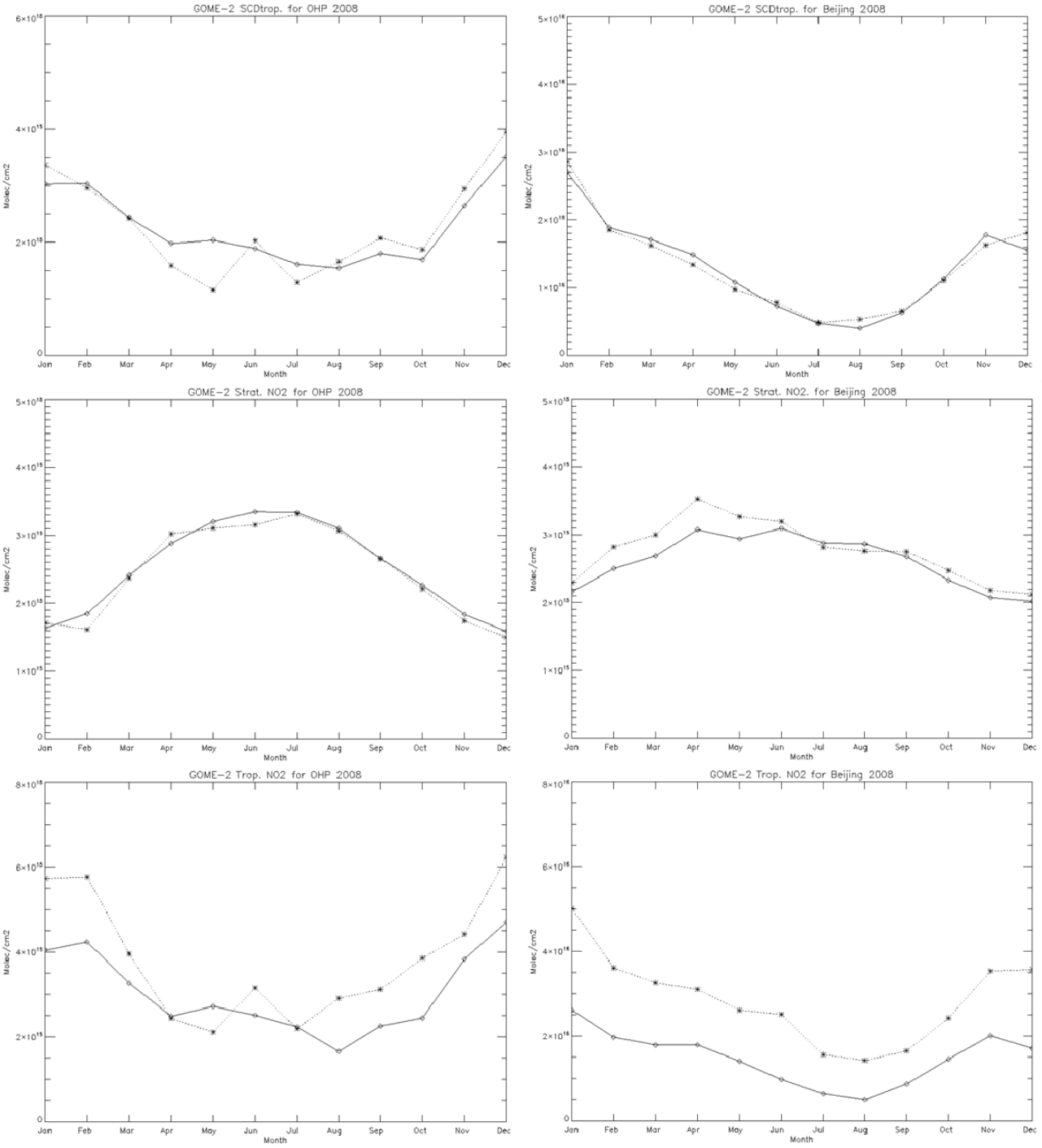

Figure 5.1.5 – Time-series of the tropospheric SCD, the stratospheric VCD and tropospheric VCD of the 2 GOME-2 products (solid line is GDP; dotted line is TEMIS) around OHP (left) and Beijing (right) during 2008.

From figure 5.1.5 we can conclude that the initial total VCDs (= SCD_total / AMF_strat.) for the GDP and TEMIS datasets are very similar. This is as expected, since the DOAS slant column settings for the two retrievals are (almost) the same. Moreover, the different way of calculating the stratospheric component (spatial filtering versus assimilation) does not have a significant impact on the calculation of the tropospheric

NO_2 column for Beijing: SCD_trop (= SCD_total - VCD_strat * AMF_strat) for both datasets are very similar. This is also as expected as in Beijing the tropospheric NO_2 columns are much larger than the stratospheric NO_2 columns. For OHP, the VCD_strat for both datasets are very similar with maximum differences of ~ 2e14 molec/cm^2. However, the tropospheric NO_2 columns for OHP are about 10 times smaller than for Beijing and therefore even these small differences in VCD_strat have a relatively large impact on the tropospheric SCD.

However, the main reason for the (much) larger tropospheric VCD in the TEMIS data for the two locations are related to the large differences between the tropopsheric AMF: over Beijing the mean AMF_trop for GDP is of ~0.85 compared to ~0.45 for TEMIS and over OHP ~0.80 compared to ~0.60. Likely reasons for the differences in AMF_trop are the different CTMs (MOZART2 vs TM4), the different emission catalogues they use, and the differences in cloud retrieval algorithms (OCRA vs FRESCO).

C. CONTINUOUS DEVELOPMENTS FOR THE VALIDATION OF GOME-2 NO_2 COLUMN DATA

C.1 New developments with the MAX-DOAS technique

A retrieval algorithm making use of a more sophisticated method involving radiative transfer modeling of the atmosphere for the conversion from SC to VC is currently under-development at BIRA-IASB [Clémer et al., 2009]. This algorithm also allows for the retrieval of information on the aerosol, which can be used to improve the NO_2 retrievals.
The development of the profiling tool has been performed in the context of the AGACC project (http://www.oma.be/AGACC/Home.html and AGACC_2008 of the end of the 1rst phase). The performance of the algorithm has been tested on simulated DSCD and a preliminary study has been carried out on data of a recent BIRA-IASB MAX-DOAS instrument installed in Beijing, China (40°N, 116.3°E) in June 2008, in the context of the AMFIC project (http://www.amfic.eu/ index.php).
In this section, the developed method for the subsequent retrieval of tropospheric aerosol extinction and NO_2 vertical profiles from MAX-DOAS measurements is briefly described and then the results obtained in Beijing are presented.

C.1.1 Retrieval of tropospheric aerosol extinction and NO_2 vertical profiles from MAX-DOAS measurements: Beijing example

Over the last years, ground-based multi-axis differential absorption spectroscopy (MAX-DOAS) has been proved to be a very promising tool for the automated retrieval of tropospheric pollutants [Wagner et al., 2004; Friess et al., 2006; Wittrock et al., 2004; Irie et al., 2008; Li et al., 2008]. As described in Section B.4.2.1 (page 34), the MAX-DOAS instruments are designed to allow for the quasi simultaneous observation of the scattered sun light in a range of different LOS directions from the horizon to the zenith, resulting in an increased sensitivity towards atmospheric absorbers present close to the surface.

One of the main obstacles for the tropospheric trace gas vertical profile retrievals is the sensitivity of the length of the light path –and thus the observed SCD of an atmospheric absorber– to the presence of aerosol in the atmosphere. To overcome this difficulty BIRA-IASB developed an algorithm to retrieve, in a first step, the aerosol extinction vertical profiles from measurements of the O_4 absorptions for different LOS. In a second step, the obtained aerosol profiles are used as input for the retrieval of tropospheric trace gas (e.g., NO_2) vertical profiles.

To retrieve the aerosol extinction vertical profiles we start from measurements of the differential absorption structures of the oxygen collision complex O_4 for different geometrical configurations (Ω, i.e., the SZA), elevation angle and relative azimuth angle) and wavelength (λ) intervals (for Beijing 2 intervals are used that covers the UV, at 345-365nm, and the VIS region, at 455-500nm). In general, the length of the light path through the atmosphere and thus the observed SCD of an atmospheric absorber depend not only on the concentration of the trace gas but also on the vertical distribution and optical properties of the aerosol present in the atmosphere. Consequently, when the vertical distribution of an absorber is well known [Greenblatt et al., 1990] and nearly constant –the O_4 concentration varies with the square of the O_2 monomer– measurements of the SCD provide information on the aerosol optical properties. Another advantage of O_4 is that it is mainly concentrated close to the surface making the observed O_4 absorption very sensitive to changes in the light path distribution due to the presence of aerosol at low altitudes. Once the aerosol extinction vertical profiles are retrieved, we are able to account for the change in the observed trace gas SCD caused by the presence of aerosol, and we can obtain the vertical profile of NO_2 in the troposphere from the measured NO_2 SCD. We will briefly describe the basic steps of the retrieval algorithm.

The schematic of the retrieval algorithm is depicted in Fig. 6.1.1.

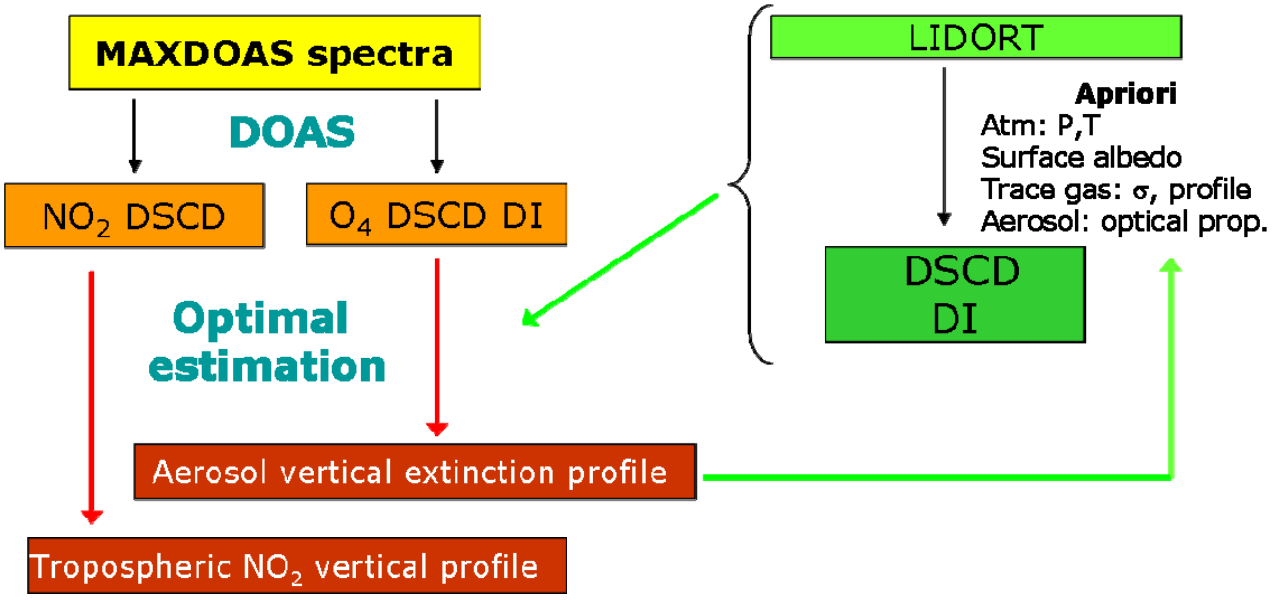

Figure 6.1.1 – Schematics of the algorithm for the retrieval of the vertical profiles of tropopsheric NO_2 and aerosols extinction. The DOAS method is applied to transform the spectral information into DSCD. The profiles are retrieved using optimal estimation for the inversion in combination with the radiative transfer code LIDORT. The aerosol profiles are retrieved first so they can be used as input for the forward model during the NO_2 profile retrievals.

The retrieval of NO_2 vertical profiles consists of two successive steps. Firstly the aerosol vertical extinction profile is retrieved and secondly the tropospheric NO_2 vertical profile is retrieved based on the obtained information on the aerosol. For both steps, the SCD of O_4/NO_2 for the different geometries and wavelength intervals need to be obtained from the measured spectra of scattered sunlight. This can be done with the so-called DOAS technique using a linear/nonlinear least-squares spectral fitting method [Platt, 1994]. Figure 6.1.2 shows the O_4 and the NO_2 DSCD ($DSCD=SCD_{off\text{-}axis}-SCD_{zenith}$) obtained from the UV window (~360nm) for the different elevation angles measured in Beijing on a clear-sky day (04 December 2008).

Now we want to retrieve the vertical profiles from the measured DSCD. To this aim we used the optimal estimation method as inversion method [Rodgers, 2000]. The forward model, describing the physics of the measurement, used here is the linearized discrete ordinate radiative transfer model (LIDORT) [Spurr et al., 2001; Spurr, 2002]. One major advantage of this code is that it includes an analytical calculation of the weighting functions needed for the inversion step. Consequently the algorithm is relatively fast, which is a major advantage when one aims for real-time automated retrievals. In case of the NO_2 profile retrieval, the aerosol extinction profile, retrieved in a previous step from the O_4 DSCD in the same wavelength interval as the NO_2 DSCD, is used in the forward model to properly account for changes in the light path cause by aerosol. More information on the algorithm can be found in [Clémer et. al, 2009].

As a first test we used the algorithm to retrieve aerosol extinction and subsequently NO_2 vertical profiles from the MAX-DOAS spectra measured in Beijing during the period November 2008 – March 2009. Figure 6.1.3 shows the time series of the daily average of the retrieved tropospheric NO_2 column. For comparison the tropospheric NO_2 columns calculated using the geometrical approach based on the measured NO_2 DSCD at 30° and 15° elevation are shown. The tropospheric NO_2 columns are calculated from the retrieved tropospheric NO_2 profiles.

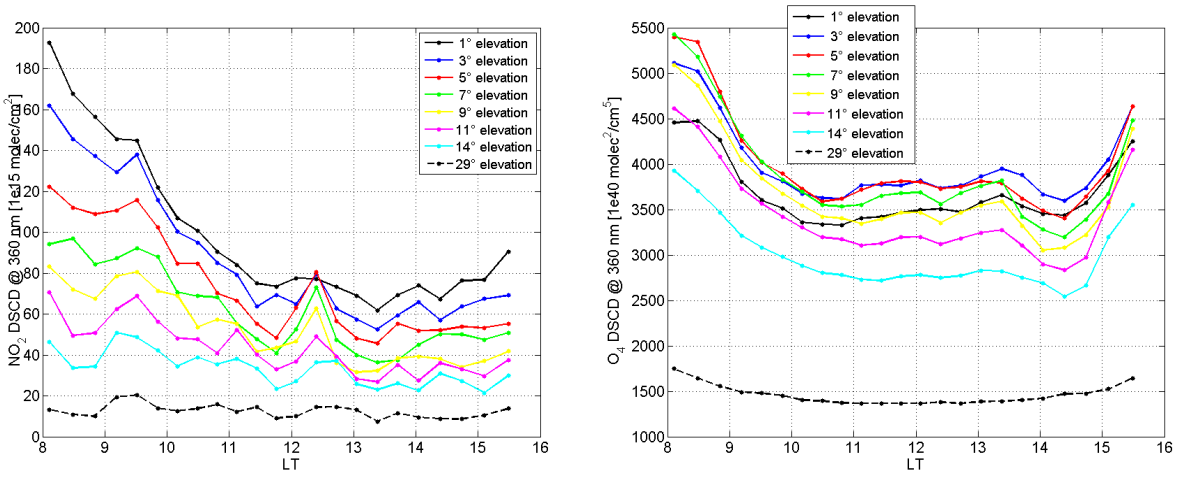

Figure 6.1.2 - The DSCD ($SCD_{off\text{-}axis}$-SCD_{zenith}) obtained from the 345-365nm window of the MAX-DOAS spectra for the different elevation angles (different colours) in Beijing on the 4th of December 2008. The O_4 DSCD are shown on the right and the NO_2 DSCD on the left.

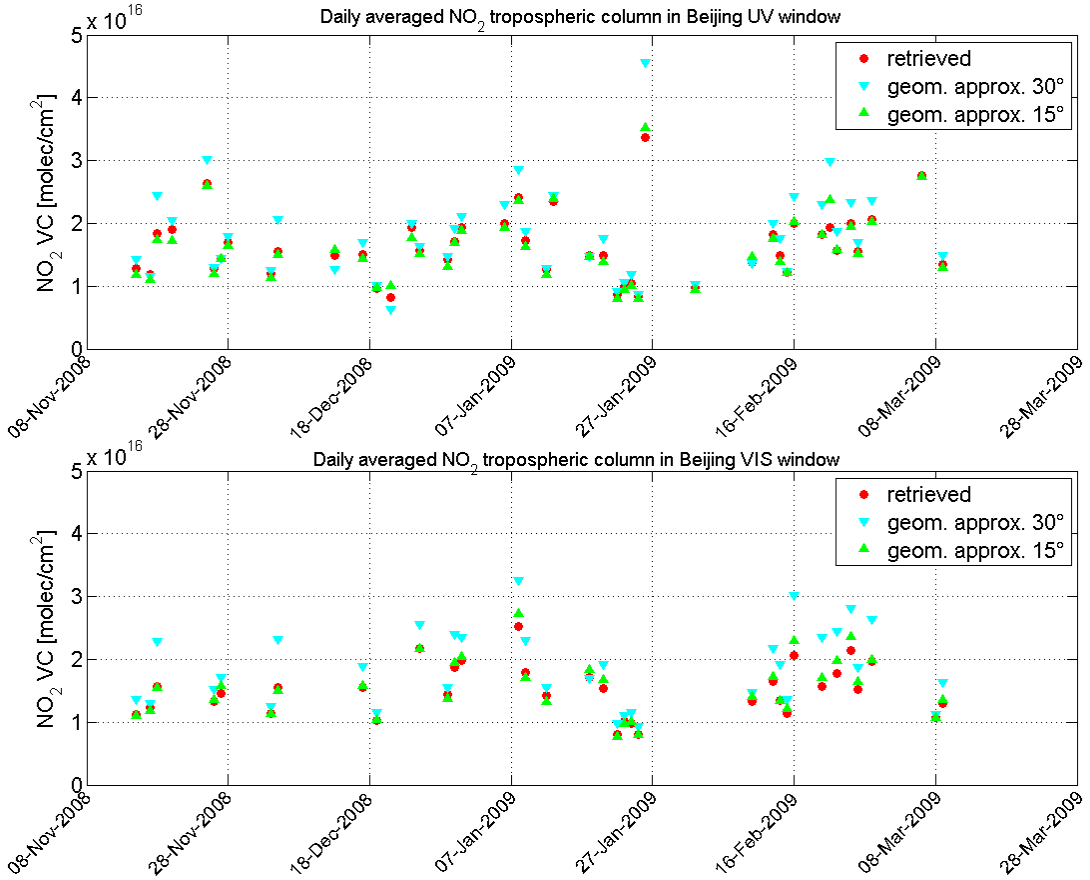

Figure 6.1.3 - Time series of the daily average of the tropospheric NO_2 column in Beijing retrieved using the profiling tool (red) and using the geometrical approximation based on the NO_2 DSCD measured at elevation 30° (cyan) and 15° (green). The upper plot is in the UV window while the lower plot is the results from the VIS window.

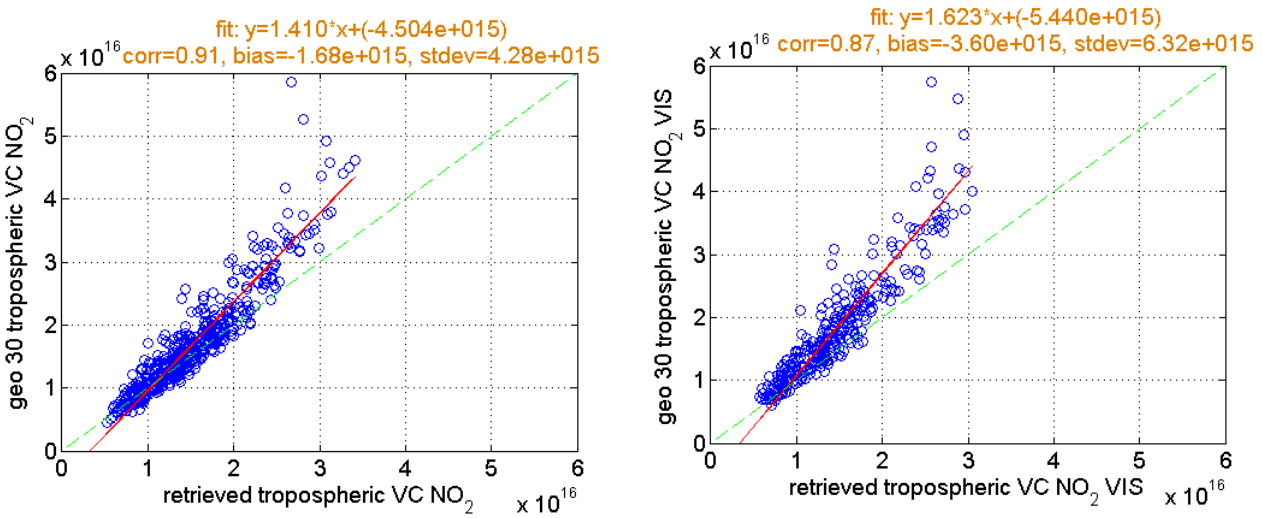

Figure 6.1.4 - Scatter plots of the tropospheric NO2 vertical columns retrieved using the profiling tool versus the vertical columns obtained using the geometrical approach (30° elevation) from the NO_2 DSCD in the UV window (left) the VIS window (right). Also shown are the linear regression fits and the corresponding statistical parameters (correlation coefficient, bias, and standard deviation).

The scatter plots shown in Fig. 6.1.4, comparing the NO_2 vertical columns obtained using the profiling tool and the geometrical approach (based on the NO_2 DSCD measured at 30° elevation) reveals a good correlation between the vertical columns obtained using these two methods.

The negative bias observed is probably related to the usage of an a-priori NO_2 vertical profile in the optimal estimation step deviating too much from the "real" profile (the vertical column of the a-priori used was quite small, i.e. ~0.5e15 molec/cm²) in combination with the low sensitivity of the profiling tool towards NO_2 present at higher altitudes (over 1km).

These first results indicate that the retrieval technique is very promising as good correlations are obtained but that more efforts are needed to choose the best settings for the inversion step. Choosing a more appropriate NO_2 a-priori profile, for example based on the NO_2 vertical column obtained using the geometrical approach, will most likely result in a reduction of the bias.

The retrieval algorithm does not only provide total tropospheric NO_2 columns but also profile information. To illustrate the power of the retrieval algorithm the full NO_2 profiles retrieved at 14h local time on a clear-sky day in December (04-Dec.-2008) are shown in Figure 6.1.5. In addition the comparison of the NO_2 DSCD measured and simulated using the retrieved NO_2 profile for all elevation angles is shown. In both wavelength intervals the simulated DSCD very well fit the measured DSCD. The difference between the NO_2 profiles retrieved in the UV (blue) and in the VIS (red) can partially explained by the different sensitivity of the retrieval in these two wavelength regions. The degree of freedom is larger for the UV allowing the retrieved profile more freedom to deviate from the a-priori profile.

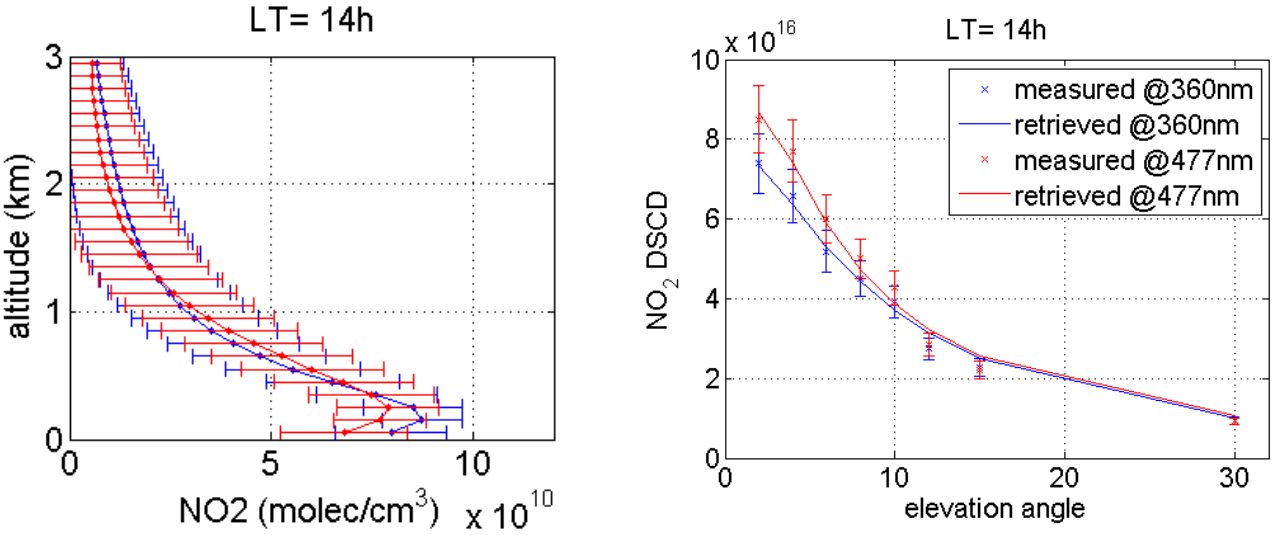

Figure 6.1.5 - Left: Example of the retrieved NO_2 profiles from MAX-DOAS measurements in the UV (blue) and VIS window (red) at 14h local time on the 4th of December 2008 in Beijing. The error bars are the retrieval errors. Right: measured NO2 DSCD (symbols) and DSCD simulated (solid lines) using the NO2 profiles shown on the left.

To conclude, the extension of the MAX-DOAS retrieval technique (from a geometrical approximation to the more sophisticated algorithm described above) is very promising. First results from the Beijing instrument show that information on aerosol can be retrieved from the MAX-DOAS instrument, that good correlations can be obtained for the tropospheric NO_2 vertical columns compared with the geometrical approximation and that the retrieval of low tropospheric NO_2 profiles is possible in several wavelength regions.
However, more efforts are still needed to select the best settings for the inversion step: choosing a more appropriate NO_2 a-priori profile, for example based on the NO_2 vertical column obtained using the geometrical approach, should improve the retrieval. This topic is under investigation at BIRA-IASB and the extension of this preliminary study done in Beijing to other locations, as OHP and possibly Brussels, is planned.
This would help in the validation of tropopsheric NO_2 of GOME-2, by improving the ground-based retrieval algorithm and making the time-series of tropopsheric columns more consistent, but also enabling the access to the vertical distribution of the NO_2 in the low troposphere.

C.2 Comparison with CHIMERE model

A further aspect proposed in the CDOP work-package 3190 is to test the sensitivity of GOME-2 data to the lower troposphere and its ability to detect geographical patterns accurately. This involves chemical-transport tools operational at BIRA-IASB and RMI and their development for specific studies performed within the O3M-SAF context.

The idea is to make use of modelling results to generate tropospheric NO_2 columns above Belgium and Europe and compare them to GOME-2 retrieved values. By means of results from the chemical transport model CHIMERE and of surface network data (e.g., from the IRCELINE network in Belgium), a correlative study of the GOME-2 perception of geographical patterns in the tropospheric NO_2 field is envisaged. Furthermore, the sensitivity of GOME-2 to high-resolution NO_2 spatial features can be investigated. This involves exploring resolution issues, e.g. NO_2 tessellation within the GOME-2 footprint at full resolution and reproducing the scene as it is seen by GOME-2.

In this section, the CHIMERE model is first shortly presented, including some evaluation of the model by comparison to in-situ NO_2 data in Belgium. Secondly, a preliminary comparison of the CHIMERE tropopsheric NO_2 results and the MAX-DOAS instrument at OHP is presented. Then, CHIMERE is used to reproduce the MAX-DOAS and GOME-2 scene, and the ratio of the modelled data is applied as a correction factor in the comparison.

C.2.1 The CHIMERE model

The chemical transport model (CTM) Chimere (Vautard et al., 2001) is able to model NO_2-concentrations for 8 different layers (or more) until an altitude of 500 hPa. Some characteristics of the CHIMERE model:

- The domain of the model is covering Europe (-10.5W, 22.5E, 35 N, 57.5N)
- It's resolution is 0.5 x 0.5 (~ 50 km²)
- The meteorological input used is from ECMWF (European Centre for Medium-Range Forecasts)
- The emission database used is from EMEP (Vestreng, 2003)

The CHIMERE model has been installed at RMI and NO_2-data has been modelled over the period from February 2007 to December 2009. A tropospheric NO_2 reference dataset is thus now available and can be easily adjusted in time as a function of the needs of the NO_2-validation team (BIRA-IASB).

In order to evaluate the performance of the modelled data, some statistics has been calculated for four stations in Belgium over the first one-year period (from 03-2007 to 02-2008). In Figure 6.2.1 an example of a validation study of observed- against modelled NO_2-data is shown for the station of Houtem.

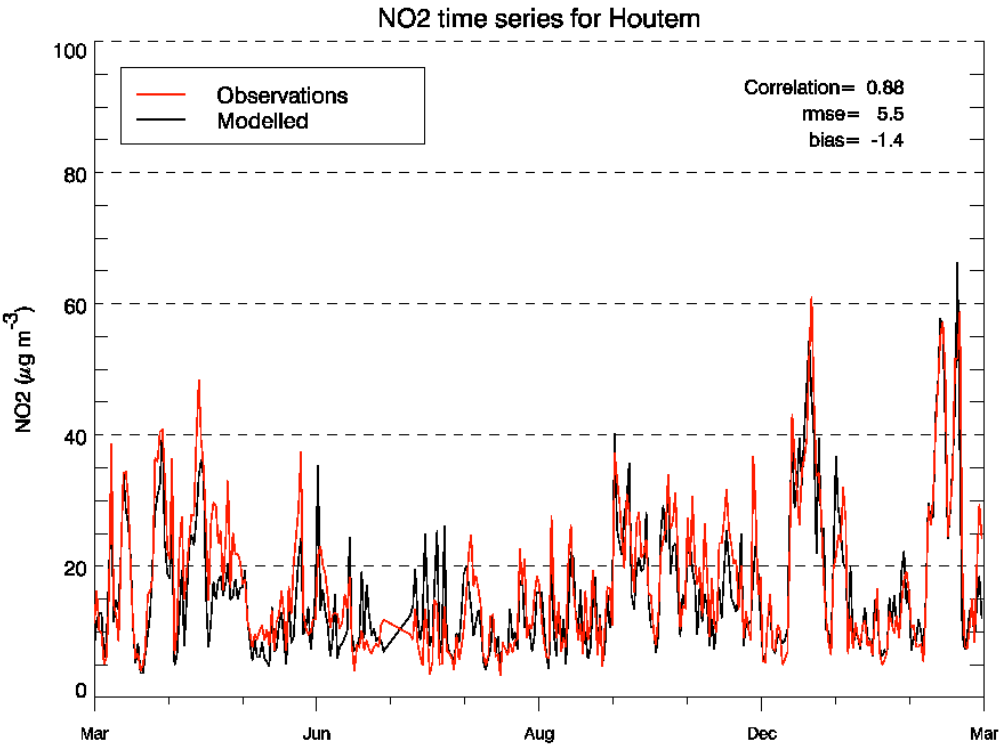

Figure 6.2.1 - Time series of modelled- and observed averaged daily mean NO_2-concentrations, during the time period 01/03/2007 - 9/02/2008.

The same evaluation has been performed for three other Belgian reference stations (WP2). The statistics are summarized in Table 6.2.1.

Station	Correlation	RMSE	Bias
Ukkel	0.78	12.8	-6.7
Dessel	0.68	8.4	-2.0
Moerkerke	0.85	6.3	-0.5
Houtem	0.88	5.5	-1.4

Table 6.2.1 - Bias, correlation and rmse for the time period 01-03-2007/29-02-2008.

C.3.2 Pilot study: CHIMERE around OHP

The CHIMERE dataset has been extracted over OHP (by interpolating the neighbouring cells) and comparisons with the MAX-DOAS columns have been performed for the period from June 2007 to December 2009 (figure 6.2.2). A relatively good agreement between the time-series is found, with the MAX-DOAS showing some higher variability in the background conditions and some significant differences during large pollution episodes.

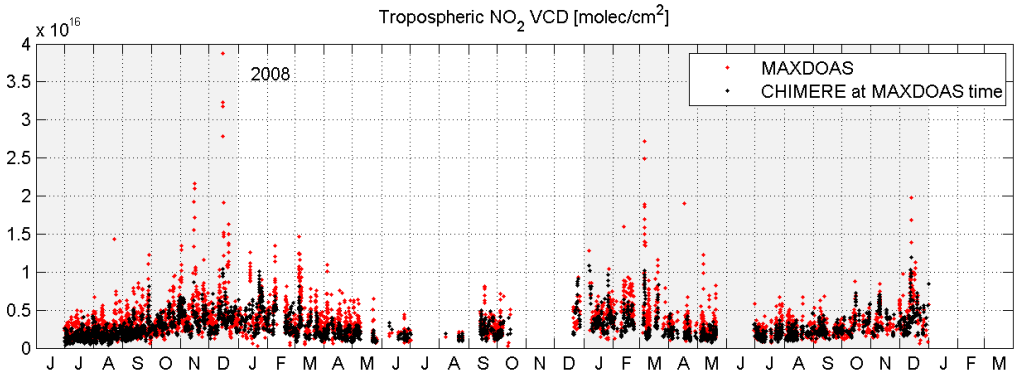

Figure 6.2.2 - Time series from June 2007 to December 2009 of modelled and observed tropospheric NO_2 columns, respectively from the CHIMERE model and the MAX-DOAS instrument.

The CHIMERE dataset has then been used around OHP to explore the sensitivity of GOME-2 to high-resolution NO_2 spatial features, and to make the link between the different horizontal sensitivities of the MAX-DOAS and the satellite pixel. Considering that a GOME-2 pixel horizontal dimensions is ~40x80km² (latitude x longitude) and a CHIMERE cell is 0.5°x0.5° (which at the OHP latitude is 55km x 55km*cos(45°), i.e. ~55x38km²), and depending on the relative position of the satellite pixel to the CHIMERE grid cells, several CHIMERE cells should be averaged in order to represent the spatial averaging performed by the satellite. An example involving 6 CHIMERE cells for one GOME-2 pixel is showed in figure 6.2.3 for a particular day in July 2007.
The idea is to calculate for every day the value seen by CHIMERE on the corresponding GOME-2 pixel and at the OHP location and to use this ratio as a correction factor for the collocation difference between the satellite and the ground-based measurements. The CHIMERE column as seen by GOME-2 is reconstructed by weighting the CHIMERE NO_2 columns with the area covered by the GOME-2 pixel, and summing over each polygon. For the MAX-DOAS, an interpolation at the OHP coordinates is performed between the neighbouring cells.
As can be seen in figure 6.2.4, presenting the scatter plot of the GOME-2 and the MAX-DOAS NO_2 tropospheric columns, this correction for the collocation difference improves slightly the comparison between the two measurements, reducing slightly the scatter and modifying the correlation coefficient from 0.63 to 0.71 and the slope of the linear fit from 0.69 to 0.73.

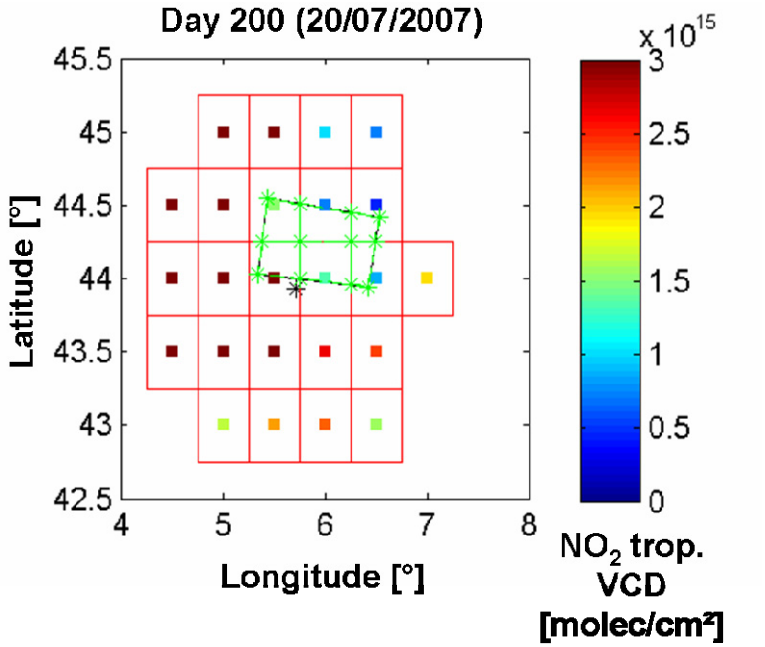

Figure 6.2.3 - Example of the spatial distribution of the tropospheric NO_2 obtained by the CHIMERE model (coloured squares) around OHP (the black * in the figure) and the position of the closest GOME-2 pixel (green rectangle) on the Julian day 200 (20/7/2007).

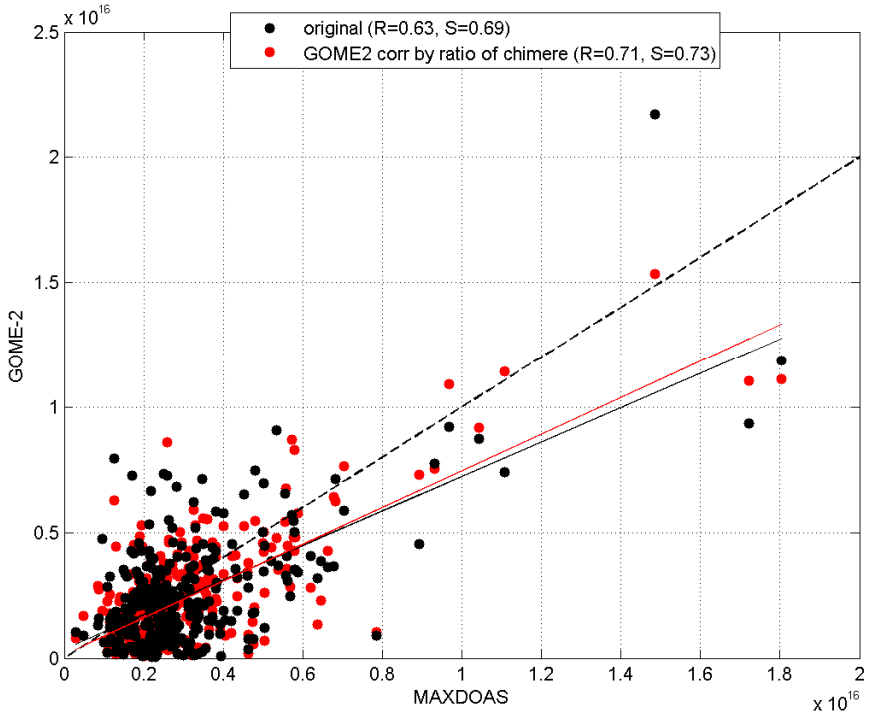

Figure 6.2.4 – Scatter plot of the closest GOME-2 pixel and the MAX-DOAS tropospheric NO2 columns over OHP. The black dots are the original comparisons, as described in Sect. B.4.2.3, and the red dots are the corrected GOME-2 data for the collocation error calculated with the CHIMERE model.

D. CONCLUSION AND PERSPECTIVES

This document reports on the validation of O3M-SAF GOME-2 NO_2 column data products retrieved at DLR with versions 4.3 and 4.4 of the GOME Data Processor (GDP), using reprocessed level-1B-R1 data based on level-0-to-1B processor version 4.0/4.1. The complexity and the "residual principle" of the tropospheric NO_2 retrieval algorithm, as well as the very small number of validation sources for tropospheric NO_2, necessitate the adoption of an end-to-end validation approach. The latter consists in a separate validation of the individual components of the retrieval chain.

A first part of the document, devoted to studies of the DOAS analysis results, gives the following conclusions:

- GOME-2 slant columns: GDP 4.3 DOAS fit results match requirements.
- DOAS fit residuals are comparable to those of ERS-2 GOME; However, the DOAS fit residual and NO2 slant column error increase with time as a result of the GOME-2 instrument degradation.
- Reprocessed GOME-2 level1B-R1 data based on level-0-to-1B processor version 4.0/4.1 modify total NO_2 results by 2 10^{13} molec.cm^{-2} or a few percent, that is, within the error bars of the correlative measurements.
- Differences between the near-real-time (NRT) and offline (OFL) processors: Monthly mean differences do not exceed 1 10^{14} molec.cm^{-2}; the general difference is within a few 10^{13} molec.cm^{-2}.

For unpolluted conditions, this validation update to four complete years of GOME-2 NO_2 column data confirms the overall good agreement with ground-based NDACC observations in the Northern Hemisphere and at polar stations, where GOME-2 data meet target requirements, but also the negative GOME-2 offset by about 0.6 10^{15} molec/cm^2 at the Southern middle latitudes with respect to NDACC and ERS-2 GOME measurements. Stratospheric validations were extended to polluted areas by filtering out, by cloud screening, GOME-2 data obviously affected by tropospheric pollution. Using this method, the tentative quantitative assessment of the agreement between GOME-2 and provisional NDACC UVVIS observations (of stratospheric/total NO_2) at the pilot station of the Observatoire de Haute Provence (OHP) confirms that the agreement ranges from -6 to +1 10^{14} molec/cm^2, that is, usually within the 10% range, with a yearly mean of -3 10^{14} molec/cm^2 and a standard deviation of .5 10^{14} molec/cm^2. The GOME-2 total column over other sites with a tropospheric NO_2 background but for unpolluted conditions also meets target requirements.

Comparisons of the GOME-2 product to MAX-DOAS tropospheric columns at the OHP are extended to three years of data. The pollution episodes are well reproduced by GOME-2 and the quantitative comparison are very encouraging, yielding a correlation coefficient of 0.67 and a linear regression slope of ~0.8. Comparison of the temporal series of the monthly mean ground-based and GOME-2 data shows a similar evolution of the seasonal behaviour, with larger values in winter (when the largest anthropogenic sources are emitted and when there is less light and thus less conversion of NO_2 into NO) and smaller in summer. The differences at the OHP for the GOME-2 GDP 4.3 data are generally within ±0.5 10^{15} molec/cm^2 (relative difference (Sat-GB)/Sat generally below ±50%), with a maximum difference of 1.8 10^{15} molec/cm^2. This first tentative of "direct" validation of the GOME-2 tropospheric NO_2 at OHP is very encouraging. Moreover, model data from CHIMERE has been used to test and consider the different horizontal sensitivities of the MAX-DOAS and the satellite pixel. A correction factor for the collocation difference has been calculated based on the model and applied to the measured data, improving the results of the comparison (both the correlation coefficient and the slope of the linear regression fit).

However, the extension of this comparison to a recent BIRA-IASB MAX-DOAS instrument installed in Beijing, China, from June 2008 to April 2009 shows that much larger differences (up to one order of magnitude) can be obtained in more polluted conditions. The difference of sensibility (due to the location of the MAX-DOAS in the city centre of Beijing) and the uncertainties in both ground-based and satellite retrievals leads to much larger differences than in the pilot study around OHP. Additional ground-based MAX-DOAS instruments are thus necessary to evaluate, under sufficiently different geophysical states of interest, the quality of the GOME-2 tropospheric NO_2 VCD. Comparisons within different pollution cases, covering a large set of tropospheric NO_2 content scenarios are needed, as well as a better distribution of MAX-DOAS instruments worldwide and harmonisation among the different retrieval and validation methods.

In order to better understand the quality of the GOME-2 GDP tropospheric NO_2 product, an additional study involving other satellite products (GOME-2 GDP and TEMIS products and SCIAMACHY TEMIS product) around OHP and Beijing has been carried out. GOME-2 GDP is in a general good agreement with GOME-2 and SCIAMACHY TEMIS products reproducing the seasonal variations, but there are some systematic differences (up to 50%) essentially due to the very different tropospheric AMF (over Beijing the mean AMF_trop for GDP is of ~0.85 compared to ~0.45 for TEMIS and over OHP ~0.80 compared to ~0.60), likely due to different assumptions of e.g., a-priori profiles and cloud schemes. More detailed comparisons are on-going.

E. REFERENCES

E.1. Peer-reviewed articles

Balis, D., J-C. Lambert, M. Van Roozendael, D. Loyola, R. Spurr, Y. Livschitz, P. Valks, V. Amiridis, P. Gerard, and J. Granville, Ten years of GOME/ERS-2 total ozone data – The new GOME Data Processor (GDP) Version 4: II Ground-based validation and comparisons with TOMS V7/V8, *Journal of Geophysical Research – Atmosphere*, Vol. 112, D07307, doi:10.1029/2005JD006376, 2007.

Blond, N., Boersma, K. F., Eskes, H. J., van der A, R. J., Van Roozendael, M., De Smedt, I., Bergametti, G., and Vautard, R. (2007), Intercomparison of SCIAMACHY nitrogen dioxide observations, in-situ measurements and air quality modeling results over Western Europe, doi:10.1029/2006JD007277, J. Geophys. Res., 2007.

Boersma K. F., H. J. Eskes, and E. J. Brinksma (2004), Error analysis for tropospheric NO_2 retrieval from space, J. Geophys. Res., vol. 109, D04311, doi:10.1029/2003JD003962, 2004.

Boersma, K. F., E. Bucsela, E. Brinksma, and J. F. Gleason (2002), NO_2, in OMI Algorithm Theoretical Basis Document, Volume IV: Trace Gas Algorithms, edited by K. Chance, pp. 15–36, KNMI, NASA/GSFC, FMI

Boersma, K. F., Eskes, H. J, Veefkind, J. P., Brinksma, E. J.,van der A, R. J., Sneep, M., van den Oord, G. H. J., Levelt, P. F., Stammes, P., Gleason, J. F., and Bucsela, E. J (2007), Near-real time retrieval of tropospheric NO2 from OMI, Atmos. Chem. Phys., 7, 2103–2118, www.atmos-chem-phys.net/7/2103/2007/

Brinksma, E., G. Pinardi, R. Braak, H. Volten, A. Richter, A. Schonhardt, M. Van Roozendael, C. Fayt, C. Hermans, R. Dirksen, T. Vlemmix, A.J.C Berkhout, D.P.J. Swart, H. Oetjen, F. Wittrock, T. Wagner, O. W. Ibrahim, G. de Leeuw, M. Moerman, L. Curier, E. A. Celarier, W. H. Knap, J. P. Veefkind, H.J. Eskes, M. Allaart, R. Rothe, A. J. M Piters, and P. Levelt (2008), The 2005 and 2006 DANDELIONS NO_2 and Aerosol Intercomparison Campaigns, J. Geophys. Res, vol. 113, D16S46, doi:10.1029/2007JD008808, 2008.

Bucsela, E. J., Celarier, E. A., Wenig, M. O., Gleason, J. F., Veefkind, J. P., Boersma, K. F., and Brinksma, E. J. (2006), Algorithm for NO_2 vertical column retrieval from the Ozone Monitoring Instrument, IEEE trans. on Geosci. Rem. Sens., 44(5), doi:10.1109/TGRS.2005.863715, 2006.

Celarier, E. A., E. J. Brinksma, J. F. Gleason, J. P. Veefkind, A. Cede, J. R. Herman, D. Ionov, F. Goutail, J-P. Pommereau, J.-C. Lambert, M. van Roozendael, G. Pinardi, F. Wittrock, A. Schönhardt, A. Richter, O. W. Ibrahim, T. Wagner, B. Bojkov, G. Mount, E. Spinei, C. M. Chen, T. J. Pongetti, S. P. Sander, E. J. Bucsela, M. O. Wenig, D. P. J. Swart, H. Volten, M. Kroon, and P. F. Levelt, Validation of Ozone Monitoring Instrument Nitrogen Dioxide Columns, J. Geophys. Res, vol. 113, D15S15, doi:10.1029/2007JD008908, 2008

Chipperfield, M. P., (1999), Multiannual simulations with a three-dimensional chemical transport model, J. Geophys. Res., 104 (D1), 1,781-1,805, 1999.

Clémer K., C. Fayt, F. Hendrick, C. Hermans, G. Pinardi, R. Spurr, P. Wang, M. Van Roozendael: Simultaneous retrieval of tropospheric aerosol extinction and NO_2 vertical profiles from MAX-DOAS measurements in Beijing, Proceedings of the 8th International Symposium on Tropospheric Profiling, 19–23 October, Delft, The Netherlands, Edited by A. Apituley, H.W.J. Russchenberg, W.A.A. Monna.

Dikty, S., Richter, A., Bovensmann, H., Wittrock, F., Weber, M., Noël, S., Burrows, J. P., Munro, R., and Lang, R.: GOME-2 level 2 products at IUP Bremen and first results on the quantification of the effects of optical degradation, EUMETSAT Meteorological Satellite Conference, Córdoba, Spain, 20-24 September 2010.

Errera, Q., and D. Fonteyn, (2001), Four-dimensional variational chemical assimilation of CRISTA stratospheric measurements, J. Geophys. Res., 106 (D11), 12,253-12,265, 2001.

Eskes H. J. and Boersma K. F. (2003), Averaging kernels for DOAS total-column satellite retrievals, Atmos. Chem. Phys., 3, 1285–1291, 2003, www.atmos-chem-phys.org/acp/3/1285/

Friedeburg, T.Wagner, F. Wittrock, D. Fonteyn, and M. De Maziere (2006), Intercomparison exercise between different radiative transfer models used for the interpretation of ground-based zenith-sky and multi-axis DOAS observations, Atmos. Chem. Phys., 6, 93–108, 2006.

Frieß, U., Monks, P. S., Remedios, J. J., Rozanov, A., Sinreich, R., Wagner, T., and Platt, U., (2006), MAX-DOAS O_4 measurements: A new technique to derive information on atmospheric aerosols: 2. Modeling studies, J. Geophys. Res., 111, D14203, doi:10.1029/2005JD006618, 2006.

Greenblatt G.D., Orlando, J.J., Burkholder J.B., and Ravishankara A.R.: Absorption measurements of oxygen between 330 and 1140 nm, J. Geophys. Res. **95**, 18577-18582, 1990.

Heckel, A., Richter, A., Tarsu, T., Wittrock, F., Hak, C., Pundt, I., Junkermann,W., and Burrows, J. P. (2005), MAX-DOAS measurements of formaldehyde in the Po-Valley, Atmos. Chem. Phys., 5, 909–918, 2005, SRef-ID: 1680-7324/acp/2005-5-909.

Hendrick, F, M. Van Roozendael, A. Kylling, A. Petritoli, A. Rozanov, S. Sanghavi, R. Schofield, C. von Friedeburg, T.Wagner, F. Wittrock, D. Fonteyn, and M. De Mazière, (2006), Intercomparison exercise between different radiative transfer models used for the interpretation of ground-based zenith-sky and multi-axis DOAS observations, Atmos. Chem. Phys., 6, 93–108, 2006, SRef-ID: 1680-7324/acp/2006-6-93.

Hendrick, F., Barret, B., Van Roozendael, M., Boesch, H., Butz, A., De Mazi`ere, M., Goutail, F., Hermans, C., Lambert, J.-C., Pfeilsticker, K., and Pommereau, J.-P. (2004), Retrieval of nitrogen dioxide stratospheric profiles from ground-based zenith-sky UV-visible observations: validation of the technique through correlative comparisons, Atmos. Chem. Phys., 4, 2091–2106, 2004, SRef-ID: 1680-7324/acp/2004-4-2091.

Hendrick, F., R. Mueller, B.M. Sinnhuber, M. Bruns, J. P. Burrows, M. P. Chipperfield, D. Fonteyn, A. Richter, M. Van Roozendael, and F. Wittrock, (2000), Simulation of BrO Diurnal Variation and BrO Slant Columns: Intercomparison Exercise Between Three Model Packages, Proceedings of the 5th European Workshop on Stratospheric Ozone, Saint Jean de Luz, France, 27 Sept.-1 Oct. 1999, Air Pollution Research Report n°73, European Commission – DG XII, Brussels.

Honninger, G., Friedeburg, C. V., and Platt, U.(2004), Multi Axis Differential Optical Absorption Spectroscopy (MAX-DOAS), Atmos. Chem. Phys., 4, 231–254, 2004, SRef-ID: 1680-7324/acp/2004-4-231.

Irie H., Kanaya Y., Akimoto H., Iwabuchi H., Shimizu A., and Aoki K.: First retrieval of tropospheric aerosol profiles using MAX-DOAS and comparison with lidar and sky radiometer measurements, Atmos. Chem. Phys. **8**, 341-350, 2008.

Johnston, P.V., and R.L. McKenzie, NO_2 Observations at 45°S during the Decreasing Phase of Solar Cycle 21, from 1980 to 1987, *Journal of Geophysical Research*, Vol. 94, pp. 3473-3486, 1989.

Koelemeijer, R. B. A., Stammes, P., Hovenier, J.W., and de Haan, J. F. (2001), A fast method for retrieval of cloud parameters using oxygen A-band measurements from Global Ozone Monitoring Experiment, J. Geophys. Res., 106, 3475–3490, 2001.

Kurylo, M. J., and R. J. Zander, The NDSC - Its status after ten years of operation, in Proc. of the Quadrennial Ozone Symposium 2000, Hokkaido Univ., Sapporo, Japan, Ed. by NASDA, 167-168, 2001.

Lambert, J.-C., M. Van Roozendael, M. De Mazière, P.C. Simon, J.-P. Pommereau, F. Goutail, A. Sarkissian, and J.F. Gleason, Investigation of pole-to-pole performances of spaceborne atmospheric chemistry sensors with the NDSC, *Journal of the Atmospheric Sciences*, Vol. 56, pp. 176-193, 1999.

Lambert, J.-C., Télédétection spatiale de l'ozone et du dioxyde d'azote dans l'atmosphère globale, PhD Thesis, Polytechnic School/Free University of Brussels, Ed. Belgian Institute for Space Aeronomy, Brussels, 291 pp., 2005.

Lang, R., Munro, R., Livschitz, Y., Dyer, R., and Lacan, A.: GOME-2 FM3 Long-Term In-Orbit Degradation - Basic Signatures After 2nd Throughput Test, EUMETSAT Technical report, EUM.OPS-EPS.DOC.09.0464, 2009.

Li X., Brauers T., Shao M., Garlang R.M., Wagner T., Deutschmann T., and Wahner A.: MAX-DOAS measurements in southern China:1. automated aerosol profile retrieval using oxygen dimmers absorptions, Atmos. Chem. Phys. Discuss. **8**, 17661-17690, 2008.

Mayer, B. and Kylling, A. (2005), Technical note: The libRadtran software package for radiative transfer calculations – description and examples of use, Atmos. Chem. Phys., 5, 1855–1877, 2005, SRef-ID: 1680-7324/acp/2005-5-1855.

Platt, U: Differential optical absorption spectroscopy (DOAS), in: Air Monitoring by Spectroscopic Techniques, Chem. Anal. Ser., edited by: Sigrist, M. W., John Wiley, New York, 127, 27–84, 1994.

Pommereau, J.-P. and F. Goutail, O_3 and NO_2 Ground-Based Measurements by Visible Spectrometry during Arctic Winter and Spring 1988, *Geophysical Research Letters*, Vol. 15, 891-894, 1988.

Richter, A., J. Leitao, A. Heckel, and J.P. Burrows (2007), Synergistic use of multiple sensors for tropospheric NO_2 measurements, ACCENT NO2 Workshop, 11 Sept. 2007, De Bilt, Netherlands.

Richter, A., J. P. Burrows, H. Nüß, C. Granier, and U. Niemeier (2005), Increase in tropospheric nitrogen dioxide over China observed from space, Nature, 437, 129–132.

Rodgers C.D.: *Inverse Methods for Atmospheric Sounding: Theory and Practice, Ser. Atmos. Oceanic Planet. Phys.*, vol. 2, edited by F.W. Taylor, World Sci., Hackensack, N.Y., 2000.

Rodgers, C. D. (1976), Retrieval of atmospheric temperature and composition from remote measurements of thermal radiation, Rev. Geophys. Space Phys., 14, 609–624, 1976.

Rodgers, C. D. (2000), Inverse Methods for Atmospheric Sounding,World Scientific, London, 2000.

Roscoe, H. K., P.V. Johnston, M. Van Roozendael, A. Richter, A. Sarkissian, J. Roscoe, K.E. Preston, J.-C. Lambert, C. Hermans, W. De Cuyper, S. Dzienus, T. Winterrath, J. Burrows, F. Goutail, J.-P. Pommereau, E. D'Almeida, J. Hottier, C. Coureul, D. Ramon, I. Pundt, L.M. Bartlett, C.T. McElroy, J.E. Kerr, A. Elokhov, G. Giovanelli, F. Ravegnani, M. Premuda, I. Kostadinov, F. Erle, T. Wagner, K. Pfeilsticker, M. Kenntner, L.C. Marquard, M. Gil, O. Puentedura, M. Yela, W. Arlander, B.A. Kåstad Høiskar, C.W. Tellefsen, K. Karlsen Tørnkvist, B. Heese, R.L. Jones, S.R. Aliwell, and R.A. Freshwater, Slant column measurements of O_3 and NO_2 during the NDSC intercomparison of zenith-sky UV-visible spectrometers in June 1996, *Journal of Atmospheric Chemistry*, Vol. 32, 281-314, 1999.

Spurr R.J.D., Kurosu T.P., Chance K.V.: A Linearized discrete Ordinate Radiative Transfer Model for Atmospheric Remote Sensing Retrieval, J. Quant. Spectrosc. Radiat. Transfer **68**, 689-735, 2001.

Spurr R.J.D.: Simulatinous derivation of intensities and weighting functions in a general preuso-spherical discrete ordinate radiative transfer treatment, J. Quant. Spectrosc. Radiat. Transfer **75**, 129-175, 2002.

Valks, P., G. Pinardi, A. Richter, J-C. Lambert, N. Hao, D. Loyola, M. Van Roozendael, and S. Emmadi, Operational total and tropospheric NO2 column retrieval for GOME-2, submitted to *Atmos. Meas. Tech., Discuss, 4, 1617-1676,* 2011.

van Noije, T. P. C., Eskes, H. J., Dentener, F. J. , Stevenson, D. S., et al.(2006), Multi-model ensemble simulations of tropospheric NO_2 compared with GOME retrievals for the year 2000, Atmos. Chem. Phys., 6, 2943–2979, 2006, http://www.atmos-chem-phys.net/6/2943/2006/.

Van Roozendael, M., D. Loyola, R. Spurr, D. Balis, J-C. Lambert, Y. Livschitz, T. Ruppert, P. Valks, P. Kenter, C. Fayt, and C. Zehner, Ten years of GOME/ERS-2 total ozone data – The new GOME Data Processor (GDP) Version 4: I Algorithm Description, *Journal of Geophysical Research – Atmosphere*, Vol. 111, D14311, doi:10.1029/2005JD006375, 2006.

Vandaele, A.-C., C. Fayt, F. Hendrick, C. Hermans, F. Humbled, *et al*., An intercomparison campaign of ground-based UV-visible measurements of NO_2, BrO, and OClO slant columns: Methods of analysis and results for NO_2, *Journal of Geophysical Research*, Vol. 110, doi:10.1029/2004JD005423, 2005.

Vandaele, A.-C., C. Hermans, P.C. Simon, M. Carleer, R. Colin, S. Fally, M.F. Mérienne, A. Jenouvrier, and B. Coquart, Measurements of NO_2 absorption cross-section from 42000 cm^{-1} to 10000 cm^{-1} (238-1000 nm) at 220 K and 294 K, *Journal of Quantitative Spectroscopy and Radiative Transfer*, Vol. 59, 171-184, 1998.

Vautard, R., Beekmann, M., Roux, J. & Gombert, D. (2001) Atmospheric Environment, 35, doi:10.1016/S1352-2310(00)00466-0.

Wagner T., J. P. Burrows, T. Deutschmann, B. Dix, C. von Friedeburg, U. Frieß, F. Hendrick, K.-P. Heue, H. Irie, H. Iwabuchi, Y. Kanaya, J. Keller, C. A. McLinden, H. Oetjen, E. Palazzi, A. Petritoli, U. Platt, O. Postylyakov, J. Pukite, A. Richter, M. van Roozendael, A. Rozanov, V. Rozanov, R. Sinreich, S. Sanghavi, and F. Wittrock, (2007), Comparison of box-air-mass-factors and radiances for Multiple-Axis Differential Optical Absorption Spectroscopy (MAX-DOAS) geometries calculated from different UV/visible radiative transfer models, Atmos. Chem. Phys., 7, 1809–1833, 2007

Wagner, T., Dix, B., Friedburg, C. v., Frieß, U., Sanghavi, S., Sinreich, R., and Platt, U. (2004), MAX-DOAS O_4 measurements: A new technique to derive information on atmospheric aerosols- Principles and information content, J. Geophys. Res., 109, D22205, doi:10.1029/2004JD004904, 2004

Wittrock, F. (2006), The retrieval of oxygenated volatile organic compounds by remote sensing techniques, PhD Thesis, 192 pp, University of Bremen, Bremen, 2006.

Wittrock, F., Oetjen, H., Richter, A., Fietkau, S., Medeke, T., Rozanov, A., and Burrows, J. P. (2004), MAX-DOAS measurements of atmospheric trace gases in Ny-Alesund – Radiative transfer studies and their application, Atmos. Chem. Phys., 4, 955–966, 2004, SRef-ID: 1680-7324/acp/2004-4-955.

E.2. Technical notes

AGACC_2008: Advanced exploitation of Ground-based measurements for Atmospheric Chemistry and Climate applications, FINAL REPORT PHASE 1, period: 15/12/2005-30/04/2008, 27/05/2008 (http://www.oma.be/AGACC/Home.html)

TN-DLR 2003: Design Document for the GOME-2 Universal Processor for Atmospheric Spectrometers, DLR Technical Note SAF/O3M/DLR/DD/001, Issue 2.0, October 2003.

TN-DLR-ATBD 2011: Algorithm Theoretical Basis Document for GOME-2 Total Column Products of Ozone, NO2, tropospheric NO2, BrO, SO2, H2O, HCHO, OClO and Cloud Properties (GDP 4.4 for O3M-SAF OTO and NTO), DLR Technical Note DLR/GOME-2/ATBD/01, 44 pp., Issue/Revision 2/D, 10 January 2011.

TN-DLR-PUM 2010: Product User Manual for GOME Total Columns of Ozone, NO_2, SO_2, BrO, H_2O, HCHO, OClO, tropospheric NO_2, and Cloud Properties (O3M-SAF OTO and NTO), DLR Technical Note DLR/GOME/PUM/01, 47 pp., Issue 2 Revision C, 19 February 2010.

Nuss et al. 2006: Nüß H., A. Richter, P. Valks, J.P. Burrows, Improvements of the NO_2 Total Column Retrieval for GOME-2, O3M SAF Visiting Scientist Activity Final Report, 11 November 2006, [http://o3saf.fmi.fi/documents.html]

Gür et al., 2005: Gür, B., P. Spietz, J. Orphal and J. Burrows (2005), Absorption Spectra Measurements with the GOME-2 FMs using the IUP/IFE-UB´s Calibration Apparatus for Trace Gas Absorption Spectroscopy CATGAS, Final Report, IUP University of Bremen, Oct. 2005.

ESA 2002: ERS-2 GOME GDP3.0 Implementation and Validation, ESA Technical Note ERSE-DTEX-EOAD-TN-02-0006, Ed. by J.-C. Lambert (IASB), 138 pp., Issue 1.0, November 2002. [http://earth.esrin.esa.it/pub/ESA_DOC/GOME/gdp3/gdp3.htm]

ESA 2004a: Algorithm Theoretical Basis Document for GOME Total Column Densities of Ozone and Nitrogen Dioxide, UPAS/GDOAS: GDP 4.0, ESA Technical Note ERSE-DTEX-EOPG-TN-04-0007, Ed. By DLR, Iss./Rev. 1/A, 15 December 2004. [http://earth.esrin.esa.it/pub/ESA_DOC/GOME/]

ESA 2004b: UPAS / GDOAS 4.0 Upgrade of the GOME Data Processor for Improved Total Ozone Columns – Delta Validation Report, ESA Technical Note ERSE-CLVL-EOPG-TN-04-0001, Ed. by J.-C. Lambert (IASB) and D. Balis (AUTH), 15 December 2004.

VAL_INITIAL_2007: Initial Validation of GOME-2 Nitrogen Dioxide Columns (GDP 4.2 OTO/NO2 and NTO/NO2): March – June 2007, IASB-BIRA Technical Note, IASB-BIRA Technical Note TN-IASB-GOME2-O3MSAF-NO2-01, 40 pp., Issue 1, Revision B, 22 October 2007.

VAL_ORR-A3_2008: ORR-A3 - GOME-2 GDP 4.2 total NO2 (NTO/OTO) validation update and initial validation of tropospheric NO_2, EUMETSAT/IASB-BIRA Technical Note, TN-IASB-GOME2-O3MSAF-NO2-02_ORR-A3, 47 pp., Issue ORR-A3, 29 April 2008.

VAL_ORR-B_2008: ORR-B rev.1 - GOME-2 GDP 4.2 total NO2 validation update (March 2007 – July 2008) and tropospheric NO2 validation set-up, EUMETSAT/IASB-BIRA Technical Note, TN-IASB-GOME2-O3MSAF-NO2-02_ORR-B_1, 52 pp., Issue ORR-B, 24 November 2008.

Vestreng (2003), Review and revision of Emission data reported to CLRTAP, EMEP status report.